University of Alberta

STOCHASTIC RESONANCE IN NANOSCALE SYSTEMS

by

Aditya A. Saha

A thesis submitted to the Faculty of Graduate Studies and Research

in partial fulfillment of the requirements for the degree of

Doctor of Philosophy

Department of Physics

© Aditya A. Saha

Spring 2011
Edmonton, Alberta

Permission is hereby granted to the University of Alberta Libraries to reproduce single copies of this thesis and to lend or sell such copies for private, scholarly or scientific research purposes only. Where the thesis is converted to, or otherwise made available in digital form, the University of Alberta will advise potential users of the thesis of these terms.

The author reserves all other publication and other rights in association with the copyright in the thesis and, except as herein before provided, neither the thesis nor any substantial portion thereof may be printed or otherwise reproduced in any material form whatsoever without the author's prior written permission.

Abstract

This thesis considers the possibility of stochastic resonance (SR) in the following nanoscale systems: (i) hard-threshold devices; (ii) averaging structures of carbon nanotubes (CNTs); (iii) myoglobin atoms; and finally (iv) tubulin dimers. The description of SR is carried out using Kramers' rate theory in the adiabatic two-state approximation for continuous systems and using Shannon's information theoretic formalism for systems with static nonlinearities. The effective potentials are modelled by asymmetric or symmetric bistable wells in a single reaction co-ordinate. Quantum considerations have not been invoked. Hence, all results are implicitly valid in the high-temperature regime of relevance to industrial applications. It is established that information transmitted by arrays of identical CNTs is maximized by non-zero noise intensities and that the response of myoglobin and tubulin dimers to ambient molecular forces (as described by the signal-to-noise ratio or SNR) is enhanced by increasing temperature. Sample calculations are shown for solvent fluctuations, ligand interactions and dipole oscillations. These results can be used to explain: (i) the effects of temperature observed in fabrication processes for CNTs; (ii) the dynamical transition observed in myoglobin and (iii) the 8.085 MHz resonance observed in microtubules.

Table of Contents

List of Figures

Chapter 1

Introduction

In conventional system theory, noise is inevitably considered as a degrading factor on the system performance. This is certainly true of all linear systems. Due to the 'irregular', non-deterministic nature of noise, it is modelled as a random process influencing system dynamics. Furthermore noise is unavoidable, it being impossible to isolate a system perfectly from its environment. All systems interact with their thermal reservoirs, which constitute a source of noisy dynamics. Even at zero temperature, when thermal (classical) fluctuations vanish, an interaction with zero-temperature reservoirs– a source of quantum noise, persists. Nonetheless, the addition of an optimal level of noise sometimes makes a nonlinear system behave in a more regular manner. Such increased 'regularity' manifests itself in a number of ways: (i) an increase in the signal energy in a certain frequency bin relative to the power of noise; (ii) an increased periodicity in residence times; (iii) an increase in synchronization between various coupled devices; and (iv) an increase in the value of information-theoretic measures for complex signals.

Stochastic Resonance (SR) is a phenomenon manifest in certain nonlinear systems whereby weak, input signals are amplified when subject to noise. This phenomenon requires three basic ingredients: (i) a system characterized by a threshold or more generally an energy activation barrier; (ii) a weak, coherent input (usually a weak periodic or semi-periodic signal); and finally (iii) a source of noise inherent in the system. The underlying mechanism of this phenomenon is simple and robust, as will be explained below.

An intuitive picture of how such noise-induced improvement occurs can be given as follows. We consider the overdamped motion of a classical particle in a symmetric double-well potential. If this system is noise-free, the particle tends to relax within the potential well where it was initially placed. Coupling to a thermal bath results

in random discrete jumps of the particle's reaction coordinate. Due to these jumps, the particle can eventually surmount the potential barrier, thereby undergoing a noise-assisted transition to the neighbouring well. These thermal activation rates are given by the celebrated Kramers' formula [94]:

$$r_K = \frac{\omega_o \omega_b}{2\pi\gamma} \exp\left(-\frac{\Delta V}{D}\right). \tag{1.1}$$

with $\omega_0^2 = V''(x_m)/m$ being the squared angular frequency at the potential minima $\pm x_m$, and $\omega_b^2 = |V''(x_b)/m|$ being the squared angular frequency at the top of the barrier x_b; and γ being the coefficient of viscosity. ΔV is the height of the potential barrier separating the two minima and $D = k_B T$ is the noise strength, related to the temperature. Thus, the thermal activation rates are functions of the barrier height and noise level. If a small periodic modulation is applied to the potential at a modulation frequency much smaller than the intrawell relaxation rate, but in itself unable to carry the particle deterministically across the potential barrier, the thermal activation rates are periodically modulated in time. Consequently, at a certain phase of the signal, the probability of undergoing a certain transition to the neighbouring well increases, whereas the probability of the opposite transition is suppressed. If we observe realizations of the stochastic process $x(t)$ for different noise strengths, we see that for some finite, optimal amount of noise, transitions between wells occur almost periodically in time. At some noise level, the waiting time $T_K(D) = 1/r_K$ between two noise-induced interwell transitions is comparable to half the time-period T_Ω of the periodic forcing. This leads us to the matching condition given by

$$T_K(D) = \frac{1}{2} T_\Omega. \tag{1.2}$$

Therefore, one feature of such noise-induced behaviour in a symmetric double-well potential is the statistical synchronization observed between (i) thermally activated hopping events from/to adjacent potential wells and (ii) the weak periodic forcing signals. For a given period of the forcing T_Ω, the time-scale matching condition can be fulfilled by tuning the noise level D_{max} to the value determined by Eq.(1.2). This somewhat counter-intuitive, cooperative effect between a signal and noise in a nonlinear system, leading to an enhanced response to the periodic force is termed stochastic resonance (SR).

The term 'Stochastic resonance' first appeared in 1981 [10], where it was proposed by Benzi as a plausible mechanism for the almost periodic occurrence of ice ages in Earth's climatic history. A statistical analysis of data pertaining to the Earth's glaciation se-

quence over the past 700,000 years indicates an average periodicity of about 100,000 years. This fact is surprising as the only comparable time-scale in Earth dynamics is the period over which the orbital eccentricity is modulated by planetary gravitational perturbations. Furthermore, these effects cause an exceedingly small variation in the solar energy flux on the Earth's surface, by itself too weak to cause the observed climatic variations. Stochastic resonance (SR) offers a simple, but by no means definitive answer to this question. Benzi and his co-workers [10] modelled global climate by a symmetric double-well potential in a single co-ordinate, namely temperature. One minimum represents an attractor corresponding to a cold, largely icy climate, the other to a warmer climate. The weak modulation of the orbital eccentricity corresponds to a weak, periodic forcing on such a system. Short-term climate fluctuations, such as annual fluctuations in solar radiation, were modelled by Gaussian white noise. In Benzi's model synchronized hopping between cold and warm climates, governed by Eq.(1.2), aid and enhance the response of the Earth's climate to otherwise weak perturbations in its orbital eccentricity.

The first experimental verification of SR was obtained in a study of the AC-driven Schmitt trigger with both a threshold and a hysteretic nonlinearity [39]. However, it was the key experiment in a bistable ring laser by McNamara and Wiesenfeld [122] which inaugurated keen interest in the SR phenomenon. Soon afterward, prominent theoretical treatments were proposed in the adiabatic limit [48, 123, 141, 73] and in the non-adiabatic regime [81, 82, 85]. Descriptions of SR in terms of linear response theory (LRT) have also been frequently proposed [34, 35, 49, 85, 73].

The unifying feature of all systems said to exhibit SR is the increased sensitivity to small perturbations at an optimal noise level. The first non-bistable systems discussed in this category were excitable systems [103]. In contrast to bistable systems, excitable systems have only one stable state, called the rest state. However, they also possess a threshold to an excited state which is not stable and decays after a refractory period. The refractory period is much longer, relative to the relaxation time of small perturbations around the stable state. A class of very simple systems which were also discovered to exhibit SR, also dwelt on extensively in this thesis, were threshold detectors [79, 80, 192, 51, 47]. It must also be mentioned that SR-like features were discovered in purely autonomous systems [72, 145].

The most prominent area for applications of stochastic resonance thus far has been in neurophysiology: SR has been demonstrated in mechanoreceptor neurons located in the tail fans of crayfish [32] and in the hair cells of crickets [100]. The investigation of SR in retinal and noisy neuron models has been done in [136, 137, 92, 91]. A detailed review is given in [126]. It is noteworthy that the notion of stochastic resonance is

not limited to the macroscopic world governed by classical physics: it has since been extended into the domain of microscopic and mesoscopic physics. The quantum analog of stochastic resonance was addressed in [105, 106, 58, 59]. It has been discovered in spatially extended pattern-forming systems [83, 102]. Other important extensions of SR include coupled systems and deterministic systems exhibiting chaos ([48] and references therein). Apart from theoretical developments [48], the SR effect has been used in many practical applications such as sonar arrays [4, 153]; flash analog-to-digital converters [111]; cochlear implants [177] and motion detection systems [67]. A prominent area of research is the investigation of stochastic resonance in nano-scale devices. Stochastic resonance hase been explored in nanotubes [98], quantum dots [78], nano-mechanical oscillators [7], nano-scaled gates [114] and nano-electronic cells [115]. Other applications are listed in [125]. The use of this phenomenon in the context of signal detection, has also received considerable interest [20, 21, 22, 23, 24, 25, 54, 155, 156, 201, 202]. The detector consists of a stochastic resonant threshold system followed by a correlator. Such detectors exhibit a marked improvement in performance over conventional, linear systems for non-Gaussian noise [20, 22, 23, 24, 25, 47, 54, 201, 202]. In this thesis, we discuss the design and construction of such a detector in greater detail.

The organization of the remainder of the thesis is as follows: in chapter 2, we present the background theory relevant to the project; in chapter 3 we discuss the design of the detector based on SR in threshold systems at length; in chapter 4 we investigate SR in arrays of carbon nanotubes; and in chapters 5 and 6 we investigate SR in myoglobin atoms and tubulin dimers respectively. Chapter 7 summarizes and concludes the document. Chapters 3, 4, 5 and 6 relate to research articles [158, 159, 160] and [161] respectively.

Chapter 2

Background theory

2.1 Characterization of stochastic resonance

In this section we discuss the simplest model that characterizes a class of symmetric, bistable systems which exhibit stochastic resonance. Such a discrete model was proposed originally as a study case by McNamara and Wiesenfeld [122], who argued that under certain conditions it gives an accurate description of most continuous bistable systems. A preliminary analytical scheme for such systems can be developed as follows.

Consider a symmetric, unperturbed system which switches between two discrete states $\pm x_m$ with rates $W_\pm$ into either state. We define $n_\pm(t)$ to be the probabilities that the system occupies either state $\pm$ at time t, i.e. $x(t) = \pm x_m$. In the presence of a periodic input signal $A(t) = A_0 \cos \Omega t$, the transition rates $W_\pm(t)$ depend periodically on time. The relevant master equation then reads

$$\frac{d}{dt} n_\pm(t) = -W_\mp(t) n_\pm(t) + W_\pm(t) n_\mp(t), \tag{2.1}$$

or, using the normalization condition $n_+(t) + n_-(t) = 1$,

$$\frac{d}{dt} n_\pm(t) = -\left[W_\pm(t) + W_\mp(t)\right] n_\pm(t) + W_\pm(t). \tag{2.2}$$

The solution of the rate equation (2.2) can be found by the standard method of integrating factor for first-order ODEs [3, 18] and is given by

$$\begin{aligned} n_\pm(t) &= g(t) \left[n_\pm(t_0) + \int_{t_0}^{t} W_\pm(\tau) g^{-1}(\tau) d\tau \right], \\ g(t) &= \exp\left(-\int_{t_0}^{t} [W_+(\tau) + W_-(\tau)] d\tau \right), \end{aligned} \tag{2.3}$$

with unspecified boundary conditions $n_{\pm}(t_0)$. Following [122, 123] we will assume the transition probability densities are periodically modulated escape rates of the Arrhenius type, given by

$$W_{\mp}(t) = r_K \exp\left[\pm \frac{A_0 x_m}{D} \cos \Omega t\right], \tag{2.4}$$

where $D = k_B T$ represents the strength of the thermal noise similar to Eq.(2.84). Since we are primarily interested in the transmission and detection of weak signals in this thesis, we will assume that the energy of the modulating signal is small compared to that of thermal noise i.e. $A_0 x_m \ll D$. In such a case, the following Taylor's series expansions can be derived in the small parameter $A_0 x_m / D$,

$$\begin{aligned} W_{\mp}(t) &= r_K \left[1 \pm \left(\frac{A_0 x_m}{D}\right) \cos \Omega t + \frac{1}{2}\left(\frac{A_0 x_m}{D}\right)^2 \cos^2 \Omega t \pm \ldots\right], \\ W_{+}(t) &+ W_{-}(t) = 2 r_K \left[1 + \frac{1}{2}\left(\frac{A_0 x_m}{D}\right)^2 \cos^2 \Omega t + \ldots\right]. \end{aligned} \tag{2.5}$$

This assumption for escape routes remains valid for small driving frequencies (adiabatic assumption). Under such an assumption the integral in Eq.(2.3) can be performed to give to first order in $A_0 x_m / D$,

$$\begin{aligned} & n_{+}(t|x_0, t_0) = 1 - n_{-}(t|x_0, t_0) \\ & = \frac{1}{2}\{\exp\left[-2 r_K (t - t_0)\right] \left[2\delta_{x_0, x_m} - 1 - \kappa(t_0)\right] + 1 + \kappa(t)\}, \end{aligned} \tag{2.6}$$

where

$$\begin{aligned} \kappa(t) &= 2 r_K / \sqrt{4 r_K^2 + \Omega^2} (A_0 x_m / D) \cos(\Omega t - \overline{\phi}) \quad \text{and} \\ \overline{\phi} &= \arctan(\Omega / 2\ r_K). \end{aligned} \tag{2.7}$$

The quantity $n_{+}(t|x_0, t_0)$ denotes the conditional probability that $x(t)$ is in state + at time t, given that its initial state $x_0 = x(t_0)$. Here, the Kronecker delta δ_{x_0, x_m} is unity when the system is initially in the state +. From the above equations, any statistical quantity of the discrete process $x(t)$ can be computed to first order in $A_0 x_m / D$. A few such quantities are:

1. the time-dependent response $\langle x(t)|x_0, t_0\rangle$ to the periodic forcing. From the defini-

tions

$$\langle x(t)|x_0,t_0\rangle = \int xP(x,t|x_0,t_0)dx \tag{2.8}$$

and

$$P(x,t|x_0,t_0) = n_+(t|x_0,t_0)\delta(x-x_m) + n_-(t|x_0,t_0)\delta(x+x_m), \tag{2.9}$$

it follows that in the asymptotic limit $t_0 \to -\infty$,

$$\lim_{t_0\to-\infty}\langle x(t)|x_0,t_0\rangle \equiv \langle x(t)\rangle_{as} = \overline{x}(D)\cos[\Omega t - \overline{\phi}(D)], \tag{2.10}$$

with

$$\begin{aligned} \overline{x}(D) &= \frac{A_0 x_m^2}{D}\frac{2r_K}{\sqrt{4r_K^2+\Omega^2}} \quad \text{and} \\ \overline{\phi}(D) &= \arctan\left(\frac{\Omega}{2r_K}\right). \end{aligned} \tag{2.11}$$

2. the auto-correlation function $\langle x(t+\tau)x(t)|x_0,t_0\rangle$. The general definition

$$\langle x(t+\tau)x(t)|x_0,t_0\rangle = \int\int xyP(x,t+\tau|y,t)P(y,t|x_0,t_0)dxdy \tag{2.12}$$

greatly simplifies in the stationary limit $t_0 \to -\infty$,

$$\begin{aligned} &\lim_{t_0\to-\infty}\langle x(t+\tau)x(t)|x_0,t_0\rangle \equiv \langle x(t+\tau)x(t)|x_0,t_0\rangle_{as} \\ &= x_m^2\exp\left(-2r_K|\tau|\right)\left[1-\kappa^2(t)\right] + x_m^2\kappa(t+\tau)\kappa(t). \end{aligned} \tag{2.13}$$

In Eq.(2.13) we can easily separate an exponentially decaying branch due to randomness and a periodically oscillating tail driven by the periodic input signal. Note that even in the stationary limit $t_0 \to -\infty$, the output signal auto-correlation depends on both times t and $t+\tau$. However in real experiments, t denotes the time of the data acquisition process. Typically, the averages implied by the definition of the auto-correlation function are taken over many sampling records of the signal $x(t)$, triggered a large number of times t within one forcing period T_Ω. Hence, the corresponding phases of the input signal $\theta = \Omega t + \phi$, are uniformly distributed between 0 and 2π. This corresponds to averaging $\langle x(t+\tau)x(t)|x_0,t_0\rangle_{as}$ with respect

to t uniformly over an entire forcing period, whereby

$$\begin{aligned}\langle\langle x(t+\tau)x(t)|x_0,t_0\rangle\rangle &= x_m^2\exp\left(-2r_K|\tau|\right)\left[1-\frac{1}{2}\left(\frac{A_0x_m}{D}\right)^2\frac{4r_K^2}{4r_K^2+\Omega^2}\right]\\ &\quad+\frac{x_m^2}{2}\left(\frac{A_0x_m}{D}\right)^2\frac{4r_K^2}{4r_K^2+\Omega^2}\cos\Omega t. \qquad (2.14)\end{aligned}$$

where the outer angular brackets $\langle\ldots\rangle$ now stand for $1/T_\Omega\int_0^{T_\Omega}[\ldots]dt$.

Before proceeding further, a few salient points in the derivation of Eqs.(2.10) and (2.13) should be outlined for the reader's benefit. From Eqs.(2.3) and (2.5) it follows that

$$g(t) = \exp\left\{-\int_{t_0}^{t}2r_K\,[1+\frac{1}{2}\left(\frac{A_0x_m}{D}\right)^2\cos^2\Omega u]du\right\}. \qquad (2.15)$$

Since the correction to $g(t)$ is seen to be of the order of $O(A_0^2)$, to first order we have the approximations $g(t)=e^{-2r_K(t-t_0)}$ and $g^{-1}(\tau)=e^{2r_K(\tau-t_0)}$. Then from Eq.(2.3) we get

$$\begin{aligned}n_+(t) &= e^{-2r_K(t-t_0)}\left[n_+(t_0)+\int_{t_0}^{t}r_K\left(1-\frac{A_0x_m}{D}\cos\Omega\tau\right)e^{2r_K(\tau-t_0)}d\tau\right],\\ &= e^{-2r_K(t-t_0)}\left[n_+(t_0)+\frac{1}{2}\left(e^{2r_K(t-t_0)}-1\right)-r_K\frac{A_0x_m}{D}\int_{t_0}^{t}\cos\Omega\tau e^{2r_K(\tau-t_0)}d\tau\right].\end{aligned} \qquad (2.16)$$

The integral in the last equation can be evaluated by the method of residues to give us

$$\int_{t_0}^{t}\cos\Omega\tau e^{2r_K\tau}d\tau=\frac{1}{2}\left[\frac{e^{2r_Kt}}{\sqrt{4r_K^2+\Omega^2}}\cos(\Omega t-\overline{\phi})-\frac{e^{2r_Kt_0}}{\sqrt{4r_K^2+\Omega^2}}\cos(\Omega t_0-\overline{\phi})\right] \qquad (2.17)$$

Substituting this result into Eq.(2.16) we get

$$\begin{aligned}n_+(t) &= e^{-2r_K(t-t_0)}\left[n_+(t_0)+\frac{1}{2}\left(e^{2r_K(t-t_0)}-1\right)-\frac{r_K}{\sqrt{4r_K^2+\Omega^2}}\right.\\ &\quad\left.\times\left(\frac{A_0x_m}{D}\right)\left\{e^{2r_K(t-t_0)}\cos(\Omega\ t-\overline{\phi})-\cos(\Omega\ t_0-\overline{\phi})\right\}\right]\\ &= \left[\frac{1}{2}(1-\kappa(t))+e^{-2r_K(t-t_0)}\{n_+(t_0)-\frac{1}{2}(1-\kappa(t_0))\}\right]. \qquad (2.18)\end{aligned}$$

where $\kappa(t)$ is as defined in Eq.(2.7). The equation for $n_-(t)$ follows similarly.

The evaluation of $\langle x(t)|x_0,t_0\rangle$ and $\langle x(t+\tau)x(t)|x_0,t_0\rangle$ involves a straight-forward evaluation of the integrals in Eqs.(2.8) and (2.12). Substituting the expressions for $n_\pm(t)$ from Eq.(2.18) into Eq.(2.8) we get

$$\langle x(t)|x_0,t_0\rangle = x_m\left(\delta_{x_0,x_m} - 1 - \kappa(t_0)\right)e^{-2r_K(t-t_0)} + x_m\kappa(t). \tag{2.19}$$

In the limit as $t_0 \to -\infty$ we get

$$\lim_{t_0\to-\infty}\langle x(t)|x_0,t_0\rangle = x_m\kappa(t) = \frac{2r_K}{4r_K^2+\Omega^2}\left(\frac{A_0x_m^2}{D}\right)^2\cos(\Omega t - \overline{\phi}). \tag{2.20}$$

Similarly substituting Eq.(2.18) into Eq.(2.12) we get

$$\begin{aligned}\langle x(t+\tau)x(t)|x_0,t_0\rangle &= \frac{x_m^2}{4}\Big[A(t,t_0)\{e^{-2r_K\tau}(1-\kappa(t)) + \kappa(t+\tau)\} \\ &\quad - B(t,t_0)\{e^{-2r_K\tau}(1+\kappa(t)) - \kappa(t+\tau)\}\Big]. \end{aligned}\tag{2.21}$$

where

$$\begin{aligned}A(t,t_0) &= e^{-2r_K(t-t_0)}(2\delta_{x_0,x_m} - 1 - \kappa(t_0)) + (1+\kappa(t)), \\ B(t,t_0) &= e^{-2r_K(t-t_0)}(2\delta_{x_0,x_m} - 1 - \kappa(t_0)) - (1-\kappa(t)).\end{aligned}\tag{2.22}$$

In the above we have evaluated the integral over x first. In the limit as $t_0 \to -\infty$ the expression simplify considerably to give us

$$\begin{aligned}&\lim_{t_0\to-\infty}\langle x(t+\tau)x(t)|x_0,t_0\rangle \\ &\frac{x_m^2}{2}\left[e^{-2r_K\tau}(1-\kappa^2(t)) + \kappa(t)\kappa(t+\tau)\right].\end{aligned}\tag{2.23}$$

We can now proceed to outline the derivation of the power spectral density and the signal-to-noise ratio.

3. The power spectral density $S(\omega)$ is defined as the Fourier transform of the averaged asymptotic autocorrelation function. Since the averaged autocorrelation function is given by Eq.(2.14) it follows that

$$S(\omega) = \frac{4r_Kx_m^2}{4r_K^2+\omega^2}\left[1 - \frac{1}{2}\left(\frac{A_0x_m}{D}\right)^2\frac{4r_K^2}{4r_K^2+\Omega^2}\right]$$

$$+\frac{\pi}{2}\left(\frac{A_0 x_m}{D}\right)^2 \frac{4x_m^2 r_K^2}{4r_K^2+\Omega^2}[\delta(\omega-\Omega)+\delta(\omega+\Omega)]. \tag{2.24}$$

The total output power, with signal plus noise, for the two-state model discussed here, is $2\pi x_m^2$, independent of the signal amplitude A_0 and frequency Ω. Hence, the effect of the input signal is to transfer power from the broadband noise background into the delta spikes of the power spectral density. It is evident from Eq.(2.24) that the energy of the signal at the frequency Ω denoted by E_S, also called the coherent energy, is given by

$$E_S = \frac{\pi}{2}\left(\frac{A_0 x_m}{D}\right)^2 \frac{4x_m^2 r_K^2}{4r_K^2+\Omega^2} \tag{2.25}$$

Similarly, the energy of the noise in the frequency bin $[\Omega - 2\pi/T_\Omega, \Omega - 2\pi/T_\Omega]$ denoted by E_N, also called the incoherent energy, is given by

$$E_N = \frac{2r_K x_m^2}{4r_K^2+\Omega^2}\left[1-\frac{1}{2}\left(\frac{A_0 x_m}{D}\right)^2 \frac{4r_K^2}{4r_K^2+\Omega^2}\right]. \tag{2.26}$$

Then it follows from Eqs.(2.25) and (2.26) that the signal-to-noise ratio (SNR), defined as the ratio of the coherent to the incoherent energy is given by

$$SNR = \frac{E_S}{E_N} = \pi\left(\frac{A_0 x_m}{D}\right)^2 r_K + O(A_0^4). \tag{2.27}$$

The residence time distribution (RTD), defined as the probability distribution of the expected time the system coordinate remains in one particular well, denoted by $N(T)$, was calculated for the two-state model in [199],[105] and [106]. To leading order in $A_0 x_m/D$ we have

$$N(T) = \mathcal{N}_0\left[1-\frac{1}{2}\left(\frac{A_0 x_m}{D}\right)^2 \cos(\Omega t)\right] r_K \exp(-r_K T), \tag{2.28}$$

with

$$\mathcal{N}_0^{-1} = 1-\frac{1}{2}\left(\frac{A_0 x_m}{D}\right)^2 /[1+(\Omega/r_K)^2]. \tag{2.29}$$

$N(T)$ can be shown to exhibit a peak structure shown in [46] with $T_n = (n-1/2)T_\Omega$. However, in this thesis the RTD has been mentioned only for completeness and this quantity will not be considered any further.

In this section the details of the symmetric two-state model exhibiting stochastic reso-

nance were studied. The two-state model can be regarded as an adiabatic approximation to any continuous bistable system, like the overdamped quartic double-well oscillator provided that the input-signal frequency is low enough for the notion of the transition rates of Eq.(2.4) to apply. The difficulty lies in the derivation of time-dependent transition rates in a continuous model. A systematic method consists of finding the unstable periodic orbits in the absence of noise, since they act as basin boundaries in an extended phase-space description [84]. Rates in periodically driven systems can be defined as the transition rates across those basin boundaries and correspond to the lowest-lying Floquet eigen-value of the time-periodic Fokker-Planck operator.

2.2 Continuous bistable systems

A two-state description of stochastic resonance is of limited utility because of the following reasons: it reduces the dynamics of the switching mechanism between two metastable states and neglects the short-time dynamics that takes place within the immediate neighbourhood of the metastable states themselves. Moreover, the goal is to describe the linear as well as nonlinear stochastic resonance response in the whole regime of modulation frequencies, extending from exponentially small Kramers rates to intrawell frequencies and higher. Phrased differently, a more elaborate approach is required to model the nonadiabatic regime of driving in the whole accessible state space of the dynamical process $x(t)$. This will be done in the class of continuous-state random systems [178, 65, 147, 190] which can be modelled in terms of the Fokker-Planck equation.

2.2.1 The Fokker-Planck description

As a generic system modelling stochastic resonance, we shall consider the random motion of a particle of mass m that moves in a bistable potential $V(x)$ and is subjected to thermal noise $\xi(t)$ of the Nyquist type at temperature T. Moreover, we perturb the particle with a periodically varying force, described in the Langevin equation

$$m\ddot{x} = m\gamma\dot{x} - V'(x) + mA_0\cos(\Omega t + \phi) + \sqrt{2m\gamma kT}\xi(t). \tag{2.30}$$

Here $\xi(t)$ denotes white Gaussian noise with zero mean and an autocorrelation function $\langle\xi(t)\xi(s)\rangle = \delta(t-s)$. The external forcing term is characterized by an amplitude A_0, an angular frequency Ω and an arbitrary but fixed initial phase ϕ. The statistically equivalent description for the corresponding probability density $p(x, v = \dot{x}, t; \phi)$ is governed by

the two-dimensional Fokker-Planck equation

$$\frac{\partial}{\partial t}p(x,v,t;\phi) = \left\{-\frac{\partial}{\partial x}v + \frac{\partial}{\partial v}[\gamma v + f(x) - A_0\cos(\Omega t+\phi)] + \gamma D\frac{\partial^2}{\partial v^2}\right\}p(x,v,t;\phi) \tag{2.31}$$

where $f(x) = -V'(x)/m$ and the diffusion coefficient is given by $D = k_BT/m$. For large values of the friction coefficient γ the inertial term given by $m\ddot{x}$ can be dropped, thereby giving us the periodically modulated Langevin equation:

$$\gamma\dot{x} = f(x) + A_0\cos(\Omega t+\phi) + \sqrt{2\gamma D}\xi(t). \tag{2.32}$$

Substituting $f(x) = (ax - bx^3)/m$, where $a > 0, b > 0$, the bistable quartic double-well potential $V(x) = -ax^2/2 + bx^4/4$. Making use of the rescaled variables:

$$\begin{aligned}\overline{x} &= x/x_m, \overline{t} = at/\gamma, \overline{A_0} = A_0/ax_m,\\ \overline{D} &= D/ax_m^2, \overline{\Omega} = \gamma\Omega/a,\end{aligned} \tag{2.33}$$

where $x = \pm x_m$ where $x_m = \sqrt{a/b}$ denote the locations of the minima of $V(x)$, the relevant Fokker-Planck equation then assumes a dimensionless form. For convenience, dropping all overbars, the Smoluchowski limit of Eq.(2.31) can be recovered:

$$\frac{\partial}{\partial t}p(x,t;\phi) = \mathcal{L}(t)p(x,t;\phi) \equiv [\mathcal{L}_0 + \mathcal{L}_{ext}]p(x,t;\phi). \tag{2.34}$$

The Fokker-Planck operator

$$\mathcal{L}_0 = -\frac{\partial}{\partial x}(x - x^3) + D\frac{\partial^2}{\partial x^2} \tag{2.35}$$

describes the unperturbed dynamics in the rescaled bistable potential

$$V(x) = -\frac{1}{2}x^2 + \frac{1}{4}x^4, \tag{2.36}$$

with barrier height $\Delta V = \frac{1}{4}$. The operator

$$\mathcal{L}_{ext} = -A_0\cos(\Omega t+\phi)\frac{\partial}{\partial x} \tag{2.37}$$

describes the effect of the external periodic forcing with amplitude A_0.

2.2.2 Floquet approach

The inertial, as well as the overdamped Brownian dynamics in Eqs.(2.31) and (2.34) describe a nonstationary Markovian process where the symmetry under time-translation is retained in a discrete manner only. The Fokker-Planck operators in Eqs.(2.31) and (2.34) are invariant under the discrete time translations $t \to t + T_\Omega$, where $T_\Omega = 2\pi/\Omega$ denotes the modulation period. Therefore, the Floquet theorem applies to the corresponding partial differential equation [43]. For a general periodic Fokker-Planck operator $\mathcal{L}(t) = \mathcal{L}(t + T_\Omega)$, defined on a multi-dimensional space of state vectors $X(t) = (x(t), v(t), \ldots)$ one finds that the relevant Floquet solutions are of the form:

$$p(X, t; \phi) = \exp(-\mu t) p_\mu(X, t; \phi) \tag{2.38}$$

with Floquet eigen-value μ and periodic Floquet modes p_μ,

$$p_\mu(X, t; \phi) = p_\mu(X, t + T_\Omega; \phi). \tag{2.39}$$

The periodic Floquet modes $\{p_\mu\}$ are the eigen-functions of the Floquet operator

$$\left[\mathcal{L}(t) - \frac{\partial}{\partial t}\right] p_\mu(X, t; \phi) = -\mu p_\mu(X, t; \phi). \tag{2.40}$$

The Floquet modes $\{p_\mu\}$ described in Eq.(2.40) are elements of the product space $L_1(X) \oplus \mathcal{T}_\Omega$, where $\mathcal{T}_\Omega$ denotes the space of functions that are periodic in time and $L_1(X)$ denotes the linear space of functions that are integrable over the state space X. As a result of the identity

$$\begin{aligned} \exp(-\mu t) p_\mu(X, t; \phi) &= \exp(-(\mu + \imath k\Omega)t) p_\mu(X, t; \phi) \exp(\imath k\Omega t) \\ &\equiv \exp(-\hat{\mu} t) \hat{p}_\mu(X, t; \phi), \end{aligned} \tag{2.41}$$

where $\hat{\mu} = \mu + \imath k\Omega$ and $k = 0, \pm 1, \pm 2, \ldots$, and $\hat{p}_\mu(X, t; \phi) = p_\mu(X, t; \phi) \exp(\imath k\Omega t) = \hat{p}_\mu(X, t + T_\Omega; \phi)$, we observe that the Floquet eigen-values can be defined only $mod(i\Omega)$. Likewise, we introduce the set of Floquet modes of the adjoint operator $\mathcal{L}^\dagger(t)$ (adjoint in $L_1(X)$), that is

$$\left[\mathcal{L}^\dagger(t) - \frac{\partial}{\partial t}\right] p^\dagger_\mu(X, t; \phi) = -\mu p^\dagger_\mu(X, t; \phi). \tag{2.42}$$

Here the sets $\{p_\mu\}$ and $\{p^\dagger_\mu\}$ are bi-orthogonal, obeying the equal-time normalization condition

$$\frac{1}{T_\Omega}\int_0^{T_\Omega} dt \int dX p_{\mu_n}(X,t;\phi)p^\dagger_{\mu_m}(X,t;\phi) = \delta_{n,m}. \tag{2.43}$$

A proof for biorthogonality used above is now given. From Eq.(2.42) it follows that

$$\begin{aligned}\left\{\left[\mathcal{L}^\dagger(t) - \frac{\partial}{\partial t}\right] p^\dagger_{\mu_m}\right\} p_{\mu_n} &= -\mu_m p^\dagger_{\mu_m} p_{\mu_n} \quad \text{and} \\ \left\{\left[\mathcal{L}^\dagger(t) - \frac{\partial}{\partial t}\right] p^\dagger_{\mu_n}\right\} p_{\mu_m} &= -\mu_n p^\dagger_{\mu_n} p_{\mu_m}.\end{aligned} \tag{2.44}$$

For brevity call the Floquet operator $\mathcal{T}$ and the adjoint operator $\mathcal{T}^\dagger$. From the adjoint property we know

$$\langle \mathcal{T}u, v\rangle = \langle u, \mathcal{T}^\dagger v\rangle. \tag{2.45}$$

Now, from Eqs.(2.44) it follows that

$$\langle p_{\mu_n}, \mathcal{T}^\dagger p^\dagger_{\mu_n}\rangle = -\mu_m \langle p_{\mu_n}, p^\dagger_{\mu_n}\rangle. \tag{2.46}$$

From Eq.(2.45) it also follows that

$$\langle p_{\mu_n}, T^\dagger p^\dagger_{\mu_n}\rangle = \langle T p_{\mu_n}, p^\dagger_{\mu_n}\rangle = -\mu_n \langle p_{\mu_n}, p^\dagger_{\mu_n}\rangle. \tag{2.47}$$

Taking the difference of the previous two equations we get

$$(\mu_n - \mu_m)\langle p_{\mu_n}, p^\dagger_{\mu_m}\rangle = 0. \tag{2.48}$$

For n, m distinct, μ_n, μ_m are also distinct. So it follows that $\langle p_{\mu_n}, p^\dagger_{\mu_m}\rangle = 0$. For n, m equal, it follows that the eigen-function must be chosen such that they satisfy the biorthogonality condition given by $\langle p_{\mu_n}, p^\dagger_{\mu_n}\rangle = 1$.

Eqs.(2.40) and (2.42) allow for a spectral representation of the time-inhomogeneous conditional probability $P(X,t|Y,s)$. With $t > s$ we find

$$P(X,t|Y,s) = \sum_{n=0}^{\infty} p_{\mu_n}(X,t;\phi)p^\dagger_{\mu_n}(Y,s;\phi)\exp[-\mu_n(t-s)] = P(X,t+T_\Omega|Y,s+\Omega) \tag{2.49}$$

If the physical system of interest occupies all microstates corresponding to the same

energy with equal probability, it is said to be ergodic, or alternatively is said to satisfy the ergodic hypothesis [40]. In some physical systems of interest, the time-scales over which the system can explore the entirety of its phase space is sufficiently large so that the ergodic hypothesis need not be valid. Examples of such system include ferromagnetic systems below the Curie temperature, systems which exhibit spontaneous symmetry breaking and spin glasses [75]. Such systems will not be considered in this thesis. A more mathematically rigorous definition of the term ergodic used in dynamical systems must necessarily be phrased using measure theory [40]. For the purposes of this thesis, such a definition will be avoided. If the ergodic hypothesis is said to be valid, the governing probability distribution is also said to be ergodic. With real parts $Re[\mu_n] > 0$ for $n > 0$, the limit $s \to -\infty$ of Eq.(2.49) yields the ergodic, time-periodic probability

$$p_{as}(X,t;\phi) = p_{\mu=0}(X,t;\phi). \tag{2.50}$$

The asymptotic probability $p_{as}(X,t;\phi)$ can be expanded into a Fourier series, i.e.

$$p_{as}(X,t;\phi) = \sum_{m=-\infty}^{\infty} a_m(X)\exp[\imath m(\Omega t+\phi)]. \tag{2.51}$$

With the arbitrary initial phase being distributed uniformly, i.e. with the probability density for ϕ given by $w(\phi) = 1/(2\pi)$, the time average of Eq.(2.52) [81]. Hence

$$\begin{aligned} \overline{p}_{as}(X) &= \frac{1}{2\pi}\int_0^{2\pi} p_{as}(X,t;\phi)d\phi, \\ &= \frac{1}{T_\Omega}\int_0^{T_\Omega} p_{\mu=0}(X,t;\phi)dt = a_0(X). \end{aligned} \tag{2.52}$$

Given the spectral representation of Eq.(2.49) for the conditional probability, the mean values and correlation functions can now be evaluated. Of particular importance in stochastic resonance is the asymptotic expectation value

$$\langle X(t)\rangle_{as} = \langle X(t)|Y_0, t_0 \to -\infty\rangle, \tag{2.53}$$

where $\langle X(t)|Y_0,t_0\rangle$ is the conditional average $\langle X(t)|Y_0,t_0\rangle = \int dX X P(X,t|Y_0,t_0)$ is the conditional average with $P(X,t|Y_0,t_0 \to -\infty)$ approaching the asymptotic time-periodic probability, the relevant asymptotic average $\langle X(t)\rangle)_{as}$ is also periodic in time and thus

admits the Fourier series representation

$$\langle X(t)\rangle_{as} = \sum_{n=-\infty}^{\infty} M_n \exp[\imath n(\Omega t + \phi)]. \tag{2.54}$$

The complex valued amplitudes $M_n \equiv M_n(\Omega, \phi)$ depend nonlinearly on both the forcing frequency Ω and the modulation amplitude A_0. Within a linear response approximation (described later in the following section) only the contributions from $|n| = 0, 1$ are non-zero. Nonlinear contributions to the stochastic resonance variable, both for the first and higher order harmonics have been implemented numerically in [81] and [85] by implementing the Floquet approach for the Fokker-Planck equation of the overdamped driven quartic double-well potential. We must now introduce a new quantity called the spectral amplification, denoted by η, defined as follows

$$\eta = [\overline{x}(D)/A_0]^2, \tag{2.55}$$

where $\overline{x}(D)$ is given by Eq.(2.11), can then be written as

$$\eta = \left(\frac{2|M_1|}{A_0}\right)^2. \tag{2.56}$$

It is empirically observed [46] that for a fixed modulation amplitude A_0 the stochastic resonance behaviour of the spectral power amplification η *decreases* upon *increasing* the forcing frequency Ω. It then follows from Eq.(2.56) that the behaviour of η versus increasing Ω at fixed noise strength D is generally that of a monotonically decreasing function. The dependence of the modulation amplitude A_0 at a fixed forcing frequency Ω is depicted in [46]. The maximum of the spectral amplification *decreases* with *increasing* amplitude A_0. Hence nonlinear response effects tend to diminish the stochastic resonance phenomenon. For a small, fixed noise strength D, when the driving frequency Ω exceeds the Kramers rate r_K, the spectral amplification η exhibits a maximum as a function of the forcing amplitude. The analog of the correlation function of a stationary process is the asymptotic time-inhomogeneous correlation

$$\langle X(t)X(t')\rangle_{as} = K(t, t'; \phi) = \int\int XYP(X, t|Y, t')p_{as}(Y, t'; \phi) \tag{2.57}$$

where $t = t' + \tau$ with $\tau > 0$ and $t' \to \infty$. An additional averaging procedure (indicated by double brackets) over a uniformly distributed phase ϕ for $K(t, t'; \phi)$ (or equivalently, a time average over one modulation cycle) yields a time-inhomogeneous, stationary cor-

relation function given by

$$\overline{K}(\tau) = \langle\langle X(t)X(t')\rangle\rangle_{as} = \frac{1}{2\pi}\int K(t,t';\phi)d\phi. \tag{2.58}$$

In terms of the Fourier amplitudes $\{M_n\}$ of Eq.(2.59) the long-time limit of $\overline{K}(\tau)$ assumes the oscillatory expression

$$\begin{aligned}\lim_{\tau\to\infty} K(\tau) &\equiv \overline{K}_{as}(\tau) = \langle\langle X(t+\tau)\rangle_{as}\langle X(t)\rangle_{as}\rangle \\ &= \sum_{n=-\infty}^{\infty} |M_n|^2 \exp(in\Omega\tau) = 2\sum_{n=1}^{\infty} |M_n|^2 \cos n\Omega\tau. \end{aligned}\tag{2.59}$$

The last expression was obtained using $M_0 = 0$ for a reflection-symmetric potential. This asymptotic result is independent of the initial phase ϕ. This is in contrast with $\langle X(t)\rangle_{as}$ as will be seen in the following section.

This oscillatory behaviour in turn yields sharp spikes at multiples of the driving frequency Ω for the power spectral density of $\overline{K}(\tau)$. Depending on the symmetry properties of the Floquet operator it is found that some of the amplitudes assume vanishing weights [81]. In particular, for a symmetric double well, all even-numbered amplitudes M_{2n} assume zero weight. Likewise a multiplicative driving $xA_0\cos\Omega t$ in Eq.(2.31) in a symmetric double well yields identically vanishing weights for all integer values of n. It should be noted that the results for the corresponding conditional probability in Eq.(2.49) for zero forcing $A_0 = 0$ reduces to the time-inhomogeneous conditional probability density. That is with $\tau = (t-s) > 0$

$$P(X,\tau|Y,0) = \sum_{n=0}^{\infty} \psi_n(X)\phi_n(Y)\exp(-\lambda_n\tau). \tag{2.60}$$

Here, for $A_0 \to 0$ the set $\{\mu_n\}$ (with $k = 0$) reduces to the set of eigen-values $\{\lambda_n\}$ of $\mathcal{L}_0$, and the sets $p_{\mu_n}(X,t)$ and $p^{\dagger}_{\mu_n}(Y,s)$ reduce to $\psi_n(X)$ and $\phi_n(Y)$, which are the eigen-functions of the operators $\mathcal{L}_0$ and $\mathcal{L}_0^{\dagger}$ respectively.

2.2.3 Linear response theory

The prominent role of stochastic resonance is to boost weak signals embedded in a noisy environment. Thus the linear response concept, or more generally the concept of perturbation theory for spectral quantities like the Floquet modes and the Floquet eigen-values are adequate for studying the basic physics which characterize stochastic resonance. Both concepts have been repeatedly invoked by several research groups [44,

122, 34, 35, 85, 86, 36]. Here we shall also focus on the linear-response concept, which also emerges as a specific application of perturbation theory. In doing so, we shall rely on the linear response theory pioneered by Kubo in [95, 96] and later extended to a wider class of stochastic processes that also admit nonthermal, stationary nonequilibrium states [65]. This extension is of particular relevance because many prominent applications of stochastic resonance in optical, chemical and biological systems operate far from thermal equilibrium. Without losing generality, we confine further analysis to a one-dimensional Markovian observable $x(t)$ subject to an external weak periodic perturbation. Following [65], the long-time limit of the response $\langle x(t)\rangle_{as}$ due to the perturbation $A(t) = A_0 \cos \Omega t$ (with $\phi = 0$), assumes to first-order the form

$$\langle x(t)\rangle_{as} = \langle x(t)\rangle_0 + \int_{-\infty}^{t} ds \chi(t-s) A_0 \cos \Omega s, \tag{2.61}$$

where $\langle x(t)\rangle_0$ denotes the stationary average of the unperturbed process. The memory kernel $\chi(t)$ of Eq.(2.61) is termed, hereafter, the response function. For an external perturbation operator of the general form

$$\mathcal{L}_{ext}(t) \equiv A_0 \cos \Omega s \Gamma_{ext}, \tag{2.62}$$

$\chi(t)$ is expressed as

$$\chi(t) = H(t) \int\int\int \; dx \; dy \; dz P_0(x, t|y, 0) x \Gamma_{ext}(y, z) p_0(z). \tag{2.63}$$

$H(t)$ denotes the Heaviside step function expressing causality of response, $p_0(z)$ is the stationary probability density of the corresponding unperturbed, generally nonthermal equilibrium process. $P_0(x, t|y, 0)$ denotes the conditional probability density and $\Gamma_{ext}(x, y)$ denotes the kernel of the operator Γ_{ext} that describes the perturbation in the master operator (either an integral or differential operator, such as in the Fokker-Planck case where $\Gamma_{ext}(x, y) = \delta'(x - y)$ for Eq.(2.37). An appealing form of the response function can be obtained by introducing the fluctuation-like quantity, denoted by $\xi(x(t))$, defined by

$$\int dy \Gamma_{ext}(x, y) p_0(y) = \int dz \mathcal{L}_0(x, z) \Gamma_{ext}(x, z) \xi(z) p_0(z). \tag{2.64}$$

where $\mathcal{L}_0(x, z)$ is the kernel of the unperturbed Fokker-Planck operator. Note that $\xi(x(t))$ satisfies $\langle \xi(x(t))\rangle_0 = 0$. The response function in Eq.(2.64) can then be expressed through

the fluctuation theorem to be

$$\chi(t) = -H(t)\frac{d}{dt}\langle x(t)\xi(x(0))\rangle. \tag{2.65}$$

For $\delta x(t) = x(t) - \langle x(t)\rangle_0$ this can be recast as

$$\chi(t) = -H(t)\frac{d}{dt}\langle \delta x(t)\xi(x(0))\rangle. \tag{2.66}$$

This result is intriguing: the linear-response function can be obtained as the time-derivative of a stationary, generally nonthermal correlation function between the two unperturbed fluctuations $\delta x(t)$ and $\xi(x(t))$. From the spectral representation of the time-homogeneous conditional probability Eq.(2.60), it follows immediately that (on assuming that the eigen-value $\lambda_0 = 0$ is not degenerate)

$$\chi(t) = H(t)\sum_{n=1}^{\infty} g_n\lambda_n \exp(-\lambda_n t). \tag{2.67}$$

The co-efficients $\{g_n\}$ are given by

$$g_n = \langle \delta x(t)\psi_n(x)\rangle_0\langle \xi(y)\phi_n(Y)\rangle_0. \tag{2.68}$$

The corresponding Fourier transform are denoted by

$$\chi(\omega) = \int_0^{\infty} \exp(-\imath\omega\tau)\chi(\tau)d\tau. \tag{2.69}$$

The real and imaginary parts of $\chi(\omega)$ can be separated as follows $\chi(\omega) = \chi'(\omega) + \imath\chi''(\omega)$. Generally, the eigen-values of the real-valued operator $\mathcal{L}_0$ are complex-valued and occur in conjugate pairs, λ_n and λ_n^* with the corresponding eigen-functions $\psi_n(x)$ and $\phi_n(x)$ introduced above. Hence, the overall real expression for $\chi(t)$ in Eq.(2.67). Substituting Eq.(2.67) into Eq.(2.61) we find the linear-response approximation

$$\langle \delta x(t)\rangle = \langle x(t)\rangle_{as} - \langle x(t)\rangle_0 = \frac{A_0}{2}\sum_{n=1}^{\infty}\lambda_n g_n\left[\frac{e^{\imath\Omega t}}{\lambda_n + \imath\Omega} + \frac{e^{-\imath\Omega t}}{\lambda_n - \imath\Omega}\right]. \tag{2.70}$$

On Fourier transforming Eq.(2.67) we get the spectral representation of $\chi(t)$

$$\chi(\omega) = \chi'(\omega) + \imath\chi''(\omega) = \sum_{n=1}^{\infty}\frac{\lambda_n g_n}{\lambda_n + \imath\omega}. \tag{2.71}$$

Therefore, Eq.(2.70) can be recast into the form

$$\langle \delta x(t) \rangle = 2|M_1| \cos(\Omega t - \overline{\phi}) \tag{2.72}$$

where the spectral amplitude $|M_1|$ and the retarded phase shift $\overline{\phi}$ are given by

$$\begin{aligned} |M_1| &= \frac{A_0}{2}|\chi(\Omega)|, \\ \overline{\phi} &= \arctan\left\{\frac{\chi''(\Omega)}{\chi'(\Omega)}\right\}. \end{aligned} \tag{2.73}$$

The above results are valid for a general nonthermal stationary system. The fluctuation $\xi(x(t))$ can be evaluated in a straight-forward manner for all one-dimensional systems modelled by the Fokker-Planck equations. Examples include stochastic resonance for optical bistability or that for coloured noise-driven bistable systems [46]. In the case of the quartic double-well potential, where the unmodulated system admits thermal equilibrium, the perturbation operator $\mathcal{L}_{ext}$ is of the gradient type: from Eq.(2.62), $\mathcal{L}_{ext}(t) = A_0 \cos\Omega t[-\partial/\partial x]$. This in turn implies that the response function obeys the well-known fluctuation-dissipation theorem known from classical equilibrium statistical mechanics [95, 96] i.e.

$$\chi(t) = -[H(t)/D]\frac{d}{dt}\langle \delta x(t)\ \delta x(0)\rangle_0, \tag{2.74}$$

where the corresponding fluctuation ξ reads $\xi(x(0)) = \delta x(0)/D$. Note that this result holds irrespective of the detailed form of the equilibrium dynamics.

2.3 Intrawell versus interwell motion

Given the spectral representation in Eq.(2.71) of the response function $\chi(t)$, we can express the two stochastic resonance quantifiers, namely the spectral amplification η of Eq.(2.56) and the signal-to-noise-ratio in terms of the spectral amplitude $|M_1|$. From Eq.(2.73) we find the spectral amplification within linear response to be

$$\eta = (2|M_1|/A_0)^2 = |\chi(\Omega)|^2. \tag{2.75}$$

In view of the unperturbed power spectral density $S_N^0(\Omega)$ of the fluctuations $\delta x(t)$, i.e.

$$S_N^0(\omega) = \int_{-\infty}^{\infty} e^{-\imath\omega\tau}\langle \delta x(t)\ \delta x(0)\rangle_0 d\tau, \tag{2.76}$$

the linear response results for the SNR reads

$$SNR = 4\pi|M_1|^2/S_N^0(\Omega) = \pi A_0^2|\chi(\Omega)|^2/S_N^0(\Omega). \tag{2.77}$$

Both stochastic resonance variables possess a spectral representation via those of $\chi(\omega)$ and $S_N^0(\omega)$. In the following, we shall implicitly assume that the noise strength D is weak. This implies that for a general bistable dynamics there exists a clear-cut separation of time scales. They are (i) the escape time scale to leave the corresponding wells i.e. the exponentially large time scale for interwell hopping, and (ii) the time scale that characterizes local relaxation within a stable state. The eigen-value λ_1 that characterizes intrawell dynamics is always real-valued and of the Kramers type [64] i.e.

$$\lambda_1 = 2r_K = r_+ + r_- \equiv \lambda, \tag{2.78}$$

where $r_\pm$ are the forward and backward transition rates respectively, which depend through the Arrhenius factor on the activation energies $\Delta\Phi_0^\pm$, where $\Phi_0(x)$ is the generalized (non-thermal equilibrium) potential associated with the unperturbed stationary probability density

$$p_0(x) = Z^{-1}(x)\exp(-\Phi_0(x)/D). \tag{2.79}$$

The relevant intrawell relaxation rates in the two wells located at $x = x_{1,2}$, where by convention we take $x_1 = -\sqrt{a/b}$ and $x_2 = \sqrt{a/b}$. The rates are estimated as the real parts of the two smallest eigenvalues ([46] and references therein) that describe the equilibration of the probability density in the vicinity of the two stable states $x_m, m = 1, 2$ respectively. For small noise intensities, these eigen-values can be approximated as

$$\begin{aligned} \lambda_2 &= \Phi_0''(\xi = x_1), \\ \lambda_3 &= \Phi_0''(\xi = x_2). \end{aligned} \tag{2.80}$$

Note that, here, the indices λ_2, λ_3 have been chosen for later convenience and do not necessarily coincide with the index ordering of the Fokker-Planck spectrum $\{\lambda_n\}$. Given these three dominant time scales, the response at weak noise is cast as the sum of the first three terms in Eq.(2.70). Truncating the summation after the third term in Eq.(2.70), for a driving phase $\phi = 0$ we then get the weak noise approximations

$$\langle \delta x(t) \rangle = \frac{A_0}{2} \sum_{n=1,2,3} \lambda_n g_n \left[\frac{e^{\imath\Omega t}}{\lambda_n + \imath\Omega} + \frac{e^{-\imath\Omega t}}{\lambda_n - \imath\Omega} \right], \tag{2.81}$$

yielding corresponding estimates for $\chi(\omega)$ and the stochastic resonance quantifiers η and the SNR. The weights g_m can be evaluated from the corresponding approximate eigenfunctions [65] or from the three-term potential ansatz for the response function [84]. For the overdamped, symmetric, quartic double-well potential given in Eq.(2.36), the spectral amplification given by Eq.(2.75) has been evaluated [85] and [86] to give

$$\eta = D^{-2}\left[\frac{4g_1^2 r_K^2}{4r_K^2+\Omega^2} + \frac{g^2\alpha^2}{\alpha^2+\Omega^2} + \frac{4g_1 g\alpha r_K(2\alpha r_K+\Omega^2)}{(4r_K^2+\Omega^2)(\alpha^2+\Omega^2)}\right], \tag{2.82}$$

where $\lambda_2 = \lambda_3 \equiv \alpha$, with $\alpha = 2$, and $g_2 = g_3 \equiv g/2$. The relevant weights g_n for $D \to 0$ read

$$\begin{aligned} g_1 &\approx 1-(1-\alpha^{-1})D + O(D^2), \\ g &= D/\alpha + O(D^2), \end{aligned} \tag{2.83}$$

and r_K is the steepest-descent approximation for the Kramers rate

$$r_K = (\sqrt{2}\pi)^{-1}\exp[-1/(4D)]. \tag{2.84}$$

On neglecting the intrawell motion, the leading-order contribution in Eq.(2.82) gives us

$$\eta \approx \frac{1}{D^2}\left[1+\frac{\pi^2}{2}\Omega^2\exp\left(\frac{1}{2D}\right)\right]. \tag{2.85}$$

This approximation exhibits the typical bell-shaped stochastic resonance behaviour as a function of increasing noise intensity. Likewise, we can evaluate the SNR for the potential under study. In the weak noise limit we have

$$S_N^0(\Omega) \approx \frac{4r_K}{4r_K^2+\Omega^2} + \frac{2g\lambda^2}{\lambda^2+\Omega^2}, \tag{2.86}$$

whence yielding the linear-response result for the SNR

$$SNR = \frac{\pi A_0^2}{2D^2}\frac{4g_1^2 r_K^2(\alpha^2+\Omega^2) + g^2\alpha^2(4r_K^2-\Omega^2) + 4\alpha g_1 r_K(2\alpha r_K+\Omega^2)}{2g_1 r_K(\alpha^2+\Omega^2) + g\alpha(4r_K^2+\Omega^2)}. \tag{2.87}$$

The plot of this result shows a bell-shaped behaviour as a function of D when Ω is not too large. Also, note that the SNR diverges as D^{-1} in the limit as $D \to 0$. This is due to intra-well contributions in Eq.(2.87). This feature is in agreement with simulations [122]. On neglecting intrawell contributions, by setting $g_2 = g_3 = 0$ we get, to leading

order, the following result:

$$SNR = \frac{\pi A_0^2}{D^2} r_K = \frac{\pi A_0^2}{\sqrt{2} D^2} \exp[-1/(4D)]. \tag{2.88}$$

Within this interwell approximation the SNR, contrary to the spectral amplification η in Eq.(2.82), is no longer dependent on the angular modulation frequency Ω. This effective two-state approximation also exhibits a bell-shaped behaviour, typical for stochastic resonance. In contrast to Eq.(2.87), the SNR vanishes for $D \to 0$. It is also observed that the leading order contribution to SNR in Eq.(2.88) is proportional to r_K, while η in Eq.(2.82) is proportional to r_K^2.

2.4 Linear time-invariant systems

Classical signal processing algorithms have been implemented with linear, time-invariant operators. The output of a linear system denoted by $y(t)$ can be characterized by "integration" against a kernel $h(t, \tau)$ located at t, as follows:

$$\begin{aligned} y(t) &= Lx(t), \\ &= \int x(\tau) h(t, \tau) d\tau. \end{aligned} \tag{2.89}$$

For numerical stability, the operator L and kernel $h(.,.)$ must have a "weak" form of continuity i.e. if f is perturbed slightly, Lf is also modified by a small amount. This weak notion of continuity can be formalized by the theory of distributions [3, 151]. The time invariance of an operator L implies that if the input $x(t)$ is delayed by τ, $x_\tau(t) = f(t-\tau)$, the output is similarly delayed by τ:

$$y(t) = Lx(t) \to y(t - \tau) = Lx(t - \tau) \tag{2.90}$$

Hence it follows that for a causal system characterized by linearity and time-invariance [112]

$$y(t) = \int_{-\infty}^{t} x(\tau) h(t - \tau) d\tau. \tag{2.91}$$

A linear time-invariant system is thus equivalent to a convolution with the impulse response h. The continuity of $x(t)$ is not necessary and the formula remains valid for any signal x such that the convolution integral in Eq.(2.91) converges. Linear time-invariant systems are characterized by their response, denoted by $h(t)$, to the Dirac impulse $\delta(t)$:

$h(t) = \delta(t)$. By the property of time-invariance it follows: $L\delta_\tau(t) = h(t-\tau)$.

The stability property of systems demands $Lx(t)$ is bounded if $x(t)$ is bounded (boundedness being defined by the L^1 norm). Since

$$\begin{aligned} |Lx(t)| &\leq \int_{-\infty}^{\infty} |x(\tau)h(t,\tau)|d\tau, \\ &\leq \sup_{\tau\in R}|x(\tau)| \int_{-\infty}^{\infty} |h(t,\tau)|d\tau, \end{aligned} \tag{2.92}$$

it is sufficient that $\int_{-\infty}^{\infty} |h(t,\tau)|d\tau < \infty$. We can say that h is stable if it is integrable. In this thesis we will only consider systems in which the last condition for bounded norm is met.

In this section we develop an general framework for the description of stochastic resonance in the manner of Chapeau-Blondeau [21]. This development is generic, and accords the advantage that it is applicable to any nonlinear system, static or dynamic. Though elements of this framework in the narrower context of specific nonlinear systems exist, this framework does not refer to any particular system. In a latter section, it is shown how an explicit realization of this general framework can be achieved using static nonlinear systems. To this end, let us consider a time-invariant nonlinear system, static or dynamic with an output denoted by $y(t)$. It is subject to the input of a periodic deterministic signal $x(t)$ with period T_s and realizations of stationary random noise denoted by $\eta(t)$. $y(t)$ is considered the steady state response of the system, when the above inputs are applied at $t \to \infty$. Due to the influence of the random input $\eta(t)$ and the deterministic input $x(t)$ the output $y(t)$, in general, will be a nonstationary random signal. However, since $x(t)$ is periodic $y(t)$ will be a cyclostationary signal with period T_s. The random output signal $y(t)$ can be expressed as the sum of its nonstationary mean $E[y(t)]$ plus the statistical fluctuations $\widetilde{y}(t)$ around the mean:

$$y(t) = E[y(t)] + \widetilde{y}(t). \tag{2.93}$$

Because of the cyclo-stationarity of $y(t)$, the nonstationary mean $E[y(t)]$ is a deterministic periodic function of t with period T_s, with well-defined Fourier coefficients given by:

$$\overline{Y_n} = \frac{1}{T_s}\int_0^{T_s} E[y(t)] \exp\left(-i2\pi nt/T_s\right) dt. \tag{2.94}$$

The statistical auto-correlation function for the output signal $y(t)$, with a fixed t and τ

is given by the expectation

$$E[y(t)y(t+\tau)] = E[\widetilde{y}(t)\widetilde{y}(t+\tau)] + E[y(t)]E[y(t+\tau)]. \tag{2.95}$$

The expectation computed above in Eq.(2.95) is a deterministic function of the variables t and τ, and is periodic in t with a period T_s. A stationary i.e. independent of t auto-correlation function $R_{yy}(\tau)$ for $y(t)$ can be constructed through a proper time averaging of $E[y(t)y(t+\tau)]$ over the semi-closed interval $[0, T_s)$ as follows:

$$R_{yy}(\tau) = \frac{1}{T_s}\int_0^{T_s} E[y(t)y(t+\tau)]dt. \tag{2.96}$$

From Eq.(2.95) it also follows

$$R_{yy}(\tau) = C_{yy}(\tau) + \frac{1}{T_s}\int_0^{T_s} E[y(t)]E[y(t+\tau)]dt. \tag{2.97}$$

where

$$C_{yy}(\tau) = \frac{1}{T_s}\int_0^{T_s} E[\widetilde{y}(t)\widetilde{y}(t+\tau)]\ dt. \tag{2.98}$$

The power spectral density of $P_{yy}(\nu)$ of $y(t)$ is defined to be the Fourier transform of the auto-correlation function $R_{yy}(\tau)$ as follows:

$$P_{yy}(\nu) = \mathcal{F}[R_{yy}(\tau)] = \int_{-\infty}^{\infty} R_{yy}\exp\left(-i2\pi\nu t\right)dt, \tag{2.99}$$

which on combining with Eq.(2.97) gives us:

$$P_{yy}(\nu) = \mathcal{F}[C_{yy}(\tau)] + \sum_{n=-\infty}^{\infty} \overline{Y_n Y_n}^{*}\delta(\nu - nT_s). \tag{2.100}$$

The power spectral density of Eq.(2.100) has the form typical of that for stochastic resonant systems: spectral lines of magnitude $|\overline{Y_n}|^2$ at integer multiples of the coherent frequency $1/T_s$, superposed on a broadband noise background given by $\mathcal{F}[C_{yy}(\tau)]$. The autocovariance $E[\widetilde{y}(t)\widetilde{y}(t+\tau)]$ and its time average $C_{yy}(\tau)$ is expected to go to zero as $|\tau| \to \infty$. $var[y(t)] = E[\widetilde{y}(t)\widetilde{y}(t)]$ denotes the nonstationary variance of $y(t)$. The stationary variance of $y(t)$, denoted by $\overline{var[y(t)]} = C_{yy}(0)$, can be found by time-averaging the above over a period T_s according to Eq.(2.98). The deterministic function $C_{yy}(\tau)$

can thus be written as

$$C_{yy}(\tau) = \overline{var[y(t)]}h(\tau), \tag{2.101}$$

where $h(\tau)$ is a deterministic even function describing the normalized shape of the stationary autocovariance which satisfies the conditions $h(0) = 1$ and $h(\tau) \to 0$ as $|\tau| \to \infty$ and has a Fourier transform denoted by $H(\nu) = \mathcal{F}[h(\tau)]$. The power spectral density of Eq.(2.100) can be expressed as

$$P_{yy}(\nu) = \overline{var[y(t)]}H(\nu) + \sum_{n=-\infty}^{\infty} \overline{Y_n Y_n}^* \delta(\nu - nT_s). \tag{2.102}$$

A classical definition of the signal-to-noise ratio (SNR) at the frequency n/T_s can be defined as the ratio of the power contained in the spectral line alone to the power contained in the noise background in a small frequency bin in which n/T_s is contained. The width of the bin ΔB is decided by the sampling frequency of the relevant system. The corresponding expression of the SNR, denoted by $\mathcal{R}$, is then given by

$$\mathcal{R}\left(\frac{n}{T_s}\right) = \frac{|\overline{Y_n}|^2}{\overline{var[y(t)]}H(n/T_s)\Delta B} \tag{2.103}$$

The above formula provides as exact expression for the output SNR which can be evaluated with the explicit knowledge of the nonstationary output mean $E[y(t)]$ and the stationary output autocovariance function $C_{yy}(\tau)$.

A further property of a stochastic resonant system subject to harmonic or quasi-harmonic signals, lies in the possibility of evaluating the phase shift between the output and the coherent periodic input. This is achieved by computing the input-output cross-correlation function. In order to do so, a few preliminary steps are required. For fixed t and τ, since the signal $s(t)$ is deterministic, it follows

$$E[s(t)y(t+\tau)] = s(t)E[y(t+\tau)]. \tag{2.104}$$

As before, in Eq.(2.95), the quantity above $E[s(t)y(t+\tau)]$ is a deterministic function of the variables t and τ, and is periodic in t with a period T_s. Likewise, the stationary cross-correlation function $R_{sy}(\tau)$ for $y(t)$ can be constructed through a proper time averaging of $E[s(t)y(t+\tau)]$ over the semi-closed interval $[0, T_s)$ as follows:

$$R_{sy}(\tau) = \frac{1}{T_s}\int_0^{T_s} s(t)E[y(t+\tau)]dt. \tag{2.105}$$

This can be interpreted as the cross-correlation function of $s(t)$ with the nonstationary output mean $E[y(t)]$. Analogously, $R_{sy}(\tau)$ in Eq.(2.105) is periodic with period T_s. Its frequency content only has components at integer multiples of $1/T_s$. Fourier transforming $R_{sy}(\tau)$ in Eq.(2.105), we obtain the cross-power spectral density, given by

$$P_{sy}(\nu) = \mathcal{F}[R_{sy}(\tau)] = \sum_{n=-\infty}^{\infty} S_n \overline{Y_n}^* \delta(\nu - nT_s), \tag{2.106}$$

where S_n represents the n^{th} Fourier coefficient of $s(t)$, defined according to Eq.(2.94). The phase shift ϕ between the mean output $E[y(t)]$ and the coherent input $s(t)$ as considered in [37], can be evaluated for a component with frequency n/T_s from the argument of the complex number $P_{sy}(n/T_s)$ as follows

$$\phi\left(\frac{n}{T_s}\right) = \arg(S_n \overline{Y_n}^*). \tag{2.107}$$

To summarize, the framework presented in this section shows how stochastic resonance in any nonlinear system can be fully characterized. In particular the output SNR and input-output phase shift can be determined solely from observations of the nonstationary output mean $E[y(t)]$ over one period and of the stationary output autocovariance $C_{yy}(\tau)$. This framework will now be used as a guideline to study stochastic resonance in the more restricted case of static nonlinearities.

2.5 Static nonlinearities

We will now consider the static, memoryless nonlinearity with the input-output transformation

$$y(t) = g[s(t) + \eta(t)] \tag{2.108}$$

where $g : R \to R$ is a bounded, though not necessarily continuous function operating on real numbers. In the special case when $\eta(t)$ represents stationary, white noise with a probability distribution function $f_\eta(u)$ and a cumulative distribution function $F_\eta(u)$. The auto-correlation function of white noise is $R_{\eta\eta}(\tau) = E[\eta(t)\eta(t+\tau)] = 2D\delta(\tau)$ and as a consequence white noise has infinite power given by $R_{\eta\eta}(0) = E[\eta^2(t)] = 2D\delta(\tau = 0)$. This artificial singularity is due to the idealized treatment of white noise. In practice, all realizations of white noise have small, but non-zero correlation time τ_c. Correspondingly, the power of such noise is large but bounded, satisfying the condition $R_{\eta\eta}(0)\tau_c \sim 2D$.

We henceforth adopt such a model for the white noise at the input.

We will also cast all succeeding formulae in the context of discrete-time signals. This will be done, for purposes of easy comparison with simulations and experimental implementations of nonlinear systems. The time scale will be discretized with a step $\Delta t \ll T_s$ such that the time period of the coherent input is an integral multiple of the time-step: $T_s = N\Delta t$. This has the effect that the white noise $\eta(t)$ only needs to have correlation time τ_c shorter than Δt and finite power $E(\eta^2) = \sigma_\eta^2$. Such a random process, when sampled at intervals of Δt acts effectively like a discrete-time white noise process $\eta(t = j\Delta t)$ with the auto-correlation function $R_{\eta\eta}(k\Delta t) = E[\eta(j\Delta t)]E[\eta(j\Delta t + k\Delta t)] = \sigma_\eta^2 \Delta t \hat{\delta}(k\Delta t)$ where $\hat{\delta}(k\Delta t)$ represents the discrete-time version of the Dirac delta function defined by

$$\hat{\delta}(k\Delta t) = \begin{cases} 1/\Delta t & \text{for } k = 0 \\ 0 & \text{for } k \neq 0 \end{cases} \tag{2.109}$$

In this realization of white noise, the power spectral density is given by

$$2D = \sigma_\eta^2 \Delta t. \tag{2.110}$$

In this discrete-time framework the treatment that will follow is exact. In order to proceed, we make the key observation that for white noise $\eta(t)$ and a static nonlinearity $g(u)$, for any fixed t any fixed $\tau \neq 0$, $y(t)$ and $y(t + \tau)$ are statistically uncorrelated. Consequently, we have the following relationship in the discrete-time framework

$$E[y(j\Delta t)y(j\Delta t + k\Delta t)] = E[y(j\Delta t)]E[y(j\Delta t + k\Delta t)], \tag{2.111}$$

for any integers j and $k \neq 0$. For the case $\tau = k\Delta t = 0$, we get

$$\begin{aligned} E[y(j\Delta t)y(j\Delta t)] &= E[\widetilde{y}^2(j\Delta t)] + E^2[y(j\Delta t)], \\ &\neq E^2[y(j\Delta t)]. \end{aligned} \tag{2.112}$$

At any fixed time $t = \Delta t$, since η_t governed by the PDF $f_\eta(u)$, the random variable $s(t) + \eta(t)$ is governed by the PDF $f_\eta(u - s(t))$. As a result, the nonstationary output mean can be explicitly computed to be

$$E[y(t)] = \int_{-\infty}^{\infty} g(u) f_\eta(u - s(t)) du \tag{2.113}$$

and the nonstationary output second-degree moment is given by

$$E[y^2(t)] = \int_{-\infty}^{\infty} g^2(u) f_\eta(u - s(t)) du. \tag{2.114}$$

It then follows that the nonstationary output variance, $var[y(t)] = E[\tilde{y}^2(t)]$, is given by

$$\begin{aligned} var[y(t)] &= \int_{-\infty}^{\infty} g^2(u) f_\eta(u - s(t)) du \\ &\quad - \left(\int_{-\infty}^{\infty} g(u) f_\eta(u - s(t)) du \right)^2. \end{aligned} \tag{2.115}$$

Substituting each individual term in Eqs.(2.111) and (2.112) with their values given by Eqs.(2.113-2.115), we get

$$\begin{aligned} E[y(j\Delta t)y(j\Delta t + k\Delta t)] &= var[y(j\Delta t)]\Delta t\hat{\delta}k\Delta t \\ &\quad + E[y(j\Delta t)]E[y(j\Delta t + k\Delta t)] \end{aligned} \tag{2.116}$$

for any integer j and k. The output autocorrelation function in a discrete-time framework can be defined through a time-average as follows

$$\begin{aligned} R_{yy}(k\Delta t) &= \overline{var(y)}\Delta t\hat{\delta}k\Delta t, \\ &\quad + \frac{1}{N} \sum_{j=0}^{N-1} E[y(j\Delta t)]E[y(j\Delta t + k\Delta t)], \end{aligned} \tag{2.117}$$

with the stationary output variance

$$\overline{var(y)} = \frac{1}{N} \sum_{j=0}^{N-1} var[y(j\Delta t)], \tag{2.118}$$

which can be explicitly computed from Eq.(2.115). The stationary output autocovariance function of Eq.(2.101), in the case of white noise and static nonlinearities, simplifies to

$$C_{yy}(k\Delta t) = \overline{var[y]}h(k\Delta t) = \overline{var[y]}\hat{\delta}(k\Delta t). \tag{2.119}$$

In the frequency domain, the discrete Fourier coefficients of the deterministic periodic signal $E[y(j\Delta t)]$ can be defined as

$$\overline{Y_n} = \frac{1}{N} \sum_{j=1}^{N-1} E[y(j\Delta t)] \exp\left(-i2\pi jn/N\right). \tag{2.120}$$

The discrete Fourier transform of R_{yy} over an integral number, given by $2M$ of periods T_s is defined by

$$P_{yy}(k\Delta t) = \mathcal{F}_{dis}[R_{yy}(k\Delta t)] = \sum_{k=-MN}^{MN-1} R_y y(k\Delta t) \exp\left(-i2\pi\nu \frac{kl}{2MN}\right) \Delta t, \quad (2.121)$$

which accords a frequency resolution of $\Delta\nu = 1/(2MN\Delta t)$.

The autocorrelation function of Eq.(2.117) is formed by a pulse at the origin with magnitude $\overline{var(y)}\Delta t$, superposed on a periodic component with period T_s. The Fourier transform of R_{yy} defined the output power spectral density P_{yy} which will be formed by a background of constant magnitude $\overline{var(y)}\Delta t$ superposed on a series of spectral lines at integral multiples of $1/T_s$. Applying Eq. (2.121) leads to

$$P_{yy}(n/T_s) = \overline{var[y]}\Delta t + \overline{Y_n Y_n}^* \frac{1}{\Delta\nu}. \quad (2.122)$$

By the condition Eq.(2.110), the first term in the above decomposition is expected to remain finite. When the horizon $M \to \infty$ then $\Delta\nu \to 0$ and the coherent spectral lines above the broadband noise background tend to Dirac delta functions. It then follows that the output SNR defined in Eq.(2.103), also denoted by $\mathcal{R}$, is given by

$$\mathcal{R}\left(\frac{n}{T_s}\right) = \frac{|\overline{Y_n}|^2}{\overline{var[y(t)]}\Delta\nu\Delta B}. \quad (2.123)$$

This gives us an explicit formula to compute the output SNR, through the Eqs. (2.113, 2.115,2.118) and (2.120) for any noise distribution $f_\eta(t)$ and any periodic input $s(t)$ transmitted through an arbitrary nonlinearity $g(u)$.

To summarize, with the SNR and the phase shift ϕ being exactly calculable from Eq.(2.107), for various harmonics of the coherent frequency $1/T_s$, we have a complete characterization of the nonlinear system suitable for the study of stochastic resonance. Since all relevant quantities lend themselves to direct numerical evaluation the present theory can be used to analyze stochastic resonance in various static nonlinear systems, as will be done later in chapter 3 of this thesis.

2.6 Statistical detection theory

We will limit out treatment to the *binary hypothesis* case where only two hypotheses are possible: $\mathcal{H}_0$, which denotes the hypothesis where the signal is absent; and $\mathcal{H}_1$, which denotes hypotheses that the signal is present. $\mathcal{H}_0$ and $\mathcal{H}_1$ are often referred to as the

null and *alternative hypotheses* respectively. We start with a few basic definitions in detection theory.

Definition. P_D denotes the *probability of Detection* which is the conditional probability of deciding $\mathcal{H}_1$ when $\mathcal{H}_1$ is true i.e. $P_D = P(\mathcal{H}_1, \mathcal{H}_1)$.

Definition. P_{FA} denotes the *probability of False Alarm* which is the conditional probability of deciding $\mathcal{H}_1$ when $\mathcal{H}_0$ is true i.e. $P_{FA} = P(\mathcal{H}_1, \mathcal{H}_0)$.

Definition. The *Test statistic* $T(x)$ is defined to be a function of the observations $\mathbf{x}$ such that where γ is called the threshold of the system.

Definition. The Receiver Operating Characteristics (ROC) of a detector is a graph of the values (P_D, P_{FA}). Such a graph summarizes the detection performance of any detector. For any given value of P_{FA}, a higher value of P_D is the hallmark of an improved, or more sensitive detector. Qualitatively, it can be said that improved detectors result in "more convex" ROCs.

Notation. A sequence of random variables which are independent and governed by the same probability distribution function are said to be independent and identically distributed or *IID* random variables.

2.6.1 The Central limit theorem

Since observations are always available in the form of a time-series we start with the Central Limit theorem which describes the asymptotic statistical properties of sums of random variables.

Theorem (Central Limit Theorem). *The sum of the sequence of IID random variables* $\{X_i\}$ *converges in law to* $\mathcal{N}(\mu, \sigma^2)$ *where the mean and variance are given by*

$$\begin{aligned} \mu &= \sum_{i=1}^{N} X_i/N, \\ \sigma^2 &= \sum_{i=1}^{N} X_i^2/N - \left\{ \sum_{i=1}^{N} X_i/N \right\}^2 . \end{aligned} \tag{2.124}$$

Sums of squares of independent Gaussian random variables are governed by the Chi-squared PDFs. Their properties are now briefly described.

2.6.2 Chi-squared (Central)

A *chi-squared* PDF with ν degrees of freedom is defined as

$$p(x) = \begin{cases} \frac{1}{2^{\frac{\nu}{2}}\Gamma(\frac{\nu}{2})} x^{\frac{\nu}{2}-1} \exp(-\frac{1}{2}x) & x > 0 \\ 0 & x < 0 \end{cases} \tag{2.125}$$

and is denoted by χ^2_ν. The degrees of freedom ν is assumed to be an integer with $\nu \geq 1$. $\Gamma(\nu)$ denotes the Gamma function defined as

$$\Gamma(\nu) = \int_0^\infty t^{\nu-1} \exp(-t) dt. \tag{2.126}$$

The Chi-squared PDF arises as the PDF of x where $x = \sum_{i=1}^{\nu} x_i^2$ if $x_i \sim \mathcal{N}(0,1)$ and the x_i's are independent and identically distributed (IID). By the latter we mean that each x_i is independent of the others and each x_i has the same PDF (identically distributed). The mean and variance are given by

$$\begin{aligned} E(x) &= \nu \\ var(x) &= 2\nu. \end{aligned} \tag{2.127}$$

A case of specific interest occurs when $\nu = 2$ so that

$$p(x) = \begin{cases} \frac{1}{2} \exp(-\frac{1}{2}x) & x > 0 \\ 0 & x < 0 \end{cases}$$

and is referred to as an *exponential* PDF. The right-tail probability for a χ^2_ν random variable is defined as

$$Q_{\chi^2_\nu}(x) = \int_x^\infty p(t) dt \tag{2.128}$$

which can be shown [1] to be

$$Q_{\chi^2_\nu}(x) = \exp(-\frac{1}{2}x) \sum_{k=0}^{\frac{\nu}{2}-1} \frac{(\frac{x}{2})^k}{k!} \nu \geq 2 \tag{2.129}$$

and for ν odd

$$Q_{\chi^2_\nu}(x) = \begin{cases} 2Q(\sqrt{x}) & \nu = 1 \\ 2Q(\sqrt{x}) + \frac{\exp(-\frac{1}{2}x)}{\sqrt{\pi}} + \sum_{k=0}^{\frac{\nu}{2}-1} \frac{(k-1)!(2x)^{k-\frac{1}{2}}}{(2k-1)!} & \nu \geq 3 \end{cases}$$

2.6.3 Chi-squared (Non-central)

A generalization of the χ^2_ν PDF arises as a result of summing the squares of IID Gaussian random variables with non-zero means. Specifically, if $x = \sum_{i=1}^{\nu} x_i^2$ where x_i's are independent and $x_i \sim \mathcal{N}(\mu_i, 1)$, then x_i has a *non-central chi-squared* PDF with ν degrees of freedom and *non-centrality parameter* $\lambda = \sum_{i=1}^{\nu} \mu_i^2$. The resulting PDF must be expressed either as an integral or as an infinite series. As an integral it is

$$p(x) = \begin{cases} \frac{1}{2}(\frac{x}{\lambda})^{\frac{\nu-2}{4}} \exp(-\frac{1}{2}x + \lambda) I_{\frac{\nu}{2}-1}(\sqrt{\lambda x}) & x > 0 \\ 0 & x < 0 \end{cases} \tag{2.130}$$

where $I_r(u)$ is the modified Bessel function of the first kind and order r. It is defined as [1] as

$$I_r(u) = \frac{(\frac{1}{2}u)^r}{\sqrt{\pi}\Gamma(r + \frac{1}{2})} \int_0^\pi \exp(u\cos\theta) \sin^{2r}\theta d\theta \tag{2.131}$$

and has the series expansion

$$I_r(u) = \sum_{k=0}^{\infty} \frac{(\frac{1}{2}u)^{(2k+r)}}{k!\Gamma(r + k + 1)}. \tag{2.132}$$

The PDF tends to a Gaussian when ν, assumed to be positive, becomes sufficiently large. Using Eq.(2.132) the PDF given by Eq.(2.130) can also be expressed as

$$p(x) = \frac{x^{\frac{\nu}{2}-1} \exp(-\frac{1}{2}(x + \lambda)}{2^{\frac{\nu}{2}}} \sum_{k=0}^{\infty} \frac{(\frac{\lambda x}{4})^k}{k!\Gamma(\frac{\nu}{2} + k)}. \tag{2.133}$$

Note that for $\lambda = 0$ this reduces to the chi-squared PDF in Eq.(2.130). The non-central Chi-squared PDF with ν degrees of freedom and noncentrality parameter λ is denoted by $\chi'^2_\nu(\lambda)$.

2.6.4 Neyman-Pearson theorem

One of the key results in statistical detection theory is the Neyman-Pearson theorem which states the criterion a detector has to satisfy in order to be optimal, for a given noise distribution.

Theorem (Neyman-Pearson) *To maximize P_D for a given $P_{FA} = \alpha$ decide $\mathcal{H}_1$ if*

$$L(\mathbf{x}) = \frac{p(\mathbf{x}; \mathcal{H}_1)}{p(\mathbf{x}; \mathcal{H}_0)} > \gamma \tag{2.134}$$

where the threshold γ is found from

$$P_{FA} = \int_{\{\mathbf{x}:L(\mathbf{x})>\gamma\}} p(\mathbf{x};\mathcal{H}_0)dx = \alpha. \tag{2.135}$$

Proof. We use Lagrange multipliers to maximize P_D for a given P_{FA}. Forming the Lagrangian

$$\begin{aligned} F &= P_D + \lambda(P_{FA} - \alpha) \\ &= \int_{R_1} p(\mathbf{x};\mathcal{H}_1)dx + \left(\lambda \int_{R_1} p(\mathbf{x};\mathcal{H}_0)dx - \lambda\alpha\right) \\ &= \int_{R_1} \left(p(\mathbf{x};\mathcal{H}_1) + \lambda p(\mathbf{x};\mathcal{H}_0)\right) dx - \lambda\alpha. \end{aligned} \tag{2.136}$$

To maximize F we should include $\mathbf{x}$ in R_1 if the integrand is positive for that value of $\mathbf{x}$ or if

$$p(\mathbf{x};\mathcal{H}_1) + \lambda p(\mathbf{x};\mathcal{H}_0) > 0 \tag{2.137}$$

When $p(\mathbf{x};\mathcal{H}_1) + \lambda p(\mathbf{x};\mathcal{H}_0) = 0$, $\mathbf{x}$ may be included in either R_0 or R_1. Assuming the PDFs are continuous, the probability of event reduces to zero. We thus decide $\mathcal{H}_1$ if

$$\frac{p(\mathbf{x};\mathcal{H}_1)}{p(\mathbf{x};\mathcal{H}_0)} > -\lambda. \tag{2.138}$$

The Lagrangian multiplier is found from the constraint and must satisfy $\lambda < 0$. Otherwise, we decide $\mathcal{H}_1$ is the likelihood ratio exceeds a negative number. Since the likelihood ratio is always non-negative, we should always decide $\mathcal{H}_1$, irrespective of the hypothesis, resulting in $P_{FA} = 1$. We let $\gamma = -\lambda$ so that finally we decide $\mathcal{H}_1$ if

$$\frac{p(\mathbf{x};\mathcal{H}_1)}{p(\mathbf{x};\mathcal{H}_0)} > \gamma \tag{2.139}$$

where the threshold $\gamma > 0$ is found from $P_{FA} = \alpha$.

It immediately follows from the Neyman-Pearson theorem is that matched (linear) filters are optimal when the noise is governed by a Gaussian PDF.

Corollary (Matched filters as optimal filters) *In the problem of detecting a known deterministic signal in white Gaussian noise, the Neyman-Pearson criterion yields the matched filter.*

Proof: The NP detector decided $\mathcal{H}_1$ if the likelihood ratio exceeds a threshold or

$$L(x) = \frac{p(x;\mathcal{H}_1)}{p(x;\mathcal{H}_0)} > \gamma \tag{2.140}$$

where $\mathbf{x} = [x[0], x[1], \ldots x[N-1]]^T$. Since

$$\begin{aligned} p(x;\mathcal{H}_1) &= \frac{1}{(2\pi\sigma^2)^{\frac{N}{2}}} \exp[-\frac{1}{2\sigma_2}\sum_{n=0}^{N-1}(x[n]-s[n])^2] \\ p(x;\mathcal{H}_0) &= \frac{1}{(2\pi\sigma^2)^{\frac{N}{2}}} \exp[-\frac{1}{2\sigma_2}\sum_{n=0}^{N-1}x^2[n]] \end{aligned} \tag{2.141}$$

We get

$$L(x) = \exp[-\frac{1}{2\sigma_2}\left(\sum_{n=0}^{N-1}(x[n]-s[n])^2] - \sum_{n=0}^{N-1}x^2[n]\right)] > \gamma. \tag{2.142}$$

Taking the logarithm (a monotonically increasing function) of both sides we get

$$l(x) = -\frac{1}{2\sigma_2}\left(\sum_{n=0}^{N-1}(x[n]-s[n])^2] - \sum_{n=0}^{N-1}x^2[n]\right) > ln\gamma. \tag{2.143}$$

Alternatively we decide $\mathcal{H}_1$ if

$$T(x) = \sum_{n=0}^{N-1} x[n]s[n] > \gamma', \tag{2.144}$$

where $\gamma' = \sigma^2\gamma + \frac{1}{2}\sum_{n=0}^{N-1}s^2[n]$. This is our NP detector, which consists of a test statistic $T(x)$ (a function of the data) and a threshold γ', which must be chosen to satisfy a certain numerical value of P_{FA}.

The performance of such a detector can be deduced as follows.

$$\begin{aligned} E(T;\mathcal{H}_0) &= E(\sum_{n=0}^{N-1} w[n]s[n]) = 0, \\ E(T;\mathcal{H}_1) &= E(\sum_{n=0}^{N-1} (s[n]+w[n])s[n]) = \mathcal{E}, \\ var(T;\mathcal{H}_0) &= var(\sum_{n=0}^{N-1} w[n]s[n]) \end{aligned}$$

$$\begin{aligned} &= \sum_{n=0}^{N-1} var(w[n])s^2[n] \\ &= \sigma^2 \sum_{n=0}^{N-1} s^2[n] = \sigma^2\mathcal{E} \\ var(T;\mathcal{H}_1) &= \sigma^2. \end{aligned} \tag{2.145}$$

In the above we have used the fact that the $w[n]$'s are uncorrelated. Thus

$$T \sim \begin{cases} \mathcal{N}(0, \sigma^2\mathcal{E}) & \text{under } \mathcal{H}_0 \\ \mathcal{N}(\mathcal{E}, \sigma^2\mathcal{E}) & \text{under } \mathcal{H}_1 \end{cases}$$

It follows

$$\begin{aligned} P_{FA} &= Prob\{T > \gamma'; \mathcal{H}_0\} \\ &= Q\left(\frac{\gamma'}{\sqrt{\sigma^2\mathcal{E}}}\right) \\ P_D &= Prob\{T > \gamma'; \mathcal{H}_1\} \\ &= Q\left(\frac{\gamma' - \mathcal{E}}{\sqrt{\sigma^2\mathcal{E}}}\right), \end{aligned} \tag{2.146}$$

where

$$Q(x) = \int_x^\infty \frac{1}{\sqrt{2\pi}} \exp\left(-\frac{1}{2}t^2\right) dt \tag{2.147}$$

where $Q(x)$ is the complementary CDF for a $\mathcal{N}(0,1)$ random variable. Since $Q(x)$ is a monotonically decreasing function it follows that the inverse function Q^{-1} is well-defined. Therefore,

$$\gamma' = \sqrt{\sigma^2\mathcal{E}}Q^{-1}(P_{FA}). \tag{2.148}$$

Substituting in Eq.(2.146) we get

$$P_D = Q\left(Q^{-1}(P_{FA}) - \sqrt{\frac{\mathcal{E}}{\sigma^2}}\right). \tag{2.149}$$

Therefore, in conclusion we can state that non-linear detectors are useful only when the PDF governing noise tends to be non-Gaussian. A general formalism of finding the system transfer functions of such nonlinear detectors will be developed in the following sections.

2.6.5 Locally optimal detectors

Generally, for the detection of a known deterministic signal $s[n]$ in IID non-Gaussian noise with PDF $p(w[n])$, we decide $\mathcal{H}_1$ if

$$\sum_{n=0}^{N-1} g_n(x[n]) > \gamma' \tag{2.150}$$

where

$$g_n(x) = \frac{p(x - As[n])}{p(x)}. \tag{2.151}$$

This non-linearity depends on the sample to which it is applied. The determination of P_{FA} and P_D for the detector of Eq.(2.150) is difficult due to the nonlinearity. Hence, we resort to asymptotic analysis. In the process we obtain an equivalent asymptotic detector. We consider the known signal $As[n]$, where $A > 0$, and examine the NP detector as $A \to 0$ or as the signal is exceedingly weak. Using Eq.(2.150) we view $g_n(x)$ as a function of A and expand it in a first-order Taylor expansion about $A = 0$. Doing so produces

$$g_n(x) = -\frac{\frac{dp(x)}{dx}}{p(x)} As[n]. \tag{2.152}$$

From Eq.(2.150) we can decide $\mathcal{H}_1$ if

$$\sum_{n=0}^{N-1} g_n(x[n]) = -\sum_{n=0}^{N-1} \frac{\frac{dp(x)}{dx}}{p(x)}|_{x=x[n]} As[n] > \gamma'. \tag{2.153}$$

2.6.6 Periodograms or energy detectors

The detection of a sinusoid in white Gaussian noise (WGN) is a common problem in many fields. Because of its wide practical utility we examine in some detail the detector structure as well as its performance. The results form the basis for many practical sonar, radar and communication systems. The general detection problem is

$$\begin{aligned} \mathcal{H}_0 : x[n] &= w[n] \quad n = 0, 1 \ldots N-1 \\ \mathcal{H}_1 : x[n] &= A\cos(2\pi n/N + \phi) + w[n] \quad n = 0, 1 \ldots N-1. \end{aligned} \tag{2.154}$$

where $w[n]$ is WGN with known variance σ^2 and the parameters $\{A, \phi\}$ are unknowns. We assume that the signal frequency is known and sampled at the Nyquist frequency resulting in the discretized observation train given in Eq.(2.154) and the sinusoid is nonzero over the entire interval $[0, N-1]$. We later present an analysis of the degradation

due to uncertainty in the estimate of the signal frequency. It is found to be of second order and subdominant to the effects of other uncertainties. The case when the signal is present only in a sub-interval of the observation length $[0, N-1]$ results in "irrelevant data". Such irrelevant data can be excised from the observation sequence by standard procedures [87]. The presence of such irrelevant data increases the time required by the detector to perform but does not diminish its accuracy or performance as a detector. However we assume that the amplitude(A) and phase(ϕ) are unknown. Here we assume that $A > 0$ as the ordered pair (A, ϕ) are not identifiable upto a phase change $(-A, \phi + 2\pi)$.

The Generalized Likelihood Ratio test decides $\mathcal{H}_1$ if

$$\frac{p(\mathbf{x}; \mathcal{H}_1)}{p(\mathbf{x}; \mathcal{H}_0)} > \gamma \tag{2.155}$$

or

$$L_G(\mathbf{x}) = \frac{\frac{1}{(2\pi\sigma^2)^{\frac{N}{2}}} \exp[-\frac{1}{2\sigma^2}\sum_{n=0}^{N-1}(x[n] - A\cos(2\pi n/N + \phi))^2]}{\frac{1}{(2\pi\sigma^2)^{\frac{N}{2}}} \exp[-\frac{1}{2\sigma^2}\sum_{n=0}^{N-1} x^2[n]]} > \gamma. \tag{2.156}$$

Now, as before, the natural logarithm, being a monotonic function, can be taken on both sides giving

$$\ln L_G(\mathbf{x}) = -\frac{1}{2\sigma^2}\left[\sum_{n=0}^{N-1} -2x[n]A\cos(2\pi n/N + \phi) + \sum_{n=0}^{N-1} A^2\cos^2(2\pi n/N + \phi)\right]. \tag{2.157}$$

Using the parameter transformation $\alpha_1 = A\cos\phi$ and $\alpha_2 = A\sin\phi$ we see that Eq.(2.157) simplifies to

$$\ln L_G(\mathbf{x}) = \frac{N}{4\sigma^2}(\alpha_1^2 + \alpha_2^2). \tag{2.158}$$

So we decide $\mathcal{H}_1$ if

$$\frac{N}{4\sigma^2}(\alpha_1^2 + \alpha_2^2) > \ln\gamma. \tag{2.159}$$

But

$$\alpha_1^2 + \alpha_2^2 = \frac{4}{N}I(f_0 = 1) \tag{2.160}$$

where $I(f_0)$ is the periodogram evaluated at $f_0 = 1$ given by

$$I(f_0 = 1) = \frac{1}{N}\left|\sum_{n=0}^{N-1} x[n]\exp(-j2\pi f_0 n)\right|^2 . \tag{2.161}$$

The form of the detector is identical to that for the Rayleigh fading model [87], though the detection performance is found to be different. This detector is also called the *incoherent* or *quadrature matched filter*. The detection performance can be found from "first principles" as follows:

$$I(f_0) = \xi_1^2 + \xi_2^2 \tag{2.162}$$

where

$$\begin{aligned} \xi_1 &= \frac{1}{\sqrt{N}}\sum_{n=0}^{N-1} x[n]\cos 2\pi f_0 n \\ \xi_2 &= \frac{1}{\sqrt{N}}\sum_{n=0}^{N-1} x[n]\sin 2\pi f_0 n. \end{aligned} \tag{2.163}$$

Since ξ_1, ξ_2 are linear transformations of $\mathbf{x}$ they are jointly Gaussian. It can be shown that for ξ

$$\begin{aligned} \xi &= \mathcal{N}(\mathbf{0}, \frac{\sigma^2}{2}\mathbf{I}) && \text{under } \mathcal{H}_0 \\ \xi &= \mathcal{N}\left(\left[\frac{\sqrt{N}}{2}A\cos\phi, \frac{\sqrt{N}}{2}A\sin\phi\right], \frac{\sigma^2}{2}\mathbf{I}\right) && \text{under } \mathcal{H}_1. \end{aligned} \tag{2.164}$$

Since under either hypothesis the random variables are independent, the PDF is related to the central χ^2 under $\mathcal{H}_0$ and to the non-central χ^2 under $\mathcal{H}_1$. It remains to calculate the defining parameters for these central and non-central χ^2 PDFs. The noncentrality parameter for the χ^2 PDF can be found as follows:

$$\lambda = \left(\frac{\sqrt{N}\frac{A}{2}\cos\phi}{\sigma/\sqrt{2}}\right)^2 + \left(\frac{\sqrt{N}\frac{A}{2}\sin\phi}{\sigma/\sqrt{2}}\right)^2 = \left(\frac{NA^2}{2\sigma^2}\right). \tag{2.165}$$

As a result

$$\begin{aligned} P_{FA} &= Prob\{I(f_0) > \gamma'; \mathcal{H}_0\} \\ &= Prob\left\{\frac{I(f_0)}{\sigma^2/2} > \frac{\gamma'}{\sigma^2/2}; \mathcal{H}_0\right\} \end{aligned}$$

$$\begin{aligned} &= Q_{\chi_2^2}\left(\frac{2\gamma'}{\sigma^2}\right) \\ &= \exp\left(-\frac{\gamma'}{\sigma^2}\right). \end{aligned} \tag{2.166}$$

And

$$\begin{aligned} P_D &= Prob\{I(f_0) > \gamma'; \mathcal{H}_1\} \\ &= Prob\left\{\frac{I(f_0)}{\sigma^2/2} > \frac{\gamma'}{\sigma^2/2}; \mathcal{H}_1\right\} \\ &= Q_{\chi_2^2(\lambda)}\left(\frac{2\gamma'}{\sigma^2}\right). \end{aligned} \tag{2.167}$$

In summary the Receiver Operating Characteristics can written as

$$P_D = Q_{\chi_2^2(\lambda)}\left(2\ln\frac{1}{P_{FA}}\right) \tag{2.168}$$

where λ is given by Eq.(2.165). Before concluding this discussion we should note that it is possible to generalize this approach to the case when the frequency of the incoming sinusoid is not known [87]. That requires repeated computation of the periodogram at various estimated frequencies and then picking the maximum amongst them as the Test statistic. The value of the frequency or the argument corresponding to the maximum is the estimate of the signal frequency. But in sonar applications, the frequency of target vessels can be assumed to be known to a high degree of accuracy. Therefore, we forego this discussion in our treatment.

In the following few sections we derive the optimal test statistics for detectors of sinusoidal signals in various environments. They are in the following increasing order of complexity: (i) unknown amplitude, known phase in Gaussian noise; (ii) unknown amplitude, known phase in non-Gaussian noise; (iii) unknown amplitude, unknown phase in Gaussian noise; and (iv) unknown amplitude, unknown phase in non-Gaussian noise. They serve as an useful preparatory exercise for the optimal statistics of Stochastic resonant detectors, to be derived later in chapter 3, and they illustrate the utility of the Neyman-Pearson criterion and Likelihood ratio test.

2.6.7 Detection of a sinusoidal signal with unknown amplitude but known phase in Gaussian noise

From the likelihood ratio test if the Neyman-Pearson criterion given by Eq.(2.134)

$$L_G(\mathbf{x}) = \frac{\frac{1}{(2\pi\sigma^2)^{\frac{N}{2}}} \exp[-\frac{1}{2\sigma^2}\sum_{n=0}^{N-1}(x[n]-As[n])^2]}{\frac{1}{(2\pi\sigma^2)^{\frac{N}{2}}} \exp[-\frac{1}{2\sigma^2}\sum_{n=0}^{N-1}x^2[n]]} > \gamma. \tag{2.169}$$

Now, as before, the natural logarithm, being a monotonic function, can be taken on both sides giving

$$\ln L_G(\mathbf{x}) = \frac{1}{2\sigma^2}\left[\sum_{n=0}^{N-1} +2x[n]As[n] - \sum_{n=0}^{N-1} A^2s^2[n]\right] > \ln\gamma. \tag{2.170}$$

From $\ln L_G > \gamma$ and some re-arrangement we get,

$$T(\mathbf{x}) = \sum_{n=0}^{N-1} x[n]s[n] > \frac{2\sigma^2\gamma + \sum_{n=0}^{N-1} A^2s^2[n]}{2A} \tag{2.171}$$

which gives us the optimal test statistic. However when A is unknown this argument cannot be repeated. In this case

$$\ln L_G(\mathbf{x}) = \frac{1}{2\sigma^2}\left[\sum_{n=0}^{N-1} +2x[n]As[n] - \sum_{n=0}^{N-1} A^2s^2[n]\right] > \ln\gamma \tag{2.172}$$

can be thought of as a quadratic equation in A as follows

$$2AB - A^2 > \gamma' \tag{2.173}$$

where

$$B = \frac{\sum_{n=0}^{N-1} x[n]s[n]}{\sum_{n=0}^{N-1} s^2[n]} \quad \text{and} \quad \gamma = \frac{2\sigma^2\ln\gamma}{\sum_{n=0}^{N-1} s^2[n]]}. \tag{2.174}$$

This can be re-written as

$$B^2 - (B-A)^2 > \gamma'. \tag{2.175}$$

Since A is indeterminate, the expression on the left-hand side has an infimum given by

$$T(\mathbf{x}) = B^2 = \left[\frac{\sum_{n=0}^{N-1} x[n]s[n]}{\sum_{n=0}^{N-1} s^2[n]}\right]^2 > \gamma'', \tag{2.176}$$

where γ'' denotes the modified threshold for the Test statistic.

2.6.8 Detection of a sinusoidal signal with unknown amplitude but known phase in general non-Gaussian noise

As before, from the Neyman-Pearson criterion as given in Eq.(2.134)

$$L_G(\mathbf{x}) = \prod_{n=0}^{N-1} \frac{p(x[n] - As[n])}{p(x[n])} > \gamma. \tag{2.177}$$

The governing PDF of the noise is denoted by p which need not be a Gaussian. Taking the natural logarithm and keeping only till the first order term in the Taylor series expansion in $As[n]$, we get

$$\ln L_G = \sum_{n=0}^{N-1} \ln \frac{p(x[n]) - p'(x[n])As[n]}{p(x[n])} > \ln \gamma. \tag{2.178}$$

On some minor rearrangement we get

$$\ln L_G = \sum_{n=0}^{N-1} \ln \left[1 - \frac{p'}{p}(x[n])As[n]\right] > \ln \gamma. \tag{2.179}$$

Taking the Taylor expansion for $\ln(1+x)$ in the argument of the logarithm, we get

$$-\left[\sum_{n=0}^{N-1} \frac{p'}{p}(x[n])s[n]\right] A + \left[\sum_{n=0}^{N-1} \left(\frac{p'}{p}(x[n])\right)^2 s^2[n]\right]^2 A^2 > \ln \gamma \tag{2.180}$$

which can be re-written as a quadratic expression in the amplitude A

$$\frac{-2AB + CA^2}{2!} = -\frac{C}{2!}(A - B/C)^2 + \frac{B^2}{2C} > \ln \gamma \tag{2.181}$$

where

$$B = \left[\sum_{n=0}^{N-1} \frac{p'}{p}(x[n])s[n]\right] \quad \text{and} \quad C = \left[\sum_{n=0}^{N-1} \left(\frac{p'}{p}(x[n])\right)^2 s^2[n]\right]^2. \tag{2.182}$$

Therefore the Test statistic is taken to be the infimum which is

$$T(\mathbf{x}) = \frac{1}{2C}\left[\sum_{n=0}^{N-1}\frac{p'}{p}(x[n])s[n]\right]^2. \tag{2.183}$$

2.6.9 Detection of sinusoidal signals with unknown amplitudes and phases in Gaussian noise

The Neyman-Pearson criterion Eq.(2.134) states

$$L_G(\mathbf{x}) = \frac{\frac{1}{(2\pi\sigma^2)^{\frac{N}{2}}}\exp[-\frac{1}{2\sigma^2}\sum_{n=0}^{N-1}(x[n]-A\cos(2\pi n/N+\phi))^2]}{\frac{1}{(2\pi\sigma^2)^{\frac{N}{2}}}\exp[-\frac{1}{2\sigma^2}\sum_{n=0}^{N-1}x^2[n]]} > \gamma. \tag{2.184}$$

Now, as before, the natural logarithm, being a monotonic function, can be taken on both sides giving

$$\begin{aligned}\ln L_G(\mathbf{x}) &= \frac{1}{2\sigma^2}\left[2A\sum_{n=0}^{N-1}\{2x[n]A\cos(2\pi n/N+\phi) - \sum_{n=0}^{N-1}A^2\cos^2(2\pi n/N+\phi)\right] \\ &= \frac{1}{2\sigma^2}\left[2A\left\{\left(\sum_{n=0}^{N-1}2x[n]A\cos(2\pi n/N)\right)\cos\phi - \left(\sum_{n=0}^{N-1}2x[n]A\sin(2\pi n/N)\right)\sin\phi\right\}\right. \\ &\quad \left. -A^2/2\left\{\sum_{n=0}^{N-1}(1+\cos(4\pi n/N+2\phi))\right\}\right]. \end{aligned} \tag{2.185}$$

This can be re-written as the quadratic

$$\ln L_G(\mathbf{x}) = \frac{1}{2\sigma^2}\left[2A\left\{B_1\cos\phi - B_2\sin\phi\right\} - A^2\frac{N}{2}\right]. \tag{2.186}$$

The above equation holds regardless of the value of ϕ. The terms $B_{1,2}$ are given by

$$B_1 = \sum_{n=0}^{N-1}x[n]\cos(2\pi n/N) \quad \text{and} \quad B_2 = \sum_{n=0}^{N-1}x[n]\sin(2\pi n/N). \tag{2.187}$$

The first term in the quadratic can be re-arranged as follows:

$$B_1\cos\phi - B_2\sin\phi = \hat{B}\cos(\phi-\beta), \tag{2.188}$$

where $\beta = \tan^{-1}(-B_2/B_1)$ and $\hat{B} = (B_1^2+B_2^2)^{1/2}$. The above expression has an infimum

$\hat{B}$. The test statistic can be taken to this infimum squared as follows,

$$T(\mathbf{x}) = \hat{B}^2 = \left(\sum_{n=0}^{N-1} x[n]\cos(2\pi n/N)\right)^2 + \left(\sum_{n=0}^{N-1} x[n]\sin(2\pi n/N)\right)^2. \quad (2.189)$$

2.6.10 Detection of a sinusoidal signal with unknown amplitude and phase in general non-Gaussian noise

The Neyman-Pearson criterion Eq.(2.134) states

$$L_G(\mathbf{x}) = \prod_{n=0}^{N-1} \frac{p(x[n] - A\cos(2\pi n/N + \phi))}{p(x[n])} > \gamma. \quad (2.190)$$

Taking the natural logarithm

$$\ln L_G = \sum_{n=0}^{N-1} \ln \frac{p(x[n]) - p'(x[n])A\cos(2\pi n/N + \phi)}{p(x[n])} > \ln\gamma. \quad (2.191)$$

Keeping only till the first order terms in the Taylor series expansion in $As[n]$,

$$\ln L_G = \sum_{n=0}^{N-1} \ln\left[1 - \frac{p'}{p}(x[n])A\cos(2\pi n/N + \phi)\right] > \ln\gamma. \quad (2.192)$$

Taking the Taylor expansion about zero, we get

$$\begin{aligned} \ln L_G &= -\left[\sum_{n=0}^{N-1} \frac{p'}{p}(x[n])\cos(2\pi n/N + \phi)\right] A + \left[\sum_{n=0}^{N-1} \left(\frac{p'}{p}(x[n])\right)^2 \cos^2(2\pi n/N + \phi)\right] A^2, \\ &= -\left[\sum_{n=0}^{N-1} \frac{p'}{p}(x[n])\cos(2\pi n/N + \phi)\right] A + \frac{NA^2}{2}. \end{aligned} \quad (2.193)$$

As in the previous section this expression can be re-written as the quadratic

$$\ln L_G(\mathbf{x}) = -A\left[B_1\cos\phi - B_2\sin\phi\right] + \frac{NA^2}{2}, \quad (2.194)$$

where $B_1 = \sum_{n=0}^{N-1} \frac{p'}{p}(x[n])\cos(2\pi n/N)$ and $B_2 = \sum_{n=0}^{N-1} \frac{p'}{p}(x[n])\sin(2\pi n/N)$. This can be further re-written as

$$\ln L_G(\mathbf{x}) = -AB + NA^2/2, \quad (2.195)$$

where $B = \hat{B}\cos(\phi - \beta)$, $\hat{B} = (B_1^2 + B_2^2)^{1/2}$ and $\beta = \tan^{-1}(-B_2/B_1)$. The above quadratic in A can be rewritten as follows,

$$\ln L_G = \frac{N}{2}\left[A^2 - 2A\frac{B}{N}\right] = \frac{N}{2}\left[\left(A - \frac{B}{N}\right)^2\right] - B^2/2N. \tag{2.196}$$

Since A and B are indeterminate, we can say that the infimum of the above expression is given by $B^2/2N$ which again is upper bounded by $(B_1^2 + B_2^2)/2N$. Therefore, the test statistic can be taken to be

$$T(\mathbf{x}) = \left(\sum_{n=0}^{N-1} \frac{p'}{p}(x[n])\cos(2\pi n/N)\right)^2 + \left(\sum_{n=0}^{N-1} \frac{p'}{p}(x[n])\sin(2\pi n/N)\right)^2. \tag{2.197}$$

This test statistic will be used in chapter 3 of this thesis to quantify the effectiveness of detectors based on the principle of stochastic resonance. On this note, we can conclude our short digression into statistical detection theory.

2.7 The theory of Beaulieu series

A recurring problem in many signal processing and communication applications is that of determining the probability density function, or equivalently the complementary distribution function, of a sum of independent random variables (RVs) each of which is governed by a given distribution function. In this chapter we outline a convergent infinite series for the computation of the complementary probability distribution function (CDF) of a sum of independent RVs. This series expansion was derived by N. C. Beaulieu [9] and has been subsequently named after its originator. It has been widely used in various areas of communication such as detection, equalization, synchronization, interference analysis and modulation. The derivation of Beaulieu series applies more generally to sums of independent RVs which do not possess the same distribution. Therefore, we outline the derivation of the infinite series when the RVs are required only to be independent. The theory is developed by first considering bounded RVs (in Sec.(2.7.1)) and then extended to the case of unbounded RVs (in Sec.(2.7.3)), as done by Beaulieu in his seminal paper [9].

2.7.1 The infinite series for bounded random variables

Beaulieu's original approach to the problem in question consisted of casting the CDF of the sum of random variables in terms of an appropriate transformation of the periodic

square wave [9]. This is manifest by the fact that the Fourier coefficients of the square wave form the "weights" in this series expansion. Before retracing this derivation some terminology will be necessary.

Let $X_i, i = 1 \ldots L$ be bounded independent RVs each with a probability density function (PDF) $f_{X_i}(x)$. Each of the random variables are assumed to be upper and lower bounded, implying $f_{X_i}(x) = 0$ for all $x_i > B_i^U$ and for all $x_i < B_i^L$. We choose to denote the sum of the L independent random variables by $X, X = \sum_{i=1}^{L} X_i$, the complementary distribution function of X by $G_X(x)$ and the PDF of X by $f_X(x)$. It follows that X is lower bounded by $B_L = \sum_{i=1}^{L} B_i^L$ and upper bounded by $B_U = \sum_{i=1}^{L} B_i^U$. Also we choose to denote the periodic square wave by $S(x)$ as follows

$$S(x) = \begin{cases} 0 & \text{for } -T/2 < x < 0 \\ 1/2 & \text{for } 0 < x < T/2 \\ 1 & \text{for } x = \pm T/2 \end{cases} \tag{2.198}$$

$$S(x + mT) = S(x), m = 0, \pm 1, \pm 2, \ldots \tag{2.199}$$

By definition of the CDF it follows that

$$G_X(\epsilon L) = Pr(X \geq \epsilon L) = E[S(X - \epsilon L)], \tag{2.200}$$

where $E[X]$ denotes the expected value of X. Eq.(2.200) is valid for $T/2 = \max[B_U - \epsilon L, \epsilon L - B_L]$ when the PDF does not have an impulse at a discontinuity of $S(X - \epsilon L)$. The square wave $S(x)$ has the Fourier series representation [18] given by

$$S(x) = \frac{1}{2} + \sum_{n=\infty, odd}^{\infty} C_n e^{jn\omega x} \text{ for } C_n = \tfrac{1}{\pi n j} \tag{2.201}$$

where $\omega = 2\pi/T$. The equality in Eq.(2.201) is in the mean square sense, and pointwise convergence is guaranteed by a Fourier theorem [27]. Combining Eqs.(2.200) and (2.201) we get

$$\begin{aligned} G_X(\epsilon L) &= \frac{1}{2} + \sum_{n=\infty, odd}^{\infty} C_n E[e^{jn\omega(X - \epsilon L)}], \\ &= \frac{1}{2} + \sum_{n=1, odd}^{\infty} \frac{E[e^{jn\omega(X-\epsilon L)}] - E[e^{-jn\omega(X-\epsilon L)}]}{n\pi j}, \\ &= \frac{1}{2} + \sum_{n=1, odd}^{\infty} \frac{E[\exp\{jn\omega(\sum_{i=1}^{L} X_i - \epsilon L)\}] - E[\exp\{-jn\omega(\sum_{i=1}^{L} X_i - \epsilon L)\}]}{n\pi j}, \end{aligned}$$

$$
\begin{aligned}
&= \frac{1}{2} + \sum_{n=1,odd}^{\infty} \frac{\prod_{i=1}^{L} E[e^{jn\omega(X_i-\epsilon)}] - \prod_{i=1}^{L} E[e^{-jn\omega(X_i-\epsilon)}]}{n\pi j}, \\
&= \frac{1}{2} + \sum_{n=1,odd}^{\infty} \frac{\left\{\prod_{i=1}^{L} A_{in} e^{j\Theta_{in}}\right\} - \left\{\prod_{i=1}^{L} A_{in} e^{-j\Theta_{in}}\right\}}{n\pi j}, \\
&= \frac{1}{2} + \sum_{n=1,odd}^{\infty} \frac{\left\{\prod_{i=1}^{L} A_{in}\right\}\left(e^{j\sum_{i=1}^{L}\Theta_{in}}\right) - \left\{\prod_{i=1}^{L} A_{in}\right\}\left(e^{-j\sum_{i=1}^{L}\Theta_{in}}\right)}{n\pi j}, \\
&= \frac{1}{2} + \sum_{n=1,odd}^{\infty} \frac{A_n e^{j\Theta_n} - A_n e^{-j\Theta_n}}{n\pi j}, \\
&= \frac{1}{2} + \frac{2}{\pi} \sum_{n=1,odd}^{\infty} \frac{A_n \sin(\Theta_n)}{n}, \qquad (2.202)
\end{aligned}
$$

where

$$
\begin{aligned}
A_{in} &= \sqrt{\{E[\cos(n\omega X_i)]\}^2 + \{E[\sin(n\omega X_i)]\}^2}, \\
\Theta_{in} &= \tan^{-1}\left(\frac{E[\sin(n\omega(X_i-\epsilon))]}{E[\cos(n\omega(X_i-\epsilon))]}\right), \qquad (2.203)
\end{aligned}
$$

and

$$
\begin{aligned}
A_n &= \prod_{i=1}^{L} A_{in}, \\
\Theta_n &= \sum_{i=1}^{L} \Theta_{in}. \qquad (2.204)
\end{aligned}
$$

In the case of L iid RVs, Eqs.(2.202-2.204) simplifies to

$$
G_X(\epsilon L) = \frac{1}{2} + \frac{2}{\pi} \sum_{n=1,odd}^{\infty} \frac{A_{in} \sin(\Theta_n)}{n}, \qquad (2.205)
$$

where A_{in} and Θ_{in} are independent of i and are given by Eqs.(2.203) and (2.204) respectively. The characteristic function of the RV X_i be denoted by $\phi_i(\nu) = E[e^{j\nu X_j}]$. Then Eq.(2.202) can be re-written in terms of the characteristic functions

$$
G_X(\epsilon L) = \frac{1}{2} + \sum_{n=1,odd}^{\infty} \frac{\prod_{i=1}^{L} \phi_i\left(\frac{2\pi n}{T}\right)\left(e^{-j\frac{2\pi n\epsilon L}{T}}\right) \prod_{i=1}^{L} \phi_i\left(-\frac{2\pi n}{T}\right)\left(e^{j\frac{2\pi n\epsilon L}{T}}\right)}{n\pi j} \qquad (2.206)
$$

or the characteristic function of the sum, denoted by $\phi(\nu)$, as follows

$$G_X(\epsilon L) = \frac{1}{2} + \sum_{n=1,odd}^{\infty} \frac{\prod_{i=1}^{L} \phi\left(\frac{2\pi n}{T}\right)\left(e^{-j\frac{2\pi n \epsilon L}{T}}\right) \prod_{i=1}^{L} \phi\left(-\frac{2\pi n}{T}\right)\left(e^{j\frac{2\pi n \epsilon L}{T}}\right)}{n\pi j}, \quad (2.207)$$

which shows that the CDF can be found using Eq.(2.202) if the characteristic function is known at countably many uniformly spaced points. The infinite series in Eq.(2.202) can be used, to compute the complementary distribution function of the sum of L independent random variables. In general, the terms of the series may decrease faster than $1/n$ because the quantities A_n and $\sin(\theta_n)$ may decrease with increasing n. Since $|\phi(\nu)| < \phi(0) = 1$ [132] the convergence rate of the series is often better for larger values of L. It may be noted that the convergence of the series to impulsive PDFs has been poor [9]. In this thesis such impulsive PDFs will not be considered for discussion.

2.7.2 Bounds for truncation error

In practical implementations infinite series expansions as given in Eqs.(2.205,2.206) and (2.207) have to be truncated after a certain threshold. This threshold is determined from the required accuracy of the algorithm. Therefore, we now proceed to derive a bound for the truncation error for the case where the PDF of X is not impulsive. As will be shown, this error can be made arbitrarily small by including large enough terms in the summation. Let S_N denote the partial sum of order N:

$$S_N = \frac{1}{2} + \frac{2}{\pi} \sum_{n=1,odd}^{N} \frac{A_n \sin(\Theta_n)}{n} \quad (2.208)$$

and let R_N denote the corresponding remainder

$$R_N = \frac{2}{\pi} \sum_{n=N+2,odd}^{\infty} \frac{A_n \sin(\Theta_n)}{n} \quad (2.209)$$

where N is odd. Then the CDF of X evaluated at ϵL, $G_X(\epsilon L)$ may be upper and lower bounded using Eqs.(2.200) and (2.202),

$$S_N - |R_N| \leq G_X(\epsilon L) \leq S_N + |R_N|. \quad (2.210)$$

These bounds are preserved if $|R_N|$ is replaced by an upper bound B_R such that $|R_N| \leq B_R$, whereby

$$S_N - B_R \leq G_X(\epsilon L) \leq S_N + B_R. \tag{2.211}$$

Using Eqs.(2.198,2.200,2.201,2.208) and (2.209) we get

$$|R_N| = |E\left[\sum_{n=-\infty,odd}^{-N-2} \frac{e^{jn\omega(X-\epsilon L)}}{\pi nj} + \sum_{n=odd,N+2}^{\infty} \frac{e^{jn\omega(X-\epsilon L)}}{\pi nj}\right]|. \tag{2.212}$$

Let

$$D_{N+1} = \sum_{n=-\infty,odd}^{-N-2} \frac{e^{jn\omega(X-\epsilon L)}}{\pi nj} + \sum_{n=odd,N+2}^{\infty} \frac{e^{jn\omega(X-\epsilon L)}}{\pi nj} \tag{2.213}$$

and

$$E_{N+1} = \sum_{n=-\infty,odd}^{-N-2} \frac{e^{jn\omega x}}{\pi nj} + \sum_{n=odd,N+2}^{\infty} \frac{e^{jn\omega x}}{\pi nj}, \tag{2.214}$$

then we may derive through repeated use of Schwarz's inequality [132]

$$\begin{aligned}
|R_N| &= |\int_{-T/2}^{T/2} f_X(x) D_{N+1}(x) dx| \\
&\leq \left(\int_{-T/2}^{T/2} f_X(x) dx \int_{-T/2}^{T/2} f_X(x) |D_{N+1}(x)|^2\right)^{1/2} \\
&= \left(\int_{-T/2}^{T/2} f_X(x) |D_{N+1}(x)|^2\right)^{1/2} \\
&\leq \left((\sup f_X(x)) \int_{-T/2}^{T/2} |D_{N+1}(x)|^2\right)^{1/2} \\
&\leq \left((\sup f_X(x)) \int_{-T/2}^{T/2} (E_{N+1}(x))^2\right)^{1/2}
\end{aligned} \tag{2.215}$$

In the above sup denotes supremum over the real line. The last equality follows from the orthogonality of the series basis functions on the interval $[-T/2, T/2]$. If $f_X(x)$ has no impulses, it follows that $\sup f_X(x) < \infty$. It then follows that there is at least one $i, i = 1, \ldots, L$ such that $\sup f_{X_i}(x_i) < \infty$. It can then be shown that $\sup f_X(x) < \sup f_{X_i}(x_i)$

for all $i = 1, 2, \ldots L$ [9]. Thus

$$|R_N| \leq \left((\sup f_{X_i}(x_i)) \int_{-T/2}^{T/2} (E_{N+1}(x))^2 dx \right)^{1/2} = B_R. \tag{2.216}$$

Since the Fourier series of Eq.(2.201) converges in the mean to $S(x)$ given in Eq.(2.198), we get as in [27]

$$\lim_{N\to\infty} \int_{-T/2}^{T/2} (E_{N+1}(x))^2 dx = 0. \tag{2.217}$$

The preceding results imply that the CDF can be computed as accurately as desired by including a sufficient number of terms in the series Eq.(2.208). A more convenient form of the result Eq.(2.216) can be obtained by using the relation [27]

$$\frac{1}{T} \int_{-T/2}^{T/2} (E_{N+1}(x))^2 dx = \frac{1}{T} \int_{-T/2}^{T/2} (S(x))^2 dx - \sum_{n=-N, noddorn=0}^{N} |C_n|^2, \tag{2.218}$$

which along with Eq.(2.216) and Eq.(2.201),

$$|R_N| \leq B_R = \left[\min_{i=1,\ldots,L} \{\sup f_{X_i}(x_r)\} \left(\frac{T}{4} - \frac{2T}{\pi^2} \sum_{n=1,odd}^{\infty} \frac{1}{n^2} \right) \right]^{1/2}. \tag{2.219}$$

This form shows that $\lim_{N\to\infty} B_R = 0$, since $\sum_{n=1,odd}^{\infty} \frac{1}{n^2} = \frac{\pi^2}{8}$. It is observed that B_R decreases monotonically with increasing N.

2.7.3 The infinite series for unbounded random variables

In the preceding section we considered a sum of bounded RVs. In this section we will generalize the results to sums of unbounded RVs. We will then apply this series to the benchmark case of a sum of Gaussian RVs in order to verify the technique.

We proceed as follows. It is assumed that the RVs X_i and their sum X are unbounded. Furthermore, on the grounds that the CDF is a bounded nondecreasing function of its argument, it is assumed that B_L and B_U can be chosen such that $\Pr(X < B_L)$ and $\Pr(X < B_L)$ are "negligible". As before, let the $\{X_i\}$ be independent RVs and let $T/2 = \max[B_U - \epsilon L, \epsilon L - B_L]$. The probability of a random variable exceeding a certain bound can be rewritten as

$$Pr(X \geq \epsilon L) = 0 \times [Pr(X < \epsilon L)] + Pr(X \geq \epsilon L)$$

and on some rearrangement it follows that

$$Pr(X \geq \epsilon L + T/2) + E([S(X - \epsilon L)] \geq Pr(X \geq \epsilon L) \geq E([S(X - \epsilon L)] - Pr(X \geq \epsilon L - T/2).$$

As $T \to \infty$, $Pr(X \geq \epsilon L) = G_X(\epsilon L) \to E([S(X - \epsilon L)]$ since $Pr(X < \epsilon L - T/2) \to 0$ and $Pr(X \geq \epsilon L - T/2) \to 0$. Therefore, we use $E([S(X - \epsilon L])$ as an approximation of $G_X(x)$. The error Δ resulting from this truncation is

$$\Delta = E([S(X - \epsilon L]) - G_X(\epsilon L). \tag{2.220}$$

Combining with Eqs.(2.198,2.200) and (2.220) we get

$$|\Delta| \leq \max\left[G_X(\epsilon L + T/2), G_X(\epsilon L - T/2)\right].$$

For symmetric distributions and for one-sided distributions the following relations hold respectively: $G_X(x) = 1 - G_X(-x)$ and $G_X(x) = 0 \forall x < 0$. In both cases Eq.(2.221) simplifies to

$$|\Delta| \leq \max\left[G_X(\epsilon L + T/2), G_X(T/2 - \epsilon L)\right].$$

or equivalently,

$$|\Delta| \leq G_X(\epsilon L + T/2)$$

where $B_L = 0$ for a one-sided distribution. The error Δ can be bounded using the Chernoff bound. In addition to the error Δ there is also an error resulting from series truncation. From Eq.(2.221) we get

$$E([S(X - \epsilon L]) = \Delta + G_X(\epsilon L) = S_N + R_N \tag{2.221}$$

which implies that

$$S_N - |R_N| - |\Delta| \leq G_X(\epsilon L) \leq S_N + |R_N| + |\Delta|. \tag{2.222}$$

The earlier upper bounds derived for sums of RVs in Eqs.(2.216) and (2.219) remain valid for sums of unbounded RVs. Thus, the series in Eqs.(2.202) and (2.207) can be used to compute the $G_X(\epsilon L)$ for sums of unbounded RVs. The error incurred from domain

truncation is upper bounded by

$$|error| \leq B_R + |\Delta|. \tag{2.223}$$

Now we will apply the technique to a sum of L zero-mean unit-variance Gaussian Random variables (RVs). For a zero-mean, unit-variance Gaussian RV, X_i we get

$$\begin{aligned} E[\cos(n\omega(X_i - \epsilon))] &= \int_{-\infty}^{\infty} \frac{1}{\sqrt{2\pi}} e^{-x^2/2} \cos(n\omega(x-\epsilon))dx, \\ &= e^{-n^2\omega^2/2} \cos(n\omega\epsilon), \\ E[\sin(n\omega(X_i - \epsilon))] &= \int_{-\infty}^{\infty} \frac{1}{\sqrt{2\pi}} e^{-x^2/2} \sin(n\omega(x-\epsilon))dx, \\ &= -e^{-n^2\omega^2/2} \sin(n\omega\epsilon), \end{aligned} \tag{2.224}$$

and using (2.202)

$$\begin{aligned} A_n &= e^{-n^2\omega^2/2}, \\ \theta_n &= -n\omega\epsilon. \end{aligned} \tag{2.225}$$

The series for the CDF of the sum of L zero-mean unit-variance Gaussian RVs can be expressed using Eqs.(2.205) and (2.225) as follows

$$G_X(\epsilon L) = \frac{1}{2} - \frac{2}{\pi} \sum_{n=1,odd}^{\infty} \frac{e^{-n^2\omega^2 L/2}}{n} \sin(n\omega\epsilon L). \tag{2.226}$$

Questions of numerical accuracy and convergence have been addressed in [9].

Chapter 3

Stochastic resonance in hard-threshold devices

3.1 Introduction

The phenomenon of stochastic resonance refers to a coupling between deterministic driving signals and random fluctuations observed in certain nonlinear dynamical systems whereby deterministic effects are amplified. Originally, stochastic resonance was studied in threshold systems driven by weak, sub-threshold signals. A study of this phenomenon in quantizers is given in [20, 25]. In that and subsequent works quantizers have since been shown to demonstrate an improvement over conventional matched filters for the detection of signals corrupted by non-Gaussian noise [20, 22, 23, 24, 25, 47, 54, 201, 202]. For reviews of quantization the reader is referred to [12, 57]. Such a quantizer-detector was designed for the detection of weak, sinusoidal signals in a marine environment [155]. Physically, this corresponds to a remote target to be detected. The detector consists of a stochastic resonant quantizer followed by a correlator. The SNR gain must be optimized in the appropriate asymptotic limit, ensuring that the detector works in the peak of its stochastic resonant regime. Hence, we refer to it as the stochastic resonant (SR) detector. SR detectors have the following advantage. It is well-known that [87] a quadrature or incoherent matched filter is the optimal detector if a signal with unknown amplitude/ phase is buried in Gaussian noise. Here, optimality refers to maximization of the probability of detection constrained by a fixed probability of false alarm. The matched filter though easy to implement and analyze, is not optimal under conditions of non-Gaussian noise prevalent in marine environments. Optimal detectors in non-Gaussian noise are nonlinear and are not easy to implement. Hence, suboptimal nonlinear detectors which

are easier to implement are often employed for the detection of signals in non-Gaussian noise. If the SNR gain is greater than unity, a combination of the SR system and a matched filter will yield a detection performance that is better than that of the matched filter alone [21]. While conventional studies of stochastic resonance search for the optimal noise level, keeping the system fixed [47, 25], in detection schemes the problem is reversed; the system parameters are optimized for a given noise level and type. This has been demonstrated by Chapeau-Blondeau for the detection of pulse trains using quantizers with optimizable thresholds [22].

In this chapter we follow a similar approach. The results are presented as follows. In Section 3.2, properties of stochastic resonance demonstrated by quantizers and their utility in signal detection are discussed qualitatively. It is shown that the maximum SNR gain is less than unity if the input noise is Gaussian, but the SNR gain can exceed unity if the noise is non-Gaussian. In Section 3.3, an algorithm for optimizing the SNR gain of the symmetric 3-level quantizer is developed, and is applied to mixture-of-Gaussian noise PDFs. In Section 3.4, the monotonic dependence of the receiver operating characteristics on the SNR gain is established. It is also observed that if the noise PDF belongs to a sub-class of the Gaussian mixture family, the asymptotic performance of the quantizer-detector is significantly better than that of the matched filter but not as good as that of the optimal nonlinear detector. Section 3.5 presents perturbative corrections due to (i) small input SNR R_{in} and (ii) minute temporal variations in the probability density function (PDF) governing the noise of the ocean. Section 3.7 contains an outline of the hardware implementation of such an SR detector. Section 3.8 contains the conclusions and future directions of work. The issue of relative stability of 2-level and 3-level quantizers is addressed in [156]. The performance of an SR detector for generalized Gaussians is given in [155].

3.2 Review: Stochastic resonance in 3-level quantizers

Our treatment of quantizers exhibiting stochastic resonance in rooted in the SNR Gain formalism given in [25]. We consider a symmetric 3-level quantizer with thresholds $-v_t, v_t$ and quantization levels $-1, 0, 1$. If the quantizer is driven by a sequence $x[n]$, the output

sequence $y[n]$ is given by the relation

$$y[n] = \begin{cases} -1 & \text{for} \quad x[n] \leq -v_t \\ 0 & \text{for} \quad -v_t < x[n] \leq v_t \\ 1 & \text{for} \quad x[n] > v_t \end{cases} \tag{3.1}$$

The input $x[n]$ is assumed to be the sum of an N-periodic sinusoidal signal with a known frequency but unknown phase and a zero-mean additive noise with variance σ^2. The input sequence can then be written as

$$x[n] = A_1 \cos\left(2\pi n/N - \phi\right) + \sigma w[n] \tag{3.2}$$

where $w[n]$ are zero-mean, unit-variance independent and identically distributed (iid) random variable with probability density function $f(x)$ and cumulative distribution function $F(x)$. The incoming signal $s[n]$ is assumed to be subthreshold such that $A_1 \leq v_t$. In the absence of input noise, the output $y[n]$ remains unchanged at the initial state. When noise is also present at the input, the output exhibits random transitions from one state to another. For a sinusoidal signal we need to consider the output SNR at the 1^{st} harmonic alone, which as discussed in [25] is given by

$$SNR_{out} = \frac{|Y_1|^2}{\overline{\sigma_y^2}} \tag{3.3}$$

where Y_1 is the 1^{st} Fourier coefficient of the sequence $E(y[n])$ and $\overline{\sigma_y^2}$ is the average of the sequence $\sigma_y^2[n]$, and are given by

$$\begin{aligned} Y_1 &= \frac{1}{N} \sum_{n=0}^{N-1} E(y[n]) \exp(j2\pi n/N) \\ \overline{\sigma_y^2} &= \frac{1}{N} \sum_{n=0}^{N-1} \sigma_y^2[n] \end{aligned} \tag{3.4}$$

Similarly the input SNR is defined as:

$$SNR_{in} = \frac{A_1^2}{4\sigma^2} \tag{3.5}$$

It may be noted that the output SNR depends on the input signal waveform and the input noise probability density function. On the other hand, the input SNR depends only on the input signal amplitude and the input noise variance. The SNR gain of such

a threshold system $\widetilde{G}$, as defined in [20], is given by

$$G = \frac{SNR_{out}}{SNR_{in}} \tag{3.6}$$

From Eqs.(3.3,3.4) and (3.5) it then follows

$$G = \frac{4\sigma^2|Y_1|^2}{A_1^2\overline{\sigma_y^2}}. \tag{3.7}$$

Claim 1: *For a symmetric 3-level quantizer with thresholds $-v_t, v_t$ and quantization levels $-1, 0, 1$, driven by a weak, subthreshold signal ($A_1 \ll v_t$ and $A_1 \ll \sigma$) and noise governed by a symmetric PDF, the SNR gain then has the following Taylor series expansion to the first nonvanishing power of A,*

$$\widetilde{G}(x) = G(x) + g_1(x)A^2 + O(A^4), \tag{3.8}$$

where the dominant term is given by

$$G(x) = \frac{2f^2(x)}{1-F(x)} \tag{3.9}$$

and the 1^{st} nonvanishing correction, subdominant to $G(x)$, can be written as

$$g_1(x) = \frac{1}{2}\left(\frac{f(x)f''(x)}{1-F(x)}\right) + \frac{1}{4}\left(\frac{f'(x)+4f^2(x)}{1-F(x)}\right)G(x). \tag{3.10}$$

Proof: For a 3-level quantizer with symmetric quantizer thresholds and levels, the expectation and variance of the output sequence $y[n]$ are given by

$$\begin{aligned} E[y(n)] &= P(y[n]=1) - P(y[n]=-1), \\ &= 1 - F(x - Ac_n) - F(-x - Ac_n), \\ \sigma_y^2[n] &= P(y[n]=1) + P(y[n]=-1) - \{E[y[n]]\}^2, \\ &= 1 - F(x - Ac_n) + F(-x - Ac_n) - \{E[y[n]]\}^2. \end{aligned}$$

where

$$A = A_1/\sigma, \quad x = v_t/\sigma, \quad c_n = \cos(2\pi n/N - \phi). \tag{3.11}$$

In deriving the above relations we have used Eqs.(3.1,3.2) and the following intermediate

relations

$$\begin{aligned} P(y[n]=1) &= P(x[n]>v_t) = P(A_1c_n+\sigma w_n > v_t) = P(w_n > (v_t - Ac_n)/\sigma) \\ &= P(w_n > x - Ac_n) = 1 - F(x - Ac_n), \\ P(y[n]=-1) &= P(x[n] \le v_t) = P(A_1c_n+\sigma w_n \le -v_t) = P(w_n \le (-v_t - Ac_n)/\sigma) \\ &= P(w_n > -x - Ac_n) = F(-x - Ac_n). \end{aligned} \tag{3.12}$$

The parameter x, referred to henceforth as the *normalized threshold* is the ratio of the normalized threshold v_t to the noise standard deviation σ. For the nondegenerate and degenerate forms of Eq.(3.1), v_t is positive and zero, respectively. Therefore, it follows that x is always non-negative. To include the first non-vanishing power of A in the quantities above, we take the Taylor series expansion to 2^{nd} order about x, to get

$$\begin{aligned} E[y(n)] &= F(x+Ac_n) - F(x-Ac_n), \\ &= 2f(x)Ac_n + \frac{f''(x)}{3}(Ac_n)^3 + O(A^5), \\ \sigma_y^2[n] &= 2 - F(x+Ac_n)] - F(x-Ac_n) - \{E[y[n]]\}^2, \\ &= 2[1-F(x)] - (f'(x)+f^2(x))(Ac_n)^2 + O(A^4). \end{aligned}$$

Substituting the above expressions into the SNR gain defined in Eqs.(3.4) and (3.7) and keeping only terms to the first order, we then get the following expansion

$$\begin{aligned} \widetilde{G}(x) &= \left[\frac{2f^2(x)}{1-F(x)} + \frac{1}{2}\left(\frac{f(x)f''(x)}{1-F(x)}\right)A^2\right]\left[1 - \frac{1}{4}\left(\frac{f'(x)+4f^2(x)}{1-F(x)}\right)A^2\right]^{-1}, \\ &= \frac{2f^2(x)}{1-F(x)} + \left[\frac{1}{2}\left(\frac{f(x)f''(x)}{1-F(x)}\right) + \frac{2f^2(x)}{1-F(x)}\frac{1}{4}\left(\frac{f'(x)+4f^2(x)}{1-F(x)}\right)\right]A^2 \ (QED). \end{aligned}$$

3.3 The unperturbed functional $G(x)$

In the weak signal limit, when $R_{in} \ll 1$, the expansion of the gain in Eq.(3.8) has an appealing and useful explanation in perturbation theory,

1. $G(x)$, the unperturbed functional, dominates the 'landscape' of $\widetilde{G}(x)$, and therefore largely determines the maxima of the gain, and the values of the normalized threshold (x) where they are attained.

2. $g_1(x)$, the first order perturbing functional, contributes small corrections of $O(A^2)$ thereupon.

The unperturbed functional $G(x)$ attains its local maxima at

$$\left\{x : \frac{dG}{dx} = 0 \text{ and } \frac{d^2G}{dx^2} < 0\right\}. \tag{3.13}$$

From Eq.(3.9) it follows

$$\frac{dG}{dx} = \frac{2f(x)}{(1-F(x))^2}C(x), \tag{3.14}$$

where $C(x)$ is the characteristic function defined as

$$C(x) = 2[1-F(x)]f'(x) + f^2(x). \tag{3.15}$$

At maxima/minima of the gain, where $\frac{dG}{dx} = 0$, it then follows

$$\frac{d^2G}{dx^2} = \frac{2f(x)}{1-F(x)}f''(x). \tag{3.16}$$

Equivalently, $G(x)$ is locally maximized at

$$\left\{x : C(x) = 0 \text{ and } f''(x) < 0\right\}. \tag{3.17}$$

Thus, finding the local maxima of $G(x)$ has reduced to the simpler algebraic problem of finding the zeros of $C(x)$. This observation helps us derive a few important qualitative properties of the unperturbed functional $G(x)$.

3.3.1 Existence of critical points

Lemma 1 (Existence): *In the real half-line R^+, there exists at least one critical point of $G(x)$.*

Proof: Assuming $f(x)$ to be positive definite, we can take the exponential form of the PDF, so that;

$$f(x) = e^{P(x)}. \tag{3.18}$$

Therefore, $f'(x) = P'(x)e^{P(x)}$ and $1 - F(x) = \int_x^\infty e^{P(u)}du$. Multiply and divide the right-hand side by $P'(x)$ and then integrate by parts to get

$$\begin{aligned} 1-F(x) &= \int_x^\infty \frac{1}{P'(u)}\left(P'(u)e^{P(u)}\right)du = \int_x^\infty \frac{1}{P'(u)}\left(\frac{d}{du}e^{P(u)}\right)du \\ &= \int_x^\infty \frac{d}{du}\left(\frac{1}{P'(u)}e^{P(u)}\right)du - \int_x^\infty \left(\frac{d}{du}\frac{1}{P'(u)}\right)e^{P(u)}du \end{aligned}$$

$$= -\frac{1}{P'(x)}e^{P(x)} + \int_x^\infty \frac{P''(u)}{P'^2(u)}e^{P(u)}du.$$

We now introduce the modified characteristic function defined as

$$\begin{aligned}\widetilde{C}(x) &= C(x)/f^2(x), \\ &= 2\frac{[1-F(x)]f'(x)}{f^2(x)} + 1. \end{aligned} \tag{3.19}$$

Since the denominator is positive definite, the functions $C(x)$ and $\widetilde{C}(x)$ have the same set of zeros. From Eq.(3.18) and Eq.(3.19), the modified characteristic function reduces to

$$\begin{aligned}\widetilde{C}(x) &= \left[2P'(x)e^{-P(x)}\int_x^\infty \frac{P''(u)}{P'^2(u)}e^{P(u)}du - 1\right], \\ &= \left[2\int_x^\infty \frac{P''(u)}{P'^2(u)}e^{P(u)}du \Big/ \left(\frac{e^{P(x)}}{P'(x)}\right) - 1\right].\end{aligned}$$

As the terms in the numerator and denominator approach zero as $x \to \infty$ we may use l'Hospital's rule, and then rearrange, to obtain

$$\widetilde{C}(x) = \left[2\frac{P''(x)}{P''(x) - P'^2(x)} - 1\right].$$

If we assume $P(x) \sim -x^{1+\alpha}$ where $\alpha > 1$ (this assumption is valid for generalized Gaussians with $p > 1$ and mixtures of Gaussians), then we have, $P'(x) \sim -(1+\alpha)x^\alpha$ and $P''(x) \sim -(1+\alpha)\alpha x^{\alpha-1}$. Therefore, it follows $\frac{P''(u)}{P''(u)-P'^2(x)} \sim \frac{\alpha}{1+\alpha}x^{-(1+\alpha)}$ which $\to 0$ as $x \to \infty$ $\forall \alpha > 0$. Thus, for all PDFs considered here

$$\lim_{x\to\infty} \widetilde{C}(x) = -1.$$

Similarly, for symmetric differentiable PDFs $f'(0) = 0$, and therefore $\widetilde{C}(0) = 1$. Since $\widetilde{C}(x)$ is a continuous function, by the intermediate value theorem [152] it must have at least one zero crossing. It follows that $G(x)$ must have at least one critical point (*QED*).

3.3.2 Non-uniqueness of critical points

Unfortunately, the uniqueness of critical points cannot be assured. This reflects the fact that $G(x)$ need not be unimodal. Deterministic global optimization algorithms for multimodal functions exist [13], but are computationally intensive. However, using some additional properties of the unperturbed functional $G(x)$, we can develop a more efficient

deterministic algorithm, the basic premise of which reads:

1. The positive real half-line (R^+) can be partitioned into disjoint intervals on which G is unimodal. These intervals can be found from the zeros of $f''(x)$, which can be calculated from detailed phenomenological studies of marine noise ([110, 140] and references therein). On each such interval, the necessarily unique maximum/minimum can be found using classical techniques (Newton's, Bisection), thereby greatly improving computational efficiency.

2. The global maximum can then be found by taking the maximum from the resulting set of local maxima/minima.

Thus, we are using *a priori* information to develop an algorithm which is necessarily specific to our problem, but is more efficient than its more generic alternative. Towards this goal, we derive a few preliminary results.

Claim 2: *At any critical point x, and in the limit as $x \to \infty$ the following equality holds*

$$G(x) = B(x), \tag{3.20}$$

where the 'Bounding function' $B(x)$ is defined as

$$B(x) = -4f'(x). \tag{3.21}$$

Proof: If x is a critical point, from Eqs.(3.14,3.15) and the assumed positivity of $f(x)$ (i.e. $f(x) > 0$), it follows that $C(x) = 0$. This equality and Eq.(3.15) gives

$$\frac{f^2(x)}{1 - F(x)} = -2f'(x).$$

Substituting in Eq.(3.9) this gives us

$$G(x) = -4f'(x) = B(x) \qquad \forall\, x : G'(x) = 0.$$

In the limit as $x \to \infty$ the numerator and denominator of Eq.(3.9) are vanishingly small. We may apply l'Hospital's rule to Eq.(3.9), which gives us, for large x:

$$\lim_{x\to\infty} G(x) = -4f'(x) = B(x) \quad (QED).$$

In qualitative terms, $G(x)$ closely 'follows' the Bounding function $B(x)$, intersecting it at all critical points and then approaching it asymptotically. A deeper link between the

functions $G(x)$ and $B(x)$ exists, as we shall now show. The zeros of $f''(x)$ and $B'(x)$ are identical and are assumed to occur at isolated points (i.e. we assume $f''(x)$ and therefore $B'(x)$ does not vanish identically over an interval). Furthermore, we assume these points are finitely many. These assumptions are satisfied by both generalized Gaussians and mixtures of Gaussians. Then we can define an ordered set of zeros of $f''(x)$ (or $B(x)$) as follows: $Z_B = \{a_1, a_2, ...a_N\}$ or

$$Z_B = \{a_j\} \quad j = 1, \ldots, N. \tag{3.22}$$

These zeros or roots can be found from phenomenological studies of governing noise PDFs [110, 140]. This induces the following sequence of disjoint intervals:

$$I_B = \{I_j\} \quad j = 0, \ldots, N, \tag{3.23}$$

where

$$\begin{aligned} I_0 &= [0, a_1], \\ I_j &= [a_j, a_{j+1}] \quad j = 1, \ldots, N-1, \\ I_N &= [a_N, \infty). \end{aligned} \tag{3.24}$$

It is observed $R^+ = \bigcup_{j=0}^{N} I_j$. The intervals in I_B thus form a partition of R^+.

Claim 3: *Any point in the interior of an interval $I_j \in I_B$ where $G'(x) = 0$, must correspond to a local maximum/minimum of $G(x)$.*

Proof: Any point where $G'(x)$ vanishes must correspond to a (i) a local maximum/ minimum ($G''(x) \neq 0$) or (ii) an inflection point ($G''(x) = 0$). At an inflection point by Eqs.(3.14,3.16,3.21), $C(x) = 0$ and $f''(x) = B'(x) = 0$. So x must be an element of Z_B and cannot be in the interior of any interval $I_j \in I_B$. This contradicts our starting assumption. Hence, x must be a local maximum/ minimum of $G(x)$ (QED).

Claim 4: *Let x_1, x_2 be successive local maxima/minima of $G(x)$. The interval (x_1, x_2) contains a zero of $f''(x)$.*

Proof: The expression for G'' at local maxima/ minima is given in Eq.(3.16). Assume without loss of generality, that $G''(x_1) < 0$ and $G''(x_2) > 0$. Therefore $f''(x_1) < 0$ and $f''(x_2) > 0$. By the intermediate value theorem the interval (x_1, x_2) must contain a zero of $f''(x)$ (QED).

Corollary: *An interval $I_j \in I_B$ may contain atmost one local maximum/ minimum of $G(x)$.*

Proof: (by contradiction) Assume two local maxima/minima of G exist in I_j. Call them x_1, x_2. By Claim 4, the interval (x_1, x_2) must contain another zero of $f''(x)$, at say a. Observe that a is in the interior of I_j. Hence $a \notin Z_B$. But Z_B is, by construction, the set of all zeros of $f''(x)$. Hence we have arrived at a contradiction (QED).

The above results can be collected into the following key lemma.

Lemma 2 (Piecewise unimodality): *Consider any interval $[x_1, x_2] = I_j \in I_B$. If $G'(x_1)$ and $G'(x_2)$ are of opposite signs, then the interval $[x_1, x_2]$ contains a unique maximum/minimum of $G(x)$. Otherwise, the interval $[x_1, x_2]$ does not contain a maximum/minimum of $G(x)$.*

Proof: By conditions of the claim, $f''(x_1), f''(x_2) = 0$. First part: if $G'(x_1)$ and $G'(x_2)$ are of the same sign or if either $G'(x_1)$ or $G'(x_2)$ equals zero, $G'(x)$ must have either null or an even number of zero crossings in the interval (x_1, x_2). If null, the case is proved. For an even number, we proceed as follows. By Claim 3, all zero crossings of $G'(x)$ in the interval (x_1, x_2) correspond to local maxima/minima of $G(x)$. Consider any two such successive local maxima/minima of $G(x)$, say y_1 and y_2. By Claim 4, (y_1, y_2) must contain yet another zero of $G'(x)$, which contradicts our starting assumption. Therefore, $G'(x)$ has no zero crossings on the interval $[x_1, x_2]$. Second part: if $G'(x_1)$ and $G'(x_2)$ have opposite signs, $G'(x)$ must have either one or a higher odd number of zero crossings in the interval $[x_1, x_2]$. In case of a higher odd number of zero crossings, pick any two. Repeat the reasoning of the first part. A similar contradiction follows. By exclusion, therefore, $G'(x)$ must have a unique zero crossing on the interval $[x_1, x_2]$. By Claim 3, this unique zero crossing must correspond to a unique local maximum/minimum of $G(x)$ (QED).

Note: We can extend Lemma 2 to include the semi-infinite interval $[a_N, \infty)$, as similar reasoning holds.

Corollary: *If $G'(a_1)$ is negative, the interval $I_0 = [0, a_1]$ contains a unique maximum/minimum of $G(x)$. If $G'(a_N)$ is positive, then the semi-infinite interval $I_N = [a_N, \infty)$ contains a unique maximum/minimum of $G(x)$. Otherwise, I_0 and I_N do not contain maxima/minima of $G(x)$.*

Proof: For symmetric PDFs $f'(0) = 0$. From Eq.(3.9) we then get $G'(0) = 8f^3(0) > 0$. From Lemma 2, it follows when $G'(a_1)$ is negative, then the interval $I_0 = [0, a_1]$ contains a unique maximum/minimum of $G(x)$. As $x \to \infty$, from Eq.(3.20) we get $G'(x) \to -4f''(x)$. If we take the exponential form of the PDF $f(x) = e^{P(x)}$, we obtain

$$\begin{aligned} f'(x) &= P'(x)e^{P(x)}, \\ f''(x) &= [P'^2(x) + P''(x)]e^{P(x)}. \end{aligned}$$

All PDFs can be described for large x as follows: (a) $P(x) \sim -x^{1+\alpha}$ where $(\alpha > 0)$ and (b) $P(x) \sim -\alpha \log(x)$ where $(\alpha > 1)$. Case (a) includes generalized Gaussians and mixtures-of- Gaussians, while Case (b) includes the Cauchy PDF. Thus, for large x, $f''(x) \sim (1+\alpha)^2 x^{2\alpha} f(x)$ and $f''(x) \sim \alpha(1+\alpha)x^{-2} f(x)$ for cases (a) and (b), respectively. Therefore, for large x $G'(x)$ is a small negative number. Hence, from Lemma 2, if $G'(a_N)$ is positive the interval $[a_N, \infty)$ contains a unique maximum/minimum of $G(x)$ (QED).

3.3.3 The global optimization algorithm

We are finally in a position to outline our global optimization algorithm, which is based on the **Piecewise Unimodality Lemma** (Lemma 2).

1. Consider the intervals in Eqs.(3.24):
   $I_0 = [0, a_1], I_j = [a_j, a_{j+1}], 1 \leq j \leq N-1, I_N = [a_N, \infty)$.

2. for $j = 0$: If $G'(0) < 0$, I_0 contains a unique maximum/minimum which may be found by Bisection (on I_0) or Newton's method (starting at either 0 or a_1). Else, ignore I_0. Increment the value of j.

   for $j = 1$ to $N-1$: If $G'(a_j)$ and $G'(a_{j+1})$ are of opposite signs, I_j contains a unique maximum/minimum which may be found by Bisection (on I_j) or Newton's method (starting at either a_j or a_{j+1}). Else, ignore I_j. Increment the value of j.

   for $j = N$: If $G(a_N)$ is positive, I_N contains a unique maximum/minimum which may be found by Bisection (on $[a_N, B]$ where B is a suitably large bound) or Newton's method (starting at a_N). Else, ignore I_N.

3. Collect the set of maxima/ minima (S) and corresponding values of the Gain $G(S)$ thus obtained. S and $G(S)$ are finite sets of cardinality at most $N+1$.

4. The global maximum denotedby G_{SR} is the maximum of all the local maxima/minima $G(S)$ and the optimal value of x is the corresponding member of S;

$$\begin{aligned} x_{opt} &= Argmax\ G(S), \\ G_{SR} &= Max\ G(S). \end{aligned} \tag{3.25}$$

In the foregoing treatment we have assumed $G'(x)$ vanishes only at isolated points. This assumption is satisfied by most PDFs. However, the algorithm can be generalized to

include the case when $G'(x)$ vanishes over an interval of finite length.

3.3.4 Computational complexity

Thus, we have reduced a multimodal optimization problem to a sequence of atmost $N+1$ unimodal optimization problems. If L is the length of the longest interval, then the worst case complexity of the above algorithm, measured by the maximum number of steps required, is given by

$$NC_{SR} = (N+1)\log_2(L/\epsilon), \tag{3.26}$$

where ϵ is the required accuracy of the root finding procedure. The roots in Eq.(3.22) which divide the search space into disjoint intervals as in Eq.(3.24) are known in the application being considered. Consequently, the complexity of finding the partition in Eq.(3.24) can be ignored. For comparison, the worst case complexity of Brent's standard algorithm for globally optimizing multi-modal functions [13] is given by

$$NC_{clas} = B\sqrt{\frac{M}{2\epsilon}}\log_2\left(B\sqrt{\frac{M}{2\epsilon}}\right), \tag{3.27}$$

where B is the upper bound of the interval $[0, B]$ over which the search for optima is conducted, and M denotes an upper bound on the second derivative of the functional being optimized, i.e. $Sup|G''(x)| \leq M$. We can make an immediate observation about the relative worst case complexities. For finite M, B and L, as $\epsilon \to 0_+$, we obtain the following scaling laws: $NC_{clas} \sim \epsilon^{-1/2}\log_2\epsilon^{-1}$ and $NC_{SR} \sim \log_2\epsilon^{-1}$. Therefore,

$$\frac{NC_{clas}}{NC_{SR}} \sim \epsilon^{-1/2}. \tag{3.28}$$

We conclude that for increasing accuracy of optimization, the complexity of the classical technique increases as $\epsilon^{-1/2}$ compared to the algorithm outlined in this chapter.

Now, we proceed to analyze the relative complexity for thicker marine noise PDFs. The acoustic noise in the ocean is produced by a variety of uncorrelated sources. The governing unit variance PDF can be modelled [110, 140] by a mixture of two Gaussians and is given by

$$f(x) = \frac{c}{\sqrt{2\pi}}\left[\alpha e^{-(cx)^2/2} + \frac{1-\alpha}{\beta}e^{-(cx)^2/2\beta^2}\right], \tag{3.29}$$

where

$$c = [\alpha + (1-\alpha)\beta^2]^{\frac{1}{2}}, \quad 0 < \alpha < 1, \beta > 0, \tag{3.30}$$

α and β denote the mixing parameter and the ratio of the deviations of the component PDFs respectively. Also,

$$f''(x) = \frac{c^3}{\sqrt{2\pi}}\left[\alpha\{(cx)^2-1\}e^{-(cx)^2/2} + \frac{1-\alpha}{\beta^3}\{(cx/\beta)^2-1\}e^{-(cx)^2/2\beta^2}\right]. \tag{3.31}$$

Thicker PDFs of this family occur when $\beta \gg 1$. In this limit it is observed [155] that the optimal value of the normalized threshold $x \to 0$. Consequently, $F(x) \to 1/2$. The values of $f(x)$ and $f''(x)$ do not reach an asymptotic limit, but from Eq.(3.29) and Eq.(3.31) are observed to scale as c and c^3, respectively. From Eq.(3.16) we know that at any maximum/minimum $G''(x) = \frac{2f(x)}{1-F(x)}f''(x)$, which then scales as c^4. Hence, the upper bound M also scales as c^4. We also know the upper bound of the search interval B scales as $\frac{1}{c}(\log c)^{1/2}$. The length of the largest unimodal interval L, which is bounded above by B, will also scale as $\frac{1}{c}(\log c)^{1/2}$. These scaling laws suggest that the relative complexity of the two algorithms scales as

$$\frac{NC_{clas}}{NC_{SR}} \sim c(\log c)^{1/2}. \tag{3.32}$$

Since for $\beta \gg 1$, $c \to (1-\alpha)^{1/2}\beta$ we infer $\frac{NC_{clas}}{NC_{SR}} \sim \beta(\log \beta)^{1/2}$. Consequently, for similar accuracy, the classical, benchmark algorithm become rapidly intractable, relative to the algorithm in the previous section, in the case of heavy-tailed marine noise PDFs.

3.3.5 Values of CPU run-time

For increasing accuracy of optimization, as $\epsilon \to 0_+$, it can be shown from Eqs.(3.27) and (3.26) that the relative worst-case complexity can be approximated by

$$\frac{C_{Brent}}{C_{PU}} \sim \left[\frac{B\sqrt{M}}{2\sqrt{2}(N+1)}\right]\epsilon^{-1/2} \tag{3.33}$$

From the values of B, M and N given in the preceding sections and an assumed value of $\epsilon = 0.001$ it can be inferred that the Piecewise unimodal algorithm will converge $10-20$ times faster than the classical Brent's algorithm.

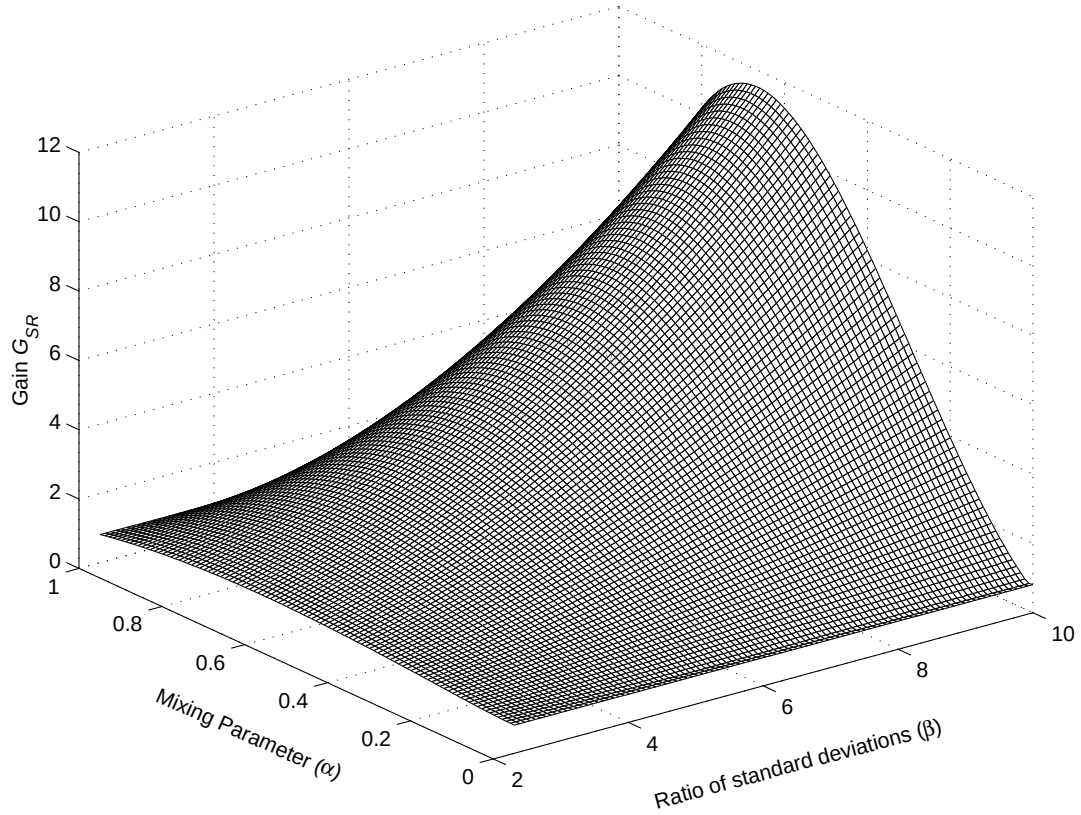

Figure 3.1: Three-dimensional plot of the gain of the SR detector in mixture-of-Gaussian noise as a function of the parameters α and β of the noise PDF.

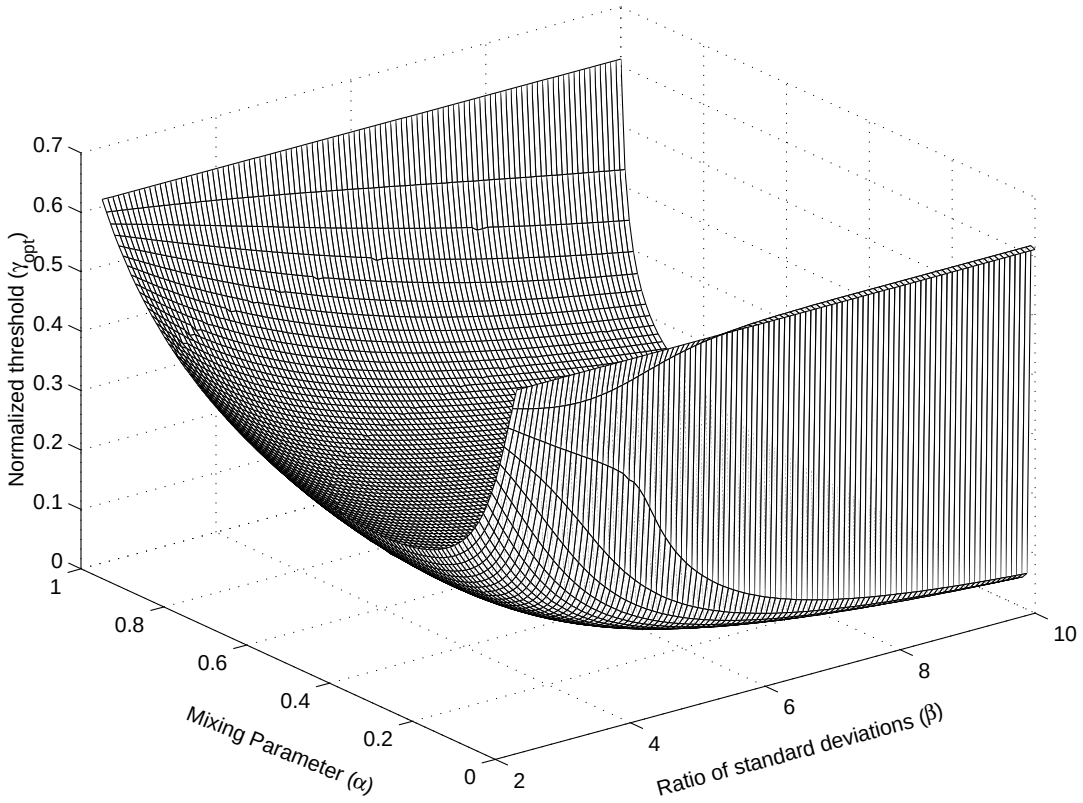

Figure 3.2: Three-dimensional plot of the normalized threshold of the SR detector in mixture-of-Gaussian noise as a function of the parameters α and β of the noise PDF.

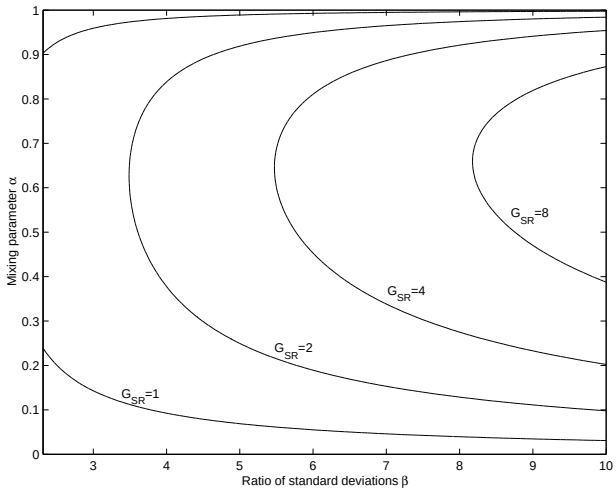

Figure 3.3: Contour plot of the gain of the SR detector in mixture-of-Gaussian noise as a function of the parameters α and β of the noise PDF.

3.3.6 Results: Mixture of Gaussians

It is apparent from Eq.(3.29) that PDFs belonging to the Gaussian mixture family can be uniquely characterized by two parameters: α and β. Therefore G_{SR} and x_{opt} are plotted as functions of both α and β in Figs.(3.1) and (3.2). It is observed that as $\alpha \to 0$ or $\alpha \to 1$, the PDF tends to a Gaussian, and the gain G_{SR} falls below unity. But for intermediate values of α, $G_{SR} \to \infty$ as $\beta \to \infty$. This divergence of G_{SR} can also be explained by asymptotic analysis. As $\beta \to \infty$, the optimal normalized threshold

$$x \to 0, c/\beta \to (1-\alpha)^{1/2} \quad \text{and} \quad c/\sqrt{2\pi}\exp(-(cx)^2/2) \to \delta(x),$$

where $\delta(.)$ denotes the Dirac delta function. Thus we have

$$\lim_{\beta\to\infty} f(x) = \alpha\delta(x) + (1-\alpha)^{3/2}/\sqrt{2\pi}\exp(-(1-\alpha)x^2/2),$$

which is a divergent(generalized) function. Consequently G_{SR} defined in Eq.(3.25) diverges. The values of (α, β) for which $G_{SR} > 1$, are identifiable from the region enclosed by the contour $G_{SR} = 1$ in Fig.(3.3). For these values of (α, β) and for the corresponding PDFs therefore, the performance of the SR detector shall be superior to that of the linear detector. For a more explicit comparison the SNR gains of the SR, linear and optimal nonlinear detectors are plotted for a fixed value of α with varying β in Fig.(3.4), and then for a fixed value of β with varying α in Fig.(3.5).

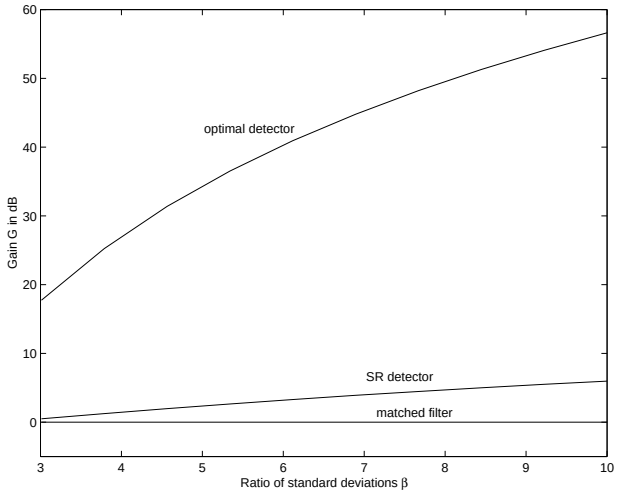

Figure 3.4: Variation of the gain of the optimal detector, SR detector and matched filter in mixture-of-Gaussian noise as a function of the parameter β of the noise PDF, with $\alpha = 0.2$.

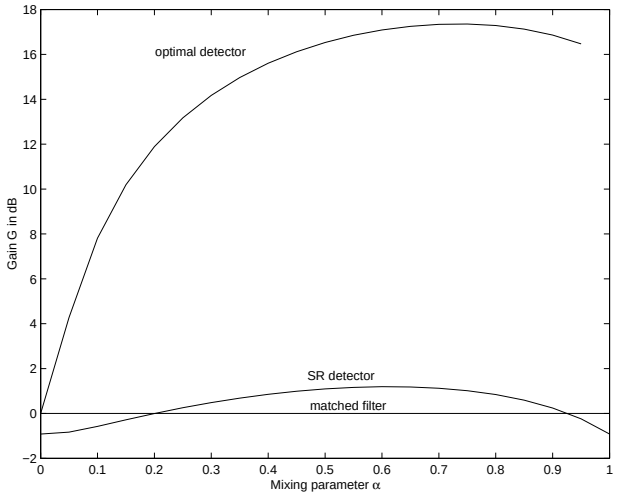

Figure 3.5: Variation of the gain of the optimal detector, SR detector and matched filter in mixture-of-Gaussian noise as a function of the parameter α of the noise PDF, with $\beta = 2.5$.

3.4 Detection statistics

In statistical detection theory it is customary to state the signal detection problem as that of testing two hypotheses: 'signal present' and 'signal absent', denoted by H_1 and H_0, respectively. The decision can be reduced to the following test:

Decide H_1 is true if $T(\mathbf{x}) > \eta$
Decide H_0 is true if $T(\mathbf{x}) < \eta$.

Here $T(\mathbf{x})$ is the Test Statistic, a function of the data vector $x[n]$, and η is the detector threshold. If the amplitude and phase of the sinusoidal signal are unknown, the Test Statistic for the optimal detector and the more conventional quadrature detector share the following generic form:

$$T(\mathbf{x}) = \left| \frac{1}{N} \sum_{n=0}^{N-1} g(x[n]) \exp(-j2\pi f_o n) \right|^2 \tag{3.34}$$

The test statistic $T(\mathbf{x})$ is therefore the periodogram of the transformed data vector $g(x[n])$ at the frequency f_0. It can be shown [87] that for this class of test statistic, under hypothesis H_0 the random variable $(2/\sigma^2)T$ has chi-squared distribution with two degrees of freedom, and that under hypothesis H_1, the random variable $(2/\sigma^2)T$ has a noncentral chi-squared distribution with two degrees of freedom and noncentrality parameter λ defined by

$$\lambda = \frac{GE_s}{2\sigma^2} = \frac{GR_{in}}{2} \tag{3.35}$$

where G is the SNR gain of the system, E_s is the energy of the signal, σ^2 is the noise power and R_{in} is the input SNR. Hence, the probability of false alarm is given by

$$\begin{aligned} P_F &= P(T > \eta; H_0) \\ &= \exp(-\eta/\sigma^2) \end{aligned} \tag{3.36}$$

and the probability of detection is given by

$$\begin{aligned} P_D &= P(T > \eta; H_1) \\ &= Q_{\chi_2'^2(\lambda)}(2\eta/\sigma^2) \end{aligned} \tag{3.37}$$

where $Q_{\chi_2'^2(\lambda)}(.)$ denotes the right-tail probability of the noncentral chi-squared PDF with two degrees of freedom and noncentrality parameter λ. The corresponding receiver operating characteristic (ROC) is given by

$$P_D = Q_{\chi_2'^2(\lambda)}\left(2\ln\frac{1}{P_F}\right) \tag{3.38}$$

For the quadrature detector or incoherent matched filter, $g_{MF}(.)$ is the identity transformation, which is the optimal transformation in Gaussian noise,

$$g_{MF}(x[n]) = x[n] \tag{3.39}$$

Since the SNR gain of the matched filter is unity, $G_{MF} = 1$ and the noncentrality parameter is given by

$$\lambda_{MF} = \frac{E_s}{2\sigma^2} = \frac{R_{in}}{2} \tag{3.40}$$

For non-Gaussian noise the optimal nonlinear transformation g_{opt} can be derived from the Neyman-Pearson criterion and is defined [87] as follows,

$$g_{\text{opt}}(\xi) = -\sigma^2\frac{f'(\xi)}{f(\xi)} \tag{3.41}$$

where $f'(\xi)$ is the derivative of the PDF $f(\xi)$. The SNR gain G_{opt} and the resulting noncentrality parameter λ_{opt} of the resulting optimal nonlinear detector [87] are given by:

$$G_{\text{opt}} = \sigma^2\int_{-\infty}^{\infty}\frac{(f'(\xi))^2}{f(\xi)}d\xi \tag{3.42}$$

$$\lambda_{opt} = \frac{G_{opt}E_s}{2\sigma^2} = \frac{G_{opt}R_{in}}{2} \tag{3.43}$$

As shown in [87] the optimal nonlinear transformation yields an effective SNR gain G_{opt} whose value is greater than unity if the noise is non-Gaussian. We can obtain a suboptimal detector of sinusoidal signals by replacing the optimal nonlinear transformation $g_{\text{opt}}(.)$ defined in Eq.(3.41) by a stochastic resonator (SR) operating at maximum gain. The SNR gain can be maximized by choosing the threshold γ_1 according to the optimization algorithm outlined in Section 3.3. The test statistic of the SR detector is therefore

given by

$$T_{SR}(\mathbf{x}) = \left| \frac{1}{N} \sum_{n=0}^{N-1} g_{\text{SR}}(x[n]) \exp(-j2\pi f_o n) \right|^2 \tag{3.44}$$

where $g_{\text{SR}}(x[n]) = y[n]$ is the output of the stochastic resonator.

Now the expressions for P_F and P_D have the form as in Eqs.(3.36, 3.37), but the parameter λ is redefined as

$$\lambda_{SR} = \frac{G_{SR} E_s}{2\sigma^2} \tag{3.45}$$

Since the ROC for the stochastic resonator is now given by

$$P_D = Q_{\chi_2'^2(\lambda_{SR})} \left(2 \ln \frac{1}{P_F} \right) \tag{3.46}$$

and $Q_{\chi_2'^2(\lambda)}(x)$ increases monotonically with λ for all x, it follows that

1. By maximizing G_{SR} we shall maximize P_D for a given P_F, thereby optimizing the detection performance of the SR detector.

2. If $G_{SR} > 1$, the SR detector performs better than the conventional matched filter.

We observe that for Gaussian mixtures, for any ordered pair (α, β) for which $G_{SR} \geq 1$, the SR detector shows an improvement over the matched filter. For $(\alpha, \beta) = (0.3, 10)$ this is borne out from the ROCs of the matched filter, SR and optimal nonlinear detectors for the low input SNR of $R_{in} = -10dB$ as shown in Fig.(3.6). When the given value of α is kept constant, the degree of improvement increases markedly as β is increased, as shown in Fig.(3.7). This is because, as observed in Section 3.3, for a fixed value of α such that $0 < \alpha < 1$, G_{SR} diverges as $\beta \to \infty$. When the given value of β is kept constant, the ROC shows improvement as α is increased from 0, but then decreases as α approaches 1. This is illustrated for $\beta = 20$ in Figs.(3.8) and (3.9). The plots of the SNR Gains and the ROCs also illustrate an interesting trend first reported in [21] namely by Chapeau-Blondeau: quantizer detectors show greater improvement over matched filter detectors as the noise PDF becomes more heavy-tailed or *leptokurtic* in nature, as is the case when $p \to 0_+$ for generalized Gaussians, and $\beta \to \infty$ for a fixed α for Gaussian mixtures.

A tentative explanation is as follows: quantizers, being threshold systems, always have bounded outputs. Thus, upon quantization, the expected output noise power is necessarily finite, regardless of the input. For increasingly leptokurtic PDFs however, the expected input noise power diverges. Therefore for matched filters, the expected

output noise power diverges. Thus, quantizers 'damp' the degenerative effects of noise more effectively than do matched filters, for more heavy tailed or leptokurtic PDFs. Hence the pronounced improvement for detectors with quantizer nonlinearity for such PDFs.

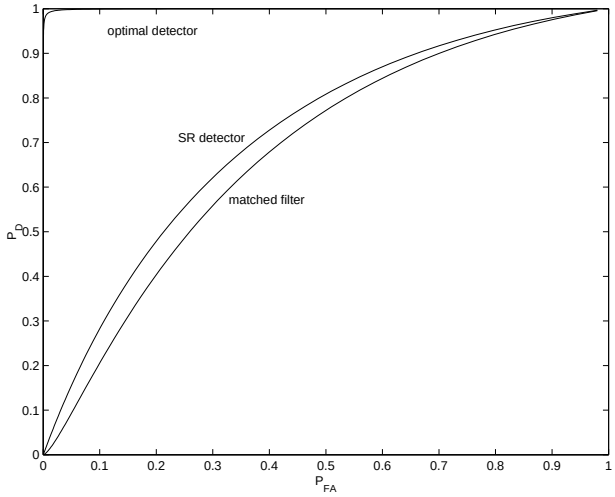

Figure 3.6: Receiver Operating Characteristics of linear, SR and optimal nonlinear detectors in mixture-of-Gaussian noise with $(\alpha, \beta) = (0.3, 10)$.

3.5 Perturbative corrections (i): due to non-zero input SNR

In this section we derive the corrections for the normalized threshold x and the SNR gain G, due to the small but nonzero input SNR R_{in}. Our approach is rooted in perturbative analysis. Here the asymptotic SNR gain G corresponds to the unperturbed cost functional which is relatively simple to optimize. In the unperturbed problem, the optimal normalized threshold and optimal gain $(x, G(x))$ can be calculated using the algorithm outlined in the previous section. Here, g_1 represents the 1^{st} order correction due to finite input SNR and corresponds to a weak, sufficiently smooth perturbing functional, subdominant to G. The resultant 1^{st} order corrections denoted by $(\delta x, \delta G(x))$ may then be computed from g_1. In order to do so, we proceed closely following the approach presented by Sakurai [163].

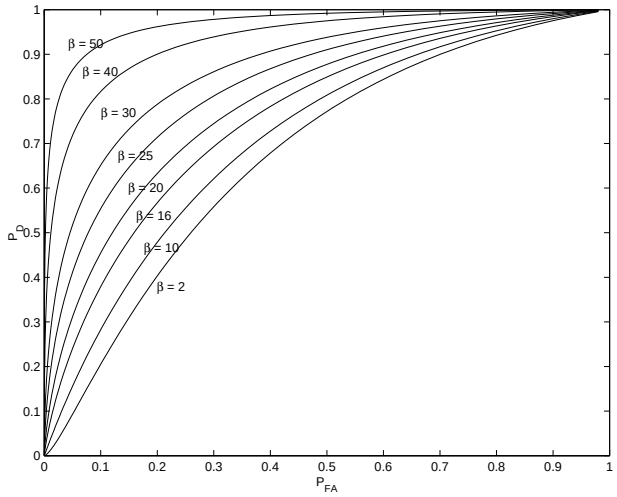

Figure 3.7: Variation of Receiver Operating Characteristics of the SR detector in mixture-of-Gaussian noise as $\beta \to \infty$, with $\alpha = 0.3$.

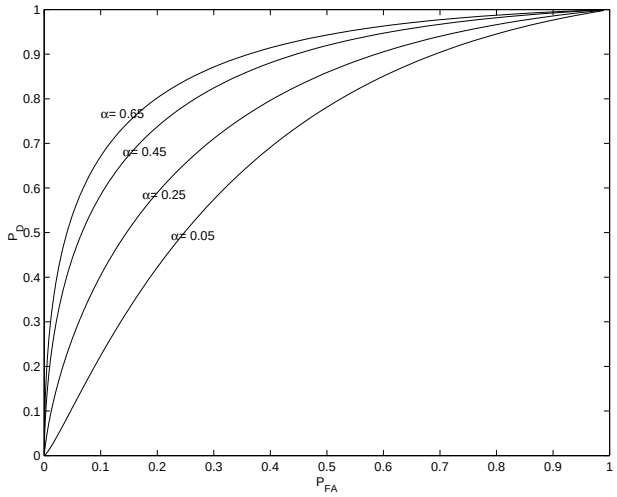

Figure 3.8: Variation of Receiver Operating Characteristics of the SR detector in mixture-of-Gaussian noise for $\alpha = 0.05, 0.25, 0.45, 0.65,$ with $\beta = 20$.

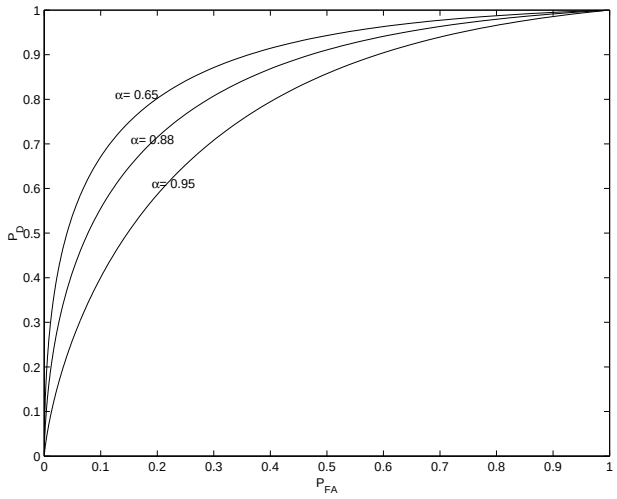

Figure 3.9: Variation of Receiver Operating Characteristics of the SR detector in mixture-of-Gaussian noise for $\alpha = 0.65, 0.88, 0.95,$ with $\beta = 20$.

If the unperturbed functional G attains its global maximum at x, then

$$G'(x) \;=\; 0, \qquad G''(x) < 0. \tag{3.47}$$

As the perturbation is subdominant and smooth, the perturbed functional $\widetilde{G} = G + g_1 A^2$ attains its global maximum at $x + \delta x$ where $\delta x \ll 1$. Therefore,

$$(G' + g_1' A^2)(x + \delta x) \;=\; 0, \qquad (G'' + g_1'' A^2)(x + \delta x) < 0.$$

Expanding in Taylor's series about x, and keeping only the first order corrections yields

$$G'(x) + G''(x)\delta x + g_1'(x) A^2 \;=\; 0. \tag{3.48}$$

Using Eqs.(3.47) and (3.48) it follows

$$\delta x \;=\; -A^2 \frac{g_1'(x)}{G''(x)}. \tag{3.49}$$

The first order correction to the SNR gain is

$$\delta G \;=\; (G + g_1 A^2)(x + \delta x) - G(x).$$

Proceeding as before by taking the Taylor's series about x, keeping only the first order

corrections and using Eq.(3.47) we obtain

$$\delta G = A^2 g_1(x). \tag{3.50}$$

The values for the correction to the threshold and SNR gain in Eqs.(3.49) and (3.50) are observed to depend on A^2 and are thus proportional to the input SNR R_{in} in the weak signal limit. The values of these corrections for the moderately high input SNR of $-20dB$ and for the mixture-of-Gaussian PDFs are shown in [157]. These figures indicate that the magnitude of the corrections increase with the SNR gain and are more pronounced for heavy-tailed PDFs. These PDFs correspond to central values of α, for fixed β and to increasing values of β, for fixed α. The input SNR, due to a mobile target vessel, varies typically between $-40dB(A = 0.01)$ and $-14dB(A = 0.2)$. The disparity between the original and corrected values of the Gain, may be expected to increase for values of input SNR higher than $-20dB$. For higher input SNRs and correspondingly higher values of A, a linearized treatment in the weak signal limit will no longer be tenable. Thus they cannot be considered here.

3.6 Perturbative corrections (ii): due to variation of marine noise PDF

The marine environment is dynamic in nature. Consequently, the PDF that governs marine noise shows considerable temporal variation. In this section, our aim will be to compute the necessary perturbative corrections to the normalized threshold (x) and the system gain (G). In order to do so, we will assume throughout that the system adjusts instantaneously to a variation in the noise PDF. This assumption is validated by the relative timescales involved; the timescale of variation of the marine noise PDF is ~ 1 hr, whereas the system response time for most sonar hardware is ~ 0.1 secs. In the manner of first order perturbation theory we will consider the change in the unperturbed functional (G) only. All other effects such as the change in the first perturbing functional (g_1) will be of higher order, and therefore subdominant. At first, we will try to keep the treatment as general as possible, and compute the corrections for all PDFs. In the subsequent section, we will restrict our attention exclusively to PDFs governing marine noise. The relevant corrections for SR quantizers in noise governed by generalized Gaussian PDFs are derived in [156].

3.6.1 General formalism

The characteristic function in Eq.(3.15) may be considered as a functional of the normalized threshold (x) and the PDF (f),

$$C(x,f) \;=\; 2[1-F(x)]f'(x)+f^2(x). \tag{3.51}$$

We have included the second argument f to explicitly denote the dependence on the noise PDF, hitherto assumed static. When the noise PDF suffers a change by δf, the system adjusts adiabatically with a change in the threshold given by δx, resulting in

$$\begin{aligned}&C(x+\delta x, f+\delta f)\\ &= 2[1-(F+\delta F)(x+\delta x)][(f'+\delta f')(x+\delta x)]+(f+\delta f)^2(x+\delta x).\end{aligned}$$

Expanding in series and keeping only till the first order corrections, we get

$$\begin{aligned}&C(x+\delta x, f+\delta f)\\ &= 2[1-F(x)]f'(x)+f^2(x)-2f'(\delta F+F'\delta x)\\ &\quad +2(1-F)(f''\delta x+\delta f')+2f(f'\delta x+\delta f).\end{aligned} \tag{3.52}$$

For optimality in the original and perturbed configurations,

$$C(x,f)=C(x+\delta x, f+\delta f)=0.$$

Therefore, from Eqs.(3.51) and (3.52) we get

$$-f'\delta F+(1-F)(f''\delta x+\delta f')+f\delta f=0,$$

which after rearrangement, yields the following expression for the correction to the threshold:

$$\delta x=\frac{f\delta f+(1-F)\delta f'-f'\delta F}{(1-F)f''}. \tag{3.53}$$

The perturbative correction to the gain can be computed in a similar manner. The unperturbed Gain in Eq.(3.15) is a functional of the normalized threshold (x) and the PDF (f),

$$G(x,f) \;=\; \frac{2f^2(x)}{1-F(x)}. \tag{3.54}$$

After the perturbations to the PDF and the normalized threshold,

$$\begin{aligned} G(x+\delta x, f+\delta f) &= \frac{2(f+\delta f)^2(x+\delta x)}{1-(F+\delta F)(x+\delta x)}, \\ &= 2\left(\frac{f^2(x)+2f\delta f+2ff'\delta x}{1-F(x)}\right)\left(1-\frac{f\delta x+\delta F}{1-F}\right)^{-1}. \end{aligned}$$

Keeping only the first order corrections, it follows that

$$\begin{aligned} &G(x+\delta x, f+\delta f) \\ &= \frac{2f^2(x)}{1-F(x)} + 4\left(\frac{f\delta f+ff'\delta x}{1-F}\right) + 2f^2\left(\frac{f\delta x+\delta F}{(1-F)^2}\right). \end{aligned} \tag{3.55}$$

The correction terms can be rearranged to give

$$\begin{aligned} &G(x+\delta x, f+\delta f) \\ &= \frac{2f^2(x)}{1-F(x)} + \frac{2f}{(1-F)^2}\left(2f'(1-F)+f^2\right)\delta x \\ &\quad + \frac{2f}{(1-F)^2}\left(2\delta f(1-F)+f\delta F\right). \end{aligned} \tag{3.56}$$

The coefficient function of δx vanishes at extremal points from Eq.(3.15). Combining Eqs.(3.55) and (3.56), we get

$$\delta G = \frac{2f}{(1-F)^2}\left(2\delta f(1-F)+f\delta F\right). \tag{3.57}$$

This relation can be simplified using the optimality criteria Eqs.(3.15,3.17) to get

$$\delta G = \frac{4}{1-F}\left(f\delta f - f'\delta F\right). \tag{3.58}$$

These formulae, while being very general, are computationally intensive as at each step they require the computation of an integral for the perturbation of the probability distribution function $\delta F(x) = \int_{-\infty}^{x} \delta f(u)du$. In addition, they require substantial memory allocation for the storage of the measured values of the perturbation δf. In the next section, we alleviate this problem by working in a restricted class of PDF relevant to the ocean acoustic scenario, namely the mixture-of-Gaussian PDFs.

3.6.2 Mixture-of-Gaussians

This class of PDF defined in Eq.(3.29) is uniquely defined by the mixing parameter (α) and the ratio of the component Gaussians (β). Therefore, the perturbation $f \to f + \delta f$, which represents a flow in function space, can be reduced to $(\alpha, \beta) \to (\alpha + \delta\alpha, \beta + \delta\beta)$ which is a flow in the space of two real variables (R^2). Since the perturbations in the parameters α and β are assumed to be independent, it follows that

$$\delta f = \frac{\partial f}{\partial \alpha}\delta\alpha + \frac{\partial f}{\partial \beta}\delta\beta.$$

Similarly,

$$\delta f' = \frac{\partial f'}{\partial \alpha}\delta\alpha + \frac{\partial f'}{\partial \beta}\delta\beta \quad \text{and} \quad \delta F = \frac{\partial F}{\partial \alpha}\delta\alpha + \frac{\partial F}{\partial \beta}\delta\beta.$$

Substituting the above formulae into Eqs.(3.56) and (3.58), we get

$$\begin{aligned} \delta x &= -\frac{1}{(1-F)f''}\left(f\frac{\partial f}{\partial \alpha} + (1-F)\frac{\partial f'}{\partial \alpha} - f'\frac{\partial F}{\partial \alpha}\right)\delta\alpha \\ &\quad -\frac{1}{(1-F)f''}\left(f\frac{\partial f}{\partial \beta} + (1-F)\frac{\partial f'}{\partial \beta} - f'\frac{\partial F}{\partial \beta}\right)\delta\beta \end{aligned} \tag{3.59}$$

and

$$\delta G = \frac{4}{1-F}\left[\left(f\frac{\partial f}{\partial \alpha} - f'\frac{\partial F}{\partial \alpha}\right)\delta\alpha + \left(f\frac{\partial f}{\partial \beta} - f'\frac{\partial F}{\partial \beta}\right)\delta\beta\right]. \tag{3.60}$$

As may be observed, by considering the perturbations in the parameters α and β, we have alleviated the need to calculate δF and to store the values of δf. Therefore, our procedure is now amenable to an application with faster run-time and scarce hardware. These corrections can be expressed in terms of standard integrals, the details of which are given in Appendix B. For illustration, these corrections are plotted for mixture-of-Gaussian PDFs in [157], for the values of $\delta\alpha = 0.1$ and $\delta\beta = 0.1$, which correspond to the average drift in parameters of the ocean on a timescale of $1hr$ [110, 140]. These corrections exhibit a similar pattern as those for finite input SNR: they are more pronounced for heavy-tailed PDFs which correspond to central values of α, for fixed β, and to increasing values of β, for fixed α. Though they are of the same overall order as, they are smaller in magnitude than the corrections due to finite input SNR. This pattern can be expected to be more pronounced for higher values of input SNR.

3.7 Hardware implementation

The instructions for the detection algorithm given in the preceding sections, can be programmed into the Texas Instruments (TI) processor (Model:TMS320C6713). This processor is a low-cost development platform designed specifically for the development of high precision signal processing applications [196]. The basic architecture is outlined below:

- An instruction set for the threshold device, the global optimization procedure and perturbative calculations can be embedded into the development platform using an assembly language, C or C++.
- Tables of the roots of the second derivative of the PDF ($f''(x)$) for various values of the mixing parameters (α, β) can be pre-computed and stored on available memory (ROM). Thus the time required for these steps is reduced to ROM look-up time. Tables for standard functions required for perturbative calculations can be similarly stored therein.

The signal is input to the threshold device and its output is tested for the detection hypothesis. The device communicates in a forward one-way loop to the control circuitry. The control circuit denotes an embedded instruction set for the global optimization routine which calculates the optimal threshold value. This part communicates with the segment of the memory which contains the locations of the roots of $f''(x)$ for various values of the mixing parameters (α, β), which characterize the PDFs which govern marine noise. The threshold device, control circuitry and the necessary ROM comprise the entire SR device to be built, and must be integrated on a single platform/ motherboard.

Conventional sonar detectors consist of the following stages: the transducer or acoustic sensor which converts incoming pressure signals in a chosen frequency to electrical signals in the same frequency; and a higher level processing stage which conducts the detection hypothesis test to decide is the signal is present or absent in that particular frequency bin [87]. In the upgraded sonar, the input signal is pre-processed by the SR device, thereby amplifying its signal content, before being led to the detection hypothesis testing stage. Thus, the SR device must be installed between the transducer and the detection hypothesis testing stages of any sonar. The advantages such a design accord are:

- The entire SR device, comprising the instruction sent and the necessary ROM can be implemented on a single commercially available DSP platform, thereby alleviating the need for custom-made hardware.

- In most modern sonars, the internal circuitry carry digital signals. The use of the SR device as an intermediate stage, therefore, avoids the need for cumbersome Analog-to-Digital (AD) and Digital-to-Analog (DA) converters.
- The resultant chip can be installed in existing, possibly remote sonar platforms as a plug-in.

3.8 Conclusions

We have investigated the convergence properties and stability of stochastic resonant (SR) detectors. The case of weak, sinusoidal signals is considered. We prove that the asymptotic expression for the SNR gain can be globally optimized by an algorithm of logarithmic complexity. The worst case complexity of this algorithm is better than that of standard algorithms in the following two cases: (i) for increasing accuracy of the optimization procedure (ii) for increasingly heavy tailed marine noise PDFs, corresponding to more turbulent ocean conditions. This improves real-time performance and avoids expensive hardware requirements. The effects of small non-zero input SNRs and drift in the marine noise PDF are found to be first order perturbative corrections. An uncertainty in the estimate of the signal frequency is found to result in a second order perturbative correction which is therefore subdominant to the former two effects. While the theoretical development is kept as general as possible, numerical simulations are carried out exclusively for the mixture-of-Gaussians, a class of PDFs which govern oceanic noise. For this class of PDFs, all corrections are expressed in terms of standard functions, making them readily implementable on sonar hardware. Numerical illustrations indicate that the SR detector is stable with respect to variations considered in a typical ocean acoustic scenario. They also indicate that non-zero input SNRs tend to be dominant amongst all corrections to the SNR gain considered. Hence, the SR detector has been shown to be a robust and viable alternative to matched field detectors. Therefore, using this device, even isolated hydrophones i.e. sonobuoys, can be upgraded economically. A conceivable generalization of this work would be to consider arrays of quantizers, with feedback. Aspects of this problem have already been studied [120, 119, 175, 201, 202]. However, the detection performance of a model incorporating all these features, such as a neural network, in a dynamic ocean acoustic scenario with correlated noise, remains to be investigated. This will be done in the future.

Chapter 4

Stochastic resonance in Carbon nanotubes

4.1 Introduction

Electrical signals can help pulse-train detection at the nanolevel. Experiments on a single-walled carbon nanotube transistor confirmed that a threshold device exhibited Stochastic resonance (SR) for finite-variance and infinite-variance noise: small amounts of noise enhanced the nanotube detector's performance [98, 99]. The experiments used a carbon nanotube field-effect transistor to detect noisy subthreshold electrical signals. Three measures of detector performance showed the SR effect: Shannon's mutual information, the normalized correlation measure, and an inverted bit error rate compared the input and output discrete-time random sequences. The nanotube detector had a threshold-like input-output characteristic in its gate effect. It produced little current for subthreshold digital input voltages that fed the transistor's gate. The observed nanotube effect was robust: it persisted even when noise with infinite-variance governed by the Cauchy distribution corrupted the signal stream.

The SR theorems in [92] give broad sufficient conditions for SR to occur in any threshold system for all possible finite-variance noise types and for most infinite-variance noise types. Simulations show that these SR theorems apply to a threshold-like ramp function that often models the transistor's current-voltage ($I - V_G$) characteristics: $Y = G(S - V_T)$ where Y is the output current, V_T is the threshold voltage and G is a nonzero gain for suprathreshold inputs $S \geq V_T$. The simulated transistor had the parameters $G = -1nA/V$ and $V_T = -2V$. The plots of Shannon's mutual information $I(S, Y)$, a normalized correlation measure $C(S, Y)$ and an inverted bit error rate $1 - BER$ show an

optimal noise standard deviation σ_{opt} in the range $(0.3, 0.5)$. The input $s_i = b_i + n_i$ was a sum of Gaussian noise n_i and binary input (Bernoulli) symbols b_i for the equally likely ON/OFF symbol pair $-1.6V$ and $-1.4V$. Experiments using a pristine (undoped) single-walled carbon nanotube transistor confirmed these predictions [98, 99]. The nanotube effect was observed as one of 4 successful combinations of input binary values with the parameter choices $ON = -1.6V$ and $OFF = -1.4V$. This SR effect occurred inspite of nanotube instabilities that caused fluctuations in the stochastic $I - V_G$ curve.

A semiconductor single-walled carbon nanotube (SWNT) can change its conductivity in response to an external electric field in a gate effect [179, 121]. The SR experiments used a chemical-vapour-deposition (CVD) grown SWNT [76, 61]. The semiconductor SWNT forms a Schottky Diode at the interface with metal so that a metal-nanotube-metal contact forms a field-effect transistor (FET) with an adjacent gate electrode [193]. The typical current-voltage $(I - V_G)$ characteristics given by

$$I = \begin{cases} G(V - V_T) & \text{for } V_G \leq V_T \\ 0 \quad \text{otherwise.} \end{cases} \tag{4.1}$$

indicate that the pristine semiconductor nanotubes act as hole-doped semiconductors at room temperatures and that nanotubes are p-type FETs [179]-[121], [6]. The transconductance G is negative and the gate voltage $V_G \leq V_T$ is suprathreshold for p-type FETs. The SR result does not specify the material or the dimensions of the threshold device and could apply to materials such as inorganic nanotubes, nanowires, nanofibers and nanoscale transistors [98]. Further details of the fabrication of such nanodevices can be found in [89] and references therein. Nanotube FET technology produces detectors that typically exhibit hysteresis. The detector is not ideal as its conductance, gate effect and hysteresis changed over time. The detector exhibited some hysteresis but not enough to prevent the SR effect. The current-voltage loop exhibits the hysteretic loop in [98]. For details of how hysteresis occurs and how it can be prevented please refer [98] and references therein.

Recent experiments have demonstrated the occurence of Stochastic Resonance (SR) in individual carbon nanotubes driven by sub-threshold binary input signals [98, 99]. In a manner typical to SR, various measures such as Shannon mutual information, input-output correlation and inverted bit-error rate increase with increasing noise intensities [98, 99] attaining a maximum at a non-zero value for the noise intensity. These results are theoretically significant as they validate certain 'forbidden interval theorems' which guarantee such non-monotonic performance of threshold systems [136, 137] under certain conditions. Signal detectors or sensors based on such nanotubes have the potential for

application to broadband or optical communication systems that use sub-microamp currents, nanolevel parallel signal processing, spread-spectrum communications or chemical detection—see [98] and references therein. Such detectors can also be interfaced with biological systems [98]. These suggested applications would require nanotubes to be driven by continuously valued input signals in contrast to sub-threshold binary input signals. This in turn would necessitate parallel arrays of nanotubes in order to avoid significant loss of information. Furthermore, individual nanotubes or nanoscaled gates produced using current fabrication technologies exhibit a variety of internal parameter variations. They also exhibit many sources of internal noise and a large number of physical defects. Alternative methods of fabrication, such as those based on self-assembling materials, fault-tolerant computing using reconfiguration or encoding strategies have been shown to be either unviable or unattainable in emergent nanotechnologies. It has been suggested that the use of redundant structures or averaging structures with mid-high redundancy factors may constitute a more realistic alternative for building reliable nanoscale gates [114, 171]. A typical cell architecture in such a case [115] consists of a parallel array of threshold devices each of which can be potentially implemented on a nanotube or a cluster of nanotubes, followed by an adder and a restitution device which restores digital levels degraded by system transfer.

The phenomenon of Stochastic resonance (SR) in such threshold systems and static nonlinearities has been extensively studied in literature [46, 19]. SR is said to occur when the response of a nonlinear system to a signal can be improved by the addition of noise [46, 126]. Conventional SR requires the signal to be 'sub-threshold' [192, 19]. Coupling many nonlinear devices in the manner suggested in [115] can lead to a variant of SR, where the sub-threshold requirement need not hold [176, 177, 117]. An immediate consequence of these results is that arrays of carbon nanotubes considered in [114, 115] are prime candidates for exhibiting SR. In this chapter, therefore, we study such a system within the related framework of quantizer-arrays [175]. In such an array, each component nanotube modeled as a quantizer performs independently noisy binary quantization, after which the measurements are summed. Henceforth, the word 'device' is used to refer to a single-walled carbon nanotube or an equivalent binary quantizer.

The main purpose of this chapter is to show that, in a manner characteristic of SR, the Shannon mutual information attainable by an array of identical nanotubes (or an *averaging structure*) will increase with increasing noise intensities, attaining a maximum at a non-zero value for the noise intensity. This result is exceedingly relevant as given current nano-fabrication processes, only arrays of carbon nanotubes with identical dimensions and chemical composition can be realized. Furthermore, such nanotubes have

inherently static electrical conduction properties. From a theoretical point-of-view, it is also interesting to consider the maximum Shannon theoretic information attainable by an array of carbon nanotubes. Ideally, the mutual information can be maximized by optimizing the threshold voltages and conductance gains dynamically, as a function of σ_η. It is shown that though the transmitted information is higher, the SR effect disappears in such a system. The remainder of this chapter is organized as follows: Section 4.2 contains the necessary background theory; Sections 4.3 and 4.4 contain the asymptotic formulas and the experimental observations affirmed respectively; and finally, Section 4.5 concludes the chapter. These results are intended to complement existing studies of bio-molecules at the nanoscale [183, 197].

4.2 Background theory

4.2.1 Mutual information in the Network

The two cases considered in this chapter are both summing networks of N threshold devices, each of which operates on the sum of a common input signal $x(t)$ and independent, identically distributed (*iid*) additive noise, $\eta_i(t), i = 1 \dots N$. The additive noise at each device has the same standard deviation σ_η. Though the noise is assumed to be of finite variance our analysis can be extended to noise distributions with infinite variance but finite dispersion. The output of each individual device $y_i(t), i = 1 \dots N$ is given by the Heaviside function with an adjustable threshold,

$$y_i(t) = H(x + \eta_i - \Theta_i) = \begin{cases} 1 & x(t) + \eta_i(t) > \Theta_i \\ 0 & \text{otherwise.} \end{cases} \tag{4.2}$$

The overall response of the network $y(t)$ is found by summing the outputs of each device, $y(t) = \sum_{i=1}^{N} y_i(t)$, and is a count of the number of devices in state 1.

If the common input signal, $x(t)$, is a random variable, then the network can be analyzed using information theory [132]. Specifically, the relative degradation in signal quality due to random noise and quantization can be measured using mutual information [132], which can be written as

$$\begin{aligned} I(x,y) &= \int_{-\infty}^{\infty} f_x(x) \left[\sum_{n=0}^{N} P_{y|x}(n|x) \log_2 P_{y|x}(n|x) \right] dx \\ &\quad - \sum_{n=0}^{N} P_y(n) \log_2 P_y(n). \end{aligned} \tag{4.3}$$

where $P_{y|x}(n|x)$ and $f_x(x)$ represent the conditional probability distribution of the output given the input and the probability density function (PDF) of the input (assumed to be known) respectively, and $P_y(n)$ represents the output probability mass function and can be obtained as

$$P_y(n) = \int_{-\infty}^{\infty} P_{y|x}(n|x) f_x(x) dx \quad n = 0, .., N. \tag{4.4}$$

Simplification of the mutual information for the binary network requires an expression for $P_{y|x}(n|x)$. This can be achieved as follows. Let $P_i(x)$ be the conditional probability of the i–th device being in state 1,

$$P_i(x) = \int_{\Theta_i - x}^{\infty} f_\eta(u) du = 1 - F_\eta(\Theta_i - x), \quad i = 1, .., N, \tag{4.5}$$

where $f_\eta(\cdot)$ and $F_\eta(\cdot)$ represent the PDF and the cumulative distribution function (CDF) governing the noise with standard deviation σ_η. The unit-variance PDF $f(\cdot)$ and the unit-variance $F(\cdot)$ are given by:

$$f(u) = \sigma_\eta f_\eta(\sigma_\eta u) \text{ and } F(u) = F_\eta(\sigma_\eta u). \tag{4.6}$$

When all threshold values $(\Theta_i)_{i=1}^N$ are not equal (henceforth referred to as configuration (i)), $P_{y|x}(n|x)$ is given by the coefficient of z^n in the power series expansion of

$$\prod_{i=1}^{N} \left[1 - P_i(x) + z P_i(x)\right]. \tag{4.7}$$

In the more restricted case when all threshold levels are equal (henceforth referred to as case (ii)), $P_{y|x}(n|x)$ is binomial,

$$P_{y|x}(n|x) = \binom{N}{n} P^n(x) \left(1 - P(x)\right)^{N-n}. \tag{4.8}$$

4.2.2 Relevance as nanotube models

The pristine (undoped) nanotubes considered in [114, 115] exhibited current-voltage characteristics that were consistent with p-type transistors. The input-output transfer function can be described by the following memoryless, threshold-like nonlinearity given by

$$I = \begin{cases} G(V - V_T) & V < V_T \\ 0 \quad \text{otherwise.} \end{cases} \tag{4.9}$$

where I and V refer to the output drain-to-source current and input gain voltage respectively. They are related by the transconductance gain G and the threshold voltage V_T, the values of which can be found by regression analysis. Typical values are $G = -1$ nA/V, $V_T = -2$ V, $3-5$ μm for the length and 2 nm for the diameter of single-walled nanotubes respectively. Such nanotubes were grown between two electrodes using a combination of chemical vapor deposition and electron-beam lithography. For more details about the manufacturing process and modes of operation the interested reader is referred to [98] and references therein.

It can be shown that the threshold device modeled by Eq.(4.2) and the nanogate considered in Eq.(4.9) are equivalent. We introduce the following unitless variables:

$$\begin{aligned} & x = -(V/|V_T| + 1); \quad \eta_i = -\delta V_i/|V_T|; \quad \Theta_i = 0; \\ & \text{and} \quad y_i = I_i/(|G||V_T|), \qquad i = 1 \ldots N. \end{aligned} \tag{4.10}$$

The index i refers to the i^{th} of N identical nanotubes in a summing array described in [114, 115]. By construction of such averaging structures, such constituent nanotubes are subject to a common input voltage V but varying voltage fluctuations δV_i and consequently produce varying output currents I_i. The set of unitless variables chosen is by no means unique, but accords us simplicity in the sections to follow. Substituting Eq.(4.10) into Eq.(4.9) it can be seen to be equivalent to Eq.(4.2) except for the following difference: they describe continuous and discrete output respectively. However, the probabilities contained in Eqs.(4.4),(4.5),(4.7) and (4.8) depend only on the input exceeding a certain value of the threshold, irrespective of the actual value of the device output. Therefore, the mutual information in Eq.(4.3) for both systems with corresponding threshold values will be equal. The same cannot be said however, of metrics such as the input-output correlation or bit-error rate. They will therefore, be excluded from consideration here. It must also be noted that due to the transformation in Eq.(4.10) all devices now have a common threshold value $\Theta_i = 0,\ i = 1 \ldots N$.

Furthermore, we consider a random input sequence where the random variable is continuous and governed by the input PDF $f_x(.)$ and the corresponding CDF $F_x(.)$. Such a model is a generalization of the Bernoulli sequences which can be as input. If we assume the PDF $f_x(.)$ to be a sum of two equally weighted Dirac delta (generalized) functions:

$$f_x(x) = \frac{1}{2}\delta(x) + \frac{1}{2}\delta(x-1), \tag{4.11}$$

the input sequence then reduces to a Bernoulli sequence. With these remarks, we can proceed to the main section of this chapter.

4.3 Asymptotic analysis

In this section we derive asymptotic expressions for the mutual information of an array in the limiting cases of high and low noise. We assume throughout that the input to each quantizer is a random signal x with finite variance σ_x^2, and mean μ_x and *iid* additive white noise with PDF $f_\eta(\cdot)$, median 0, and finite variance σ_η^2. The key results are:

- In the high noise limit, the mutual information for both configurations are equivalent and decay quadratically;
- in low noise, the mutual information of configuration (i) has a maximum at zero noise and decreases linearly with increasing noise intensities;
- in the low noise limit the mutual information of configuration (ii) however, increases in a sub-linear manner from unity. From these limiting values, it is apparent that the transmitted information should be maximized at a non-zero value for the noise intensity.

In the following section the asymptotic formulas are stated without derivation. All derivations and relevant details are relegated to Appendix C.

4.3.1 Asymptotic equivalence in high noise

We show equivalence of the two configurations by deriving the dominant values for the mutual information for both configurations at high noise levels and showing that they are the same.

Formula 1: For a summing network of N asymmetric 2-level quantizers—where the threshold levels $(\Theta_i)_{i=1}^N$ either (i) can assume independent non-identical values, or (ii) are constrained to be equal—and where the input to each is the sum of a random signal x and *iid* additive white noise, the mutual information defined in Eq.(4.3), in the high-noise limit given by $\sigma_\eta^2 \gg N\sigma_x^2$, has the asymptotic form

$$I(x,y) = \frac{2N}{\log 2} f^2(0) \frac{\sigma_x^2}{\sigma_\eta^2} + \mathcal{O}(1/\sigma_\eta^3), \tag{4.12}$$

where $f(\cdot)$ represents the unit-variance PDF governing noise, given by $f(u) = \sigma_\eta f_\eta(\sigma_\eta u)$. An illustration of such high-noise behavior for a few widely-used PDFs is given in Fig. (4.3.1).

The value of the mutual information given by Eq.(4.12) depends explicitly only on the number of devices N in the system. The fluctuations due to variations in nan-

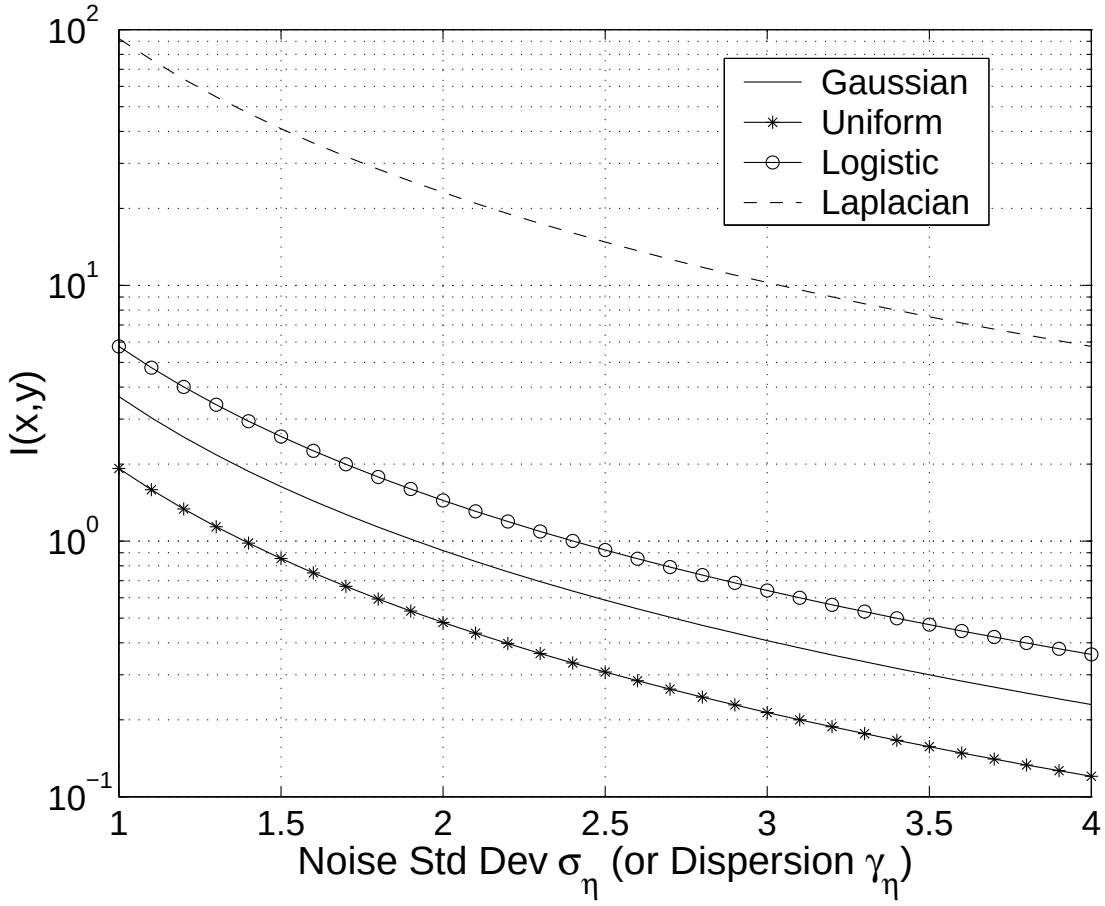

Figure 4.1: Asymptotic behavior of mutual information of a summing network of carbon nanotubes in either configurations (i) or (ii) under high noise (with number of devices $N = 8$ and Gaussian input noise of intensity $\sigma_x^2 = 1$).

otube parameters such as conductance, gate voltage and hysteresis will therefore be sub-dominant to this term in the high noise limit. Also, for PDFs with infinite variance but finite dispersion the formula in Eq.(4.12) must be modified to read:

$$I(x,y) = \frac{2N}{\log 2} f^2(0) \frac{\sigma_x^2}{\gamma_\eta^2} + \mathcal{O}\left(\frac{1}{\gamma_\eta^3}\right), \tag{4.13}$$

where $f(\cdot)$ represents the *unit-dispersion* PDF governing noise, given by $f(u) = \gamma_\eta f_\eta(\gamma_\eta u)$.

4.3.2 Limiting behavior of configuration (i) in low noise

In this section we consider a parallel array of nanotubes with threshold levels $\{\Theta_i\}_{i=1}^N$ that can assume independent non-identical values. When $\sigma_\eta = 0$ the set of thresholds attain distinct (non-degenerate) values which can be arranged in the following strictly increasing order $\Theta_1 < \ldots \Theta_i < \Theta_{i+1} \ldots < \Theta_N$. Therefore the conditional probabilities in Eq.(4.5) are given by:

$$P_i(x) = H\left(x - \Theta_i\right). \tag{4.14}$$

It then follows that

$$\begin{aligned} P_{y/x}(0/x) &= 1 - H\left(x - \Theta_1\right), \\ P_{y/x}(i/x) &= H\left(x - \Theta_i\right) - H\left(x - \Theta_{i+1}\right), \\ P_{y/x}(N/x) &= H\left(x - \Theta_N\right). \end{aligned} \tag{4.15}$$

Consequently, the unconditional probabilities defined in Eq.(4.4) simplify to:

$$\begin{aligned} P_y(0) &= \int_{-\infty}^{\Theta_1} f_x(x)dx = \frac{1}{N+1}, \\ P_y(i) &= \int_{\Theta_i}^{\Theta_{i+1}} f_x(x)dx = \frac{1}{N+1}, \\ P_y(N) &= \int_{\Theta_N}^{\infty} f_x(x)dx = \frac{1}{N+1}. \end{aligned} \tag{4.16}$$

It can be shown that the mutual information defined in Eq.(4.3) attains a maximum value given by $I(x,y) = \log_2(N+1)$ when the unconditional probabilities defined in Eq.(4.4) attain a common value of $P_y(n) = 1/(N+1)$ for all values of $n = 1 \ldots N$. Our basic approach will be to compute the corrections to the above unperturbed value for small but non-zero noise intensities. In order to do this, a few preliminaries are necessary. It

can be shown (Ineqs.(C.3,C.4) in Appendix C) that the probabilities $P_i(x)$ and $1-P_i(x)$ can be upper bounded as follows:

$$\begin{aligned} P_i(x) &\leq f\left(\frac{\Theta_i - x}{\sigma_\eta}\right)\left(\frac{\sigma_\eta}{\Theta_i - x}\right) \text{ for } x > \Theta_i, \\ 1 - P_i(x) &\leq f\left(\frac{x - \Theta_i}{\sigma_\eta}\right)\left(\frac{\sigma_\eta}{x - \Theta_i}\right) \text{ for } x < \Theta_i, \\ & \qquad i = 1, .., N. \end{aligned} \tag{4.17}$$

The upper bounds of $P_i(x)$ and $1 - P_i(x)$ on the right-hand sides of the Ineqs.(4.17) decay rapidly as $\sigma_\eta \to 0$. In the immediate neighborhood of a certain threshold value Θ_j, it then follows that $P_j(x) \approx 1$ when $j < i$; $P_j(x) \approx 0$ when $j > i$; and that

$$\prod_{j=1}^{N} \left[1 - P_j(x) + zP_j(x)\right] \approx z^{i-1}\left[1 - P_i(x) + zP_i(x)\right]. \tag{4.18}$$

The coefficient of z^n in the power series Eq.(4.7) or Eq.(4.18) give us $P_{y|x}(n|x)$. Consequently, in the neighborhood of Θ_i, we have

$$\begin{aligned} P_{y/x}(i-1/x) &= 1 - P_i(x) = F\left(\frac{\Theta_i - x}{\sigma_\eta}\right), \\ P_{y/x}(i/x) &= P_i(x) = 1 - F\left(\frac{\Theta_i - x}{\sigma_\eta}\right). \end{aligned} \tag{4.19}$$

Alternatively, they can be rearranged to get the following sequence of relations:

$$\begin{aligned} P_{y/x}(0/x) &= F\left(\frac{\Theta_1 - x}{\sigma_\eta}\right) \qquad x \sim \Theta_1, \\ P_{y/x}(i/x) &= \begin{cases} 1 - F\left(\frac{\Theta_i - x}{\sigma_\eta}\right) & \forall x \sim \Theta_i \\ F\left(\frac{\Theta_{i+1} - x}{\sigma_\eta}\right) & \forall x \sim \Theta_{i+1} \end{cases} \\ P_{y/x}(N/x) &= 1 - F\left(\frac{\Theta_N - x}{\sigma_\eta}\right) \qquad x \sim \Theta_N. \end{aligned} \tag{4.20}$$

Now, we will find the implications of these relations on the unconditional probabilities $P_y(n)$. Therefore, the values of quantities such as $P_y(n)$, represented as integrals containing these terms, as in Eq.(4.4), are largely determined in the immediate neighborhood of Θ_i. This property can be used to greatly simplify the expressions for the mutual information as $\sigma_\eta \to 0$ as is now shown. Now we can proceed to the main formula of

this section.

Formula 2: For a summing network of N carbon nanotubes with threshold levels $(\Theta_i)_{i=1}^N, i = 1 \dots N$ that can assume independent non-identical values, the mutual information defined in Eq.(4.3), in the limit as $\sigma_\eta \to 0$, has the following asymptotic form

$$I(x, y) = \log_2(N + 1) + 2(B_1 B_2)\sigma_\eta + \mathcal{O}(\sigma_\eta^2), \tag{4.21}$$

where $B_1 = \sum_{i=1}^N f_x(\Theta_i)$ and $B_2 = \int_{-\infty}^{\infty} F(u) \log_2 F(u) du$.

4.3.3 Limiting behavior of configuration (ii) in low noise

In this section we will find the limiting value of the mutual information $I(x, y)$ of a parallel array of nanotubes with equal threshold levels as $\sigma_\eta \to 0$. We proceed as follows: the empirical values for the noise-free case are taken as "unperturbed values"; the correction induced due to small but non-zero σ_η are then found. This correction is found to be sub-linear.

When $\sigma_\eta = 0$, it is observed $\Theta = 0$. The probability of any device being on defined in Eq.(4.5) is given by the Heaviside function:

$$P_i(x) \quad = \quad H\,(x) \quad i = 1, 2 \dots N.. \tag{4.22}$$

For low noise levels (σ_η nonzero but small) the following occurs: for positive x the probability of a single device being on decreases by a modest amount say $\epsilon(x)$; for negative x the probability of a single device being off increases by a similarly modest amount, also denoted here by $\epsilon(x)$. This can be encapsulated into the following definition:

$$\epsilon(x) = \begin{cases} P_{1/x} = 1 - F\left(\frac{\Theta - x}{\sigma_\eta}\right) & \forall x < 0 \\ 1 - P_{1/x} = F\left(\frac{\Theta - x}{\sigma_\eta}\right) & \forall x \geq 0 \end{cases} \tag{4.23}$$

From the observed value $\Theta = 0$ and Eq.(C.2) it then follows:

$$\epsilon(x) = \begin{cases} F\left(\frac{x}{\sigma_\eta}\right) & \forall x < 0 \\ 1 - F\left(\frac{x}{\sigma_\eta}\right) & \forall x \geq 0 \end{cases} \tag{4.24}$$

The above expressions and Eq.(C.2) make evident that $\epsilon(x)$ is symmetric. The average

of $\epsilon(x)$ given by Eq.(4.23) can then be defined by

$$\overline{\epsilon} = \int_{-\infty}^{\infty} f_x(x)\epsilon(x)dx = 2\int_0^{\infty} f_x(x)\left[1 - F(x/\sigma_\eta)\right]dx. \tag{4.25}$$

The second expression is derived using the symmetry of $\epsilon(x)$ and Eq.(4.24). The probabilities in Eq.(4.8) on being linearized in terms of $\epsilon(x)$ can be expressed as:

$$\text{For } x < 0: \quad \begin{cases} P(0/x) = 1 - N\epsilon(x), \\ P(1/x) = N\epsilon(x). \end{cases} \tag{4.26}$$

$$\text{For } x > 0: \quad \begin{cases} P(N-1/x) = N\epsilon(x), \\ P(N/x) = 1 - N\epsilon(x). \end{cases} \tag{4.27}$$

All other probabilities are of the order $\epsilon^2(x)$ and are therefore sub-dominant to these values. Substituting Eqs.(4.26) and (4.27) into Eq.(4.4) yields:

$$\begin{aligned} P_y(0) &= P_y(N) = \frac{1}{2}\left[1 - N\overline{\epsilon}\right], \\ P_y(1) &= P_y(N-1) = \frac{1}{2}N\overline{\epsilon}. \end{aligned} \tag{4.28}$$

In deriving these relations we have used (i) the symmetry of $f_x(x)$ which implies $\int_{-\infty}^{0} f_x(x)dx = \int_0^{\infty} f_x(x)dx = 1/2$ and (ii) the additional symmetry of $\epsilon(x)$ which implies $\int_{-\infty}^{0} f_x(x)\epsilon(x)dx = \int_0^{\infty} f_x(x)\epsilon(x)dx = \overline{\epsilon}/2$. We are now in a position to derive the main result of this section.
Formula 3: For a summing network of N nanotubes with a common voltage threshold Θ, the mutual information defined in Eq.(4.3), in the limit as $\sigma_\eta \to 0$, has the following asymptotic form:

$$I = 1 + N\left[\left(I_2 - I_1 \log_2 I_1\right)\sigma_\eta - I_1\sigma_\eta \log_2 \sigma_\eta\right] + \mathcal{O}(\sigma_\eta^2), \tag{4.29}$$

where I_1 and I_2 are constants related to integrals of the unit-variance complementary distribution function and are given by: $I_1 = 2f_x(0)\left[\int_0^{\infty}\left(1 - F(u)\right)du\right]$ and $I_2 = 2f_x(0)\left[\int_0^{\infty}\left(1 - F(u)\right)\log_2\left(1 - F(u)\right)du\right]$. Illustrations of such low-noise behavior for a few widely-used PDFs are given in Fig. (4.3.3).

A few other observations can also be made. For low σ_η the dominant component of Eq. (4.29) is given by:

$$I \sim 1 - NI_1\sigma_\eta \log_2 \sigma_\eta. \tag{4.30}$$

Since I_1 is positive definite, it follows that $I(x, y)$ should *increase* with σ_η. Such non-monotonic variation with noise intensity indicates the existence of a supra-threshold

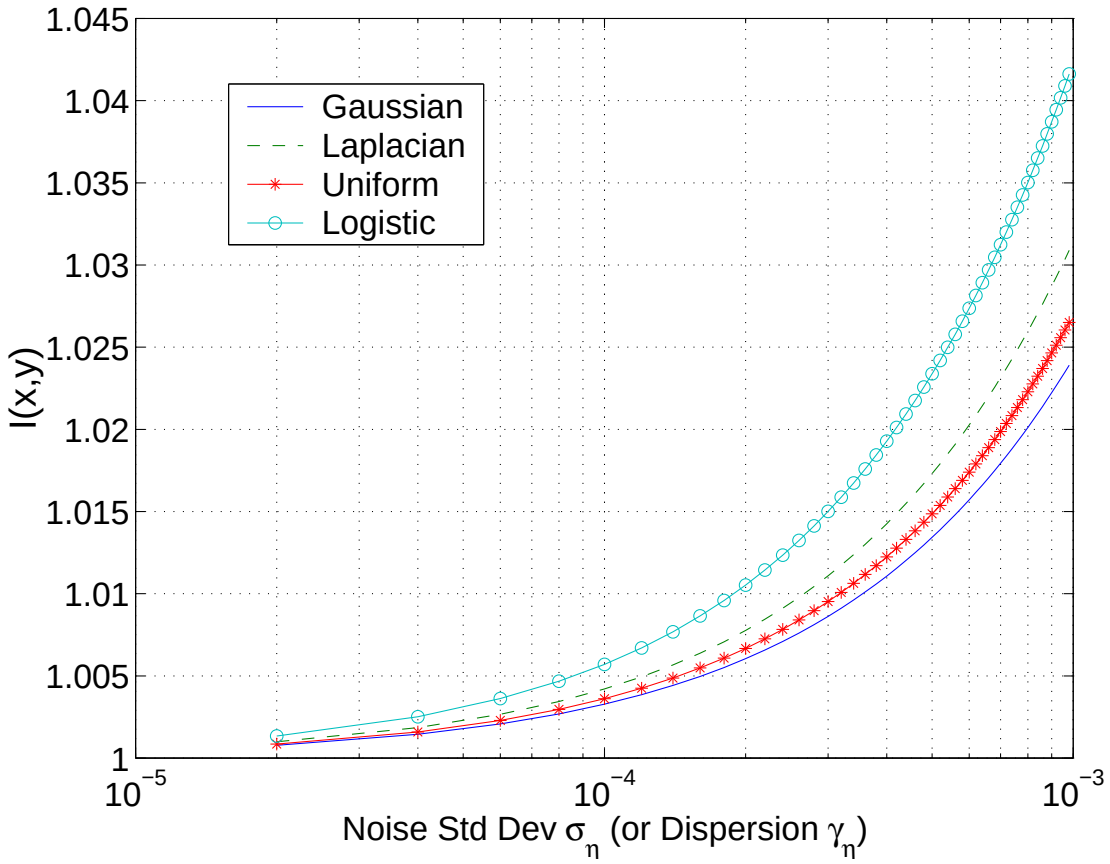

Figure 4.2: Asymptotic behavior of mutual information of a summing network of carbon nanotubes in configuration (ii) under low noise (with number of devices $N = 8$ and Gaussian input noise of intensity $\sigma_x^2 = 1$).

stochastic resonant (SSR) peak for this configuration. As before, for PDFs with infinite variance but finite dispersion the formula in Eq. (4.29) must be modified to:

$$I = 1 + N\left[\left(I_2 - I_1 \log_2 I_1\right)\gamma_\eta - I_1 \gamma_\eta \log_2 \gamma_\eta\right] + \mathcal{O}(\gamma_\eta^2). \tag{4.31}$$

We conclude this section with the following remark: due to the dimensionless quantities introduced in Eq.(4.10), the formulas derived in this section given in Eqs.(4.12,4.21) and (4.29) can be seen to be similarly unitless and therefore dimensionally consistent.

4.4 Continuity with experiments

The importance of the preceding calculations lies in the fact that they demonstrate theoretically that the stochastic resonance (SR) phenomenon can be observed in arrays of carbon nanotubes [114, 115]. For low σ_η it follows from Eq.(4.30) the mutual information increases with the rate I' which can be found from differentiating Eq.(4.30). Since for small arguments the natural logarithm diverges to $-\infty$ [152], it constitutes the dominant term in the result and gives us: $I' \sim -\frac{NI_1}{\log 2}\log \sigma_\eta$. For low σ_η being considered, this term is strictly positive. For high σ_η we know from Eq.(4.12) the mutual information decreases with the rate $I' = \frac{-4N}{\log 2} f^2(0)\frac{\sigma_x^2}{\sigma_\eta^3}$. For high σ_η being considered, this term is strictly negative. It follows [152] that the mutual information defined in Eq.(4.3) must have a stationary point, where $I' = 0$ for the intermediate range of noise intensities (alternatively, the continuous function I' must have a zero-crossing for intermediate values of σ_η). By virtue of the preceding arguments for low and high σ_η, such a stationary point must be a local maximum corresponding to the SR peak. An analytical estimate of the location of the SR peak however, seems far from straight-forward.

It has also been demonstrated that SR can occur for finite dispersion but infinite variance noise distributions. As earlier remarks show, such PDFs are amenable to our treatment. An example is the Cauchy distribution, which has a PDF given by

$$f_{\gamma_\eta}(x) = \frac{1}{\pi}\frac{\gamma_\eta}{\gamma_\eta^2 + x^2}. \tag{4.32}$$

The importance of the Cauchy PDF lies in the fact that it can be used to test the robustness of the SR effect in nanotubes to infinite variance noise.

Nanotube FET technology produces detectors that typically exhibit hysteresis [98]. Such a detector is not ideal as its conductance, gate voltage and hysteresis change over time. It has been shown that in the high noise limit such variations will have negligible effect on the mutual information values for an array of nanodevices. The effect of

variations in a parameter can be taken into account more rigorously by invoking the central limit theorem [132] as in [114, 115]. Analytical expressions for the mean and variance of important nanotube parameters with variations in these properties can be found in [114, 115].

4.5 Implications for nanoelectronics and conclusions

This chapter gives theoretical arguments for the possible observation of stochastic resonance (SR) in carbon nanotubes. It has been repeatedly observed [114, 171] that cell architectures based on the averaging of multiple nanodevices alleviate the three main problems of the nanodevices at the gate level: high defect ratios, large parameter variability and reduced noise margins. Such architectures make possible the construction of reliable mid/large nanocircuits. Such *averaging structures* have low implementation complexity which further reduces fabrication defects. Such averaging structures are studied in two distinct configurations: (i) when all constituent nanotubes have dynamic, adjustable conductance parameters; and (ii) when they have equal, static parameters. Configuration (ii) is realizable using current technology and can demonstrate the SR phenomenon. Configuration (i) is neither currently realizable nor can demonstrate the SR phenomenon, but provides an upper bound on the transmitted information attainable with such structures. Both configurations are equivalent at high noise. In addition, there seems to be a growing realization that quantum coherence plays an important role in mesoscopic systems, even at temperatures where intrinsic decoherence was formerly thought to be dominant [93]. The results presented in this chapter, being based on classical information theory, can provide a benchmark to gauge or constrain the effects of quantum coherence on such nano-architectures. Further analytical results, such as the effects of empirical models of inter-device coupling, parasitic capacitance and device hysteresis will be published in a forthcoming work. The focus will be on real-time, industrial nanocircuits based on SR, as has been done in nanomechanical structures [7] and neuronal arrays [69]. Example applications to be cited include the development of low-power flat-panel displays; electron microscope sources, fuel cells and finally "ultracapacitors" [98]. It must be stressed that such SR-based nanodevices are made possible due to the enhanced transmission accorded by SR and the unique thermal and mechanical properties of carbon nanotubes. It is also stressed that these results are of relevance to existing nano-scale studies of filaments and molecules [183, 197].

Chapter 5

Stochastic resonance in myoglobin

5.1 Introduction

Myoglobin is one of the most well-characterized functional proteins, its function being to store oxygen supplied by blood until its release for some form of metabolic activity. In this capacity it is crucial for supporting intense levels of aerobic activity and for biological sustenance during hypoxic (low oxygen) conditions. In addition to this widely accepted role in cellular oxygen transport and oxygen buffering, recent experiments have revealed that myoglobin scavenges [42] and produces nitric oxide (NO) [29] during oxygenated and deoxygenated conditions respectively. An excess of nitric oxide reduces cardiac muscle contractility and decreases the heart rate. By reacting rapidly with and thereby removing excess nitric oxide, oxygenated myoglobin protects cellular respiration [42]. However, nitric oxide also suppresses the production of damaging reactive oxygen species (ROS) [29]. Therefore, by generating nitric oxide from circulating nitrite in cardiac muscle cells under hypoxic stress, deoxygenated myoglobin acts as a mediator in limiting tissue damage due to restricted blood flow [29].

The dynamics of myoglobin have been variously studied using phonon-assisted Mossbauer scattering [2], standard X-ray crystallography [128], Mossbauer absorption spectroscopy [134, 135, 129], time-resolved spectroscopy [131] and inelastic scattering of synchrotron radiation [133]. Interest in the dynamics of such functional proteins, stems from the fact that their biological functioning is influenced by the structure fluctuations and conformational changes that are induced by binding to ligands and substrates. In the case of myoglobin, small diatomic ligands such as Oxygen which bind to the iron atom in the heme group enter and leave via the Histidine gate (His-64) [168]. The molecular oxygen binds at the active site of the protein and one of the six co-ordinations of the

iron atom. The process of binding and releasing of the ligand is reversible [5]. It is now widely accepted that proteins exist in numerous conformations which provide a reservoir of entropy essential for its functioning [41, 45]. Large scale protein motions such as the exit of a ligand from the protein interior follow the dielectric fluctuations in the bulk solvent, whereas fast fluctuations are controlled by fluctuations in the hydration shell. The former and latter are respectively termed α- and β- fluctuations in analogy to such relaxations in glasses [41].

Experiments using flash photolysis indicate an effective potential with a single reaction co-ordinate [131]. A double well potential has been used to explain elastic incoherent neutron scattering data on myoglobin [31]. Other experiments have used inelastic Rayleigh scattering of Mossbauer radiation to determine the temperature dependence of the mean-square displacement (MSD), denoted by $< x^2 >$, in myoglobin [133]. Some experimental results for myoglobin were analyzed using non-Gaussian statistical methods [187, 188]. In the low-temperature (below 180K) range the temperature dependence is observed to be linear. In the high-temperature (above 180K) range the slope of the curve increases dramatically, by more than a factor of ten in one case. The low-temperature behavior was attributed to harmonic motions of the protein and the high-temperature behavior was attributed to diffusive motion limited by bonding forces within the protein [133]. An explanation for this phenomenon involving thermal fluctuations in a system with multiple potential minima corresponding to the protein's stable conformations was provided in [189]. These results were in agreement with the results of conformational kinetics [131]; more intensive molecular dynamics simulations performed for myoglobin [174, 173]; and experimental measurements of the iron atom's positional fluctuations measured by Mossbauer absorption spectroscopy [134, 135, 129].

Though the results of [41, 45] raise doubts about the validity of such models, such multi-well potentials offer a template for the study of stochastic resonance (SR) [46, 64, 94, 122]. In this chapter, we explore some implications of Kramers' rate theory [64, 94] for such a multi-well potential, including the possibility of stochastic resonance [46, 64, 94, 122]. Stochastic resonance (SR) refers to the phenomenon whereby the addition of random noise enhances the propagation of signals within the system. This phenomenon has been observed in numerous biological detection systems such as sensory neurons [104], mechano-receptor cells of crayfish [32], cercal systems of crickets [100] and passive receptors of electrical signals in paddlefish (*Polyodon spathula*). At the sub-cellular level SR has been observed experimentally in an artificial system of ion channels [11] and theoretically in a single Shaker potassium channel [55]. An important biomedical application of SR concerns the use of electrical and mechanical noise to detect

sub-threshold mechanical cutaneous stimuli [28]. For other details and references on the topic the interested reader is referred to [63]. The remainder of this chapter is organized as follows: Section 5.2 provides necessary background; Section 5.3 presents the main results concerning vibrational statistics and harmonic response; and finally Section 5.4 concludes the chapter.

5.2 Background theory

The necessary background consists of the asymmetric bimodal potential postulated earlier for myoglobin [189]; and a few relevant quantities which follow from Kramers' rate theory applied to such an asymmetric potential [77, 194]. They are now briefly reviewed.

5.2.1 An effective potential for the problem

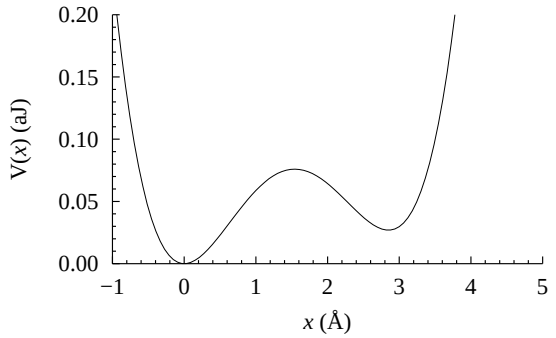

Figure 5.1: The effective bimodal potential of myoglobin as given in Eq.(5.1).

The notion of a potential with multiple minima has often been invoked for myoglobin [31, 187, 188, 189]. A self-consistent model [189] postulated an effective potential of the form:

$$V(x) = ax^4 + bx^3 + cx^2 + V_0, \tag{5.1}$$

with the coefficients

$$a = 1.52 \times 10^{-20} J/A^4, \quad b = 4.33 \times 10^{-21} J/A^3,$$
$$c = -5.29 \times 10^{-20} J/A^2. \tag{5.2}$$

A plot of the potential given by Eq.(5.1) has been illustrated in Fig.(5.1). The motivation

for a model of this form can be found in [131]. The positions and the depths of the potential wells are denoted by $x_{1,2}$ and $V_{1,2}$, where S_1 and S_2 refer to the deep and shallow wells respectively. Their numerical values are found to be $x_1 = -1.4302\mathring{A}, x_2 = 1.2166\mathring{A}, V_1 = 34.5kJ/mol$ and $V_2 = 22.4kJ/mol$ [189].

The Langevin equation for the damped motion of a particle of mass m in the effective potential is given by

$$m\ddot{x} + \gamma\dot{x} = F(x) + \xi(t), \tag{5.3}$$

where x denotes the reaction co-ordinate of the effective potential or the amplitude of the "principal mode"; m denotes the mass; γ denotes the viscosity; $F(x) = -\frac{\partial V(x)}{\partial x}$ denotes the deterministic force due to the effective potential; $\xi(t)$ denotes the random force. The fluctuating random force $\xi(t)$ denotes Gaussian white noise with zero mean, and obeys the fluctuation-dissipation theorem given by:

$$\begin{aligned} < \xi(t) > &= 0, \\ < \xi(t)\xi(t') > &= E_\xi \delta(t - t'), \end{aligned} \tag{5.4}$$

where $E_\xi = 2\gamma k_B T$. The probabilities of inter-well transitions between S_1 and S_2, given by Kramers' rate theory [94, 64] in the overdamped limit, are

$$\begin{aligned} p_{12} &= W_1 = \frac{\sqrt{V''(x_1)|V''(0)|}}{2\pi\gamma} e^{-V_1/k_B T}, \\ p_{21} &= W_2 = \frac{\sqrt{V''(x_2)|V''(0)|}}{2\pi\gamma} e^{-V_2/k_B T}. \end{aligned} \tag{5.5}$$

The numerical values were found from Eq.(5.1) to be:

$$\begin{aligned} W_1 &= \frac{2.4828}{\gamma} \times 10^{-20} J/A^2 e^{-V_1/k_B T}, \\ W_2 &= \frac{2.2906}{\gamma} \times 10^{-20} J/A^2 e^{-V_2/k_B T}. \end{aligned} \tag{5.6}$$

We can now outline quantitative estimates for the mean-squared displacement (MSD) and the signal-to-noise ratio (SNR) which follow from Kramers' theory [94, 64].

5.2.2 Preliminary results from Kramers' theory

When considering inter-well transitions the details of intra-well dynamics can be conveniently ignored. The master equation governing the change of probabilities of states S_1

and S_2 [122] is given by

$$\begin{aligned} \dot{\pi_1} &= W_2\pi_2 - W_1\pi_1, \\ \dot{\pi_2} &= W_1\pi_1 - W_2\pi_2. \end{aligned} \tag{5.7}$$

From the solution of Eq.(5.7) given by [122] it follows that the long-time limiting values of the probabilities and the inter-well mean-squared displacement are given by

$$\begin{bmatrix} \pi_1 \\ \pi_2 \end{bmatrix} = \frac{1}{W_1 + W_2} \begin{bmatrix} W_2 \\ W_1 \end{bmatrix}, \tag{5.8}$$

$$\begin{aligned} MSD_{inter} &= < x^2(t)|x_0, t_0 > - (< x(t)|x_0, t_0 >)^2 , \\ &= (x_1 - x_2)^2 \frac{W_1 W_2}{(W_1 + W_2)^2}. \end{aligned} \tag{5.9}$$

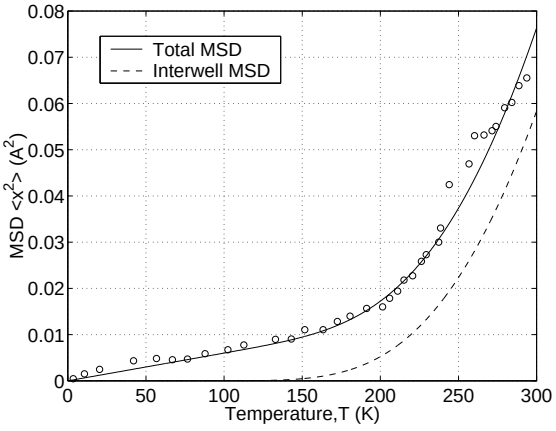

Figure 5.2: The inter-well mean squared displacement (MSD) and total mean squared displacement (MSD) in myoglobin as given by Kramers' rate theory and the effective bimodal potential as given in Eq.(5.1).

A plot of the inter-well MSD given by Eq.(5.9) has been illustrated in Fig.(5.2). A comparison with the experimental data shown in [189] reveals that though this approach correctly predicts the increase in MSD observed in the temperature range $180 - 300$K, it is inadequate in the low-temperature regime. The low-temperature spectral data are dominated by intra-well motions. Therefore, a more complete description requires analysis of intra-well motion as will be done later.

We now investigate the response of such an asymmetric potential to weak, periodic

forcing. Such forcing terms can originate in biologically transduced vibrations or from the coupling of the myoglobin globule to glass-forming solvent fluctuations [45, 41, 108]. The modified effective potential then reads

$$V(x) = ax^4 + bx^3 + cx^2 + V_0 + Ax\cos(\omega_s t). \tag{5.10}$$

If the amplitude A is assumed to be sub-dominant to the depth of the potential wells V_1 and V_2 such that $A \ll V_1, V_2$, the modified time-dependent interwell transition probabilities denoted by $W_1(t)$ and $W_2(t)$ are found to be:

$$\begin{aligned} W_1(t) &= W_1\left[1 - \frac{Ax_1}{k_BT}\cos(\omega_s t)\right], \\ W_2(t) &= W_2\left[1 - \frac{Ax_2}{k_BT}\cos(\omega_s t)\right]. \end{aligned} \tag{5.11}$$

For the asymmetric bistable potential well the auto-correlation function is given by [77, 194] to be

$$C(\tau)_{inter} = R_0 + R_1 e^{-\mu|\tau|} + \frac{A^2 R_2}{2}\left(e^{j\omega_s|\tau|} + e^{j\omega_s|\tau|}\right), \tag{5.12}$$

where μ, R_0, R_1 amd R_2 are given by [77, 194];

$$\begin{aligned} &\mu = W_1 + W_2, \\ &R_0 = \left(\frac{x_2W_1 + x_1W_2}{W_1 + W_2}\right)^2; R_1 = \frac{(x_1 - x_2)^2 W_1 W_2}{(W_1 + W_2)^2}; \\ &R_2 = \frac{(x_1 - x_2)^4 (W_1W_2)^2}{2(k_BT)^2(W_1 + W_2)^2((W_1 + W_2)^2 + \omega^2)}. \end{aligned} \tag{5.13}$$

The power spectral density for positive frequencies is given by [77, 194]:

$$< S(\omega) >_{inter} = R_1 \frac{2\mu}{\mu^2 + \omega^2} + \pi A^2 R_2 \delta(\omega - \omega_s). \tag{5.14}$$

The SNR, defined as the ratio of the strength of the output signal and the output broadband noise evaluated at the signal frequency, denoted by R can be found from [77] to be:

$$R = \frac{\pi A^2 (x_1 - x_2)^2 W_1 W_2}{4(k_BT)^2(W_1 + W_2)}. \tag{5.15}$$

For solvent-driven fluctuations the surface tension coefficient for a droplet of molecular

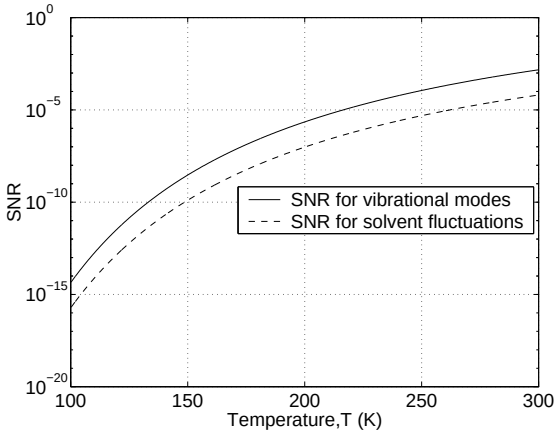

Figure 5.3: The signal-to-noise-ratio (SNR) in a myoglobin globule due to (i) molecular vibrational modes or (ii) fluctuations in the hydration shell.

size a_M [108] is given by

$$\sigma_0 = \frac{3}{4}\frac{k_B T}{a_M^2}\ln\left(\frac{a_M^2}{d_L^2 \pi e}\right). \tag{5.16}$$

Here d_L represents the Lindemann length, which characterizes the motional freedom in the solvent [108]. Approximating the molecule as a sphere of radius a_M (of surface area $4\pi a_M^2$) and combining Eqs.(5.4) and (5.16) we get

$$A^2 = \frac{6\pi\gamma k_B T}{\tau_0}\ln\left(\frac{a_M^2}{d_L^2 \pi e}\right). \tag{5.17}$$

For α fluctuations of the solvent shell which couple to the fluctuations of myoglobin [41, 45], the rate constant is given by the Vogel-Tammann-Fulcher relation to be:

$$(1/\tau_0) = f_1 \exp\{-f_2/(T - T_G)\}, \tag{5.18}$$

where $f_1 = 8.74 \times 10^{12} s^{-1}$, $f_2 = 2670$K and $T_G = 105$K, as experimentally determined [170]. The theoretical basis for the Vogel-Tammann-Fulcher relation can be found from [50]. In accordance with [108] we have taken $a_M/d_L \sim 10$. Relevant values of γ can be found from [71].

Protein-ligand interactions at large distances are described by the sum of the Lennard-

Jones potential and the Coulomb potential [191]:

$$V(r) = V_{LJ}(r) + V_C(r). \tag{5.19}$$

The Lennard-Jones potential is an empirical relation used to describe the effects of Hydrogen bonds between molecules, and for myoglobin [172] is given by

$$V_{LJ}(r) = 4U\left((\sigma/r)^{12} - (\sigma/r)^6\right), \tag{5.20}$$

where $\sigma = 3.165\mathring{A}$ and $U = -41.8kJ/mol$. The Coulomb potential for myoglobin and an approaching ligand interacting through their permanent dipole moments along the equatorial plane is given by

$$V_C(r) = \frac{k_e p_1 p_2}{\epsilon(r) r^3}. \tag{5.21}$$

k_e represents the Coulomb constant given by $k_e = 8.789 \times 10^9 Nm^2/C^2$. The dipole moments of myoglobin, Carbon monoxide (CO) and Nitric Oxide (NO) are 172 D, 0.112 D amd 0.07 D respectively. The distance dependent permittivity $\epsilon(r)$ is empirically given by

$$\epsilon(r) = \epsilon_1 + \frac{\epsilon_2}{1 + \epsilon_3 \exp(-\lambda r)}, \tag{5.22}$$

where $\epsilon_1 = -8.55$, $\epsilon_2 = 69.95$, $\epsilon_3 = 7.78$ and $\lambda = 0.2539/\mathring{A}$. For our sample calculations we have taken $A = -\frac{\partial V}{\partial r}$ at $r = 4\mathring{A}$. The effects of temperature dependence of dipole moments and the permittivity were found to be negligible. Though a distinct peak is absent, these results show that Kramers' theory predicts that the response of a myoglobin globule to ambient, biomolecular forces are enhanced by increasing temperatures. The SNR due to Kramers' theory given by Eq.(5.15) is independent of the driving frequency. This is no longer the case when intra-well motion is considered, as will be shown later.

5.3 Effect of intra-well motion

In this section we will compute the mean-squared displacement (MSD) and the signal-to-noise ratio (SNR) due to intra-well motion of myoglobin atoms in a multi-well potential. The canonical approach requires the numerical solution of the Langevin equation [122]. However, in this chapter we follow an alternative approach. A massive particle trapped in a multi-well potential can execute two distinct forms of motion: transitions from

one well to another (termed inter-well transitions); and vibrations within a well (termed intra-well motion [122]). Observables such as the MSD and SNR due to inter-well motion can be found from Kramers' theory as given by Eqs.(5.9) and (5.15). However, the effect of intra-well motion on these quantities remains to be found. This is now done.

5.3.1 MSD due to intra-well motion

For motion in the neighborhood of the meta-stable state $x_n,\ n = 1, 2$ we can use the harmonic approximation $F(x) = -m\omega_n^2(x - x_n)$ in Eq.(5.3), in the manner of [75], thereby getting

$$m\ddot{x} + \gamma\dot{x} - m\omega_n^2 x = \xi(t). \tag{5.23}$$

The oscillation frequencies for the two meta-stable states are given by $\omega_n^2 = V''(x_n)/m,\ n = 1, 2$. Taking the Fourier transform we get

$$X(\omega) = \frac{\xi(\omega)}{m(\omega^2 - \omega_n^2) + i\gamma\omega}. \tag{5.24}$$

The power spectral density is given by

$$\frac{\begin{array}{c} < X^*(\omega')X(\omega) >= \\ < \xi^*(\omega')\xi(\omega) > \end{array}}{(m(\omega'^2 - \omega_n^2) - i\gamma\omega')(m(\omega^2 - \omega_n^2) + i\gamma\omega)}. \tag{5.25}$$

From Eq.(5.4) it follows that

$$\begin{aligned} < \xi(\omega) > &= 0, \\ < \xi^*(\omega')\xi(\omega) > &= 2\pi E_\xi \delta(\omega - \omega'). \end{aligned} \tag{5.26}$$

Therefore,

$$< X^*(\omega')X(\omega) >= \frac{2\pi E_\xi \delta(\omega - \omega')}{(m(\omega^2 - \omega_n^2))^2 + (\gamma\omega)^2}. \tag{5.27}$$

The auto-correlation function is then given by

$$< x(t)x(t') > = \frac{E_\xi}{2\pi}\int_{-\infty}^{\infty} \frac{e^{i\omega(t'-t)}d\omega}{[(m(\omega^2 - \omega_n^2))^2 + (\gamma\omega)^2]}. \tag{5.28}$$

It follows that the MSD in the n^{th} well, characterized by frequency ω_n, is given by

$$\begin{aligned} < x^2(t) >_n &= \frac{E_\xi}{2\pi}\int_{-\infty}^{\infty}\frac{d\omega}{[(m(\omega^2-\omega_n^2))^2+(\gamma\omega)^2]} \\ &= \frac{E_\xi}{2m\gamma\omega_n^2} = \frac{k_BT}{m\omega_n^2}. \end{aligned} \tag{5.29}$$

The intra-well MSD is given by the sum of $< x^2(t) >_1$ and $< x^2(t) >_2$ weighted by the probabilities of the two states:

$$\begin{aligned} &MSD_{intra} = \pi_1 < x^2(t) >_1 + \pi_2 < x^2(t) >_2 \\ &= \left[\frac{W_2}{(W_1+W_2)}\frac{k_BT}{m\omega_1^2} + \frac{W_1}{(W_1+W_2)}\frac{k_BT}{m\omega_2^2}\right]. \end{aligned} \tag{5.30}$$

Therefore, combining Eqs.(5.9) and (5.30), we get:

$$\begin{aligned} &MSD = (x_1-x_2)^2\frac{W_1W_2}{(W_1+W_2)^2} + \\ &\left[\frac{W_2}{(W_1+W_2)}\frac{k_BT}{m\omega_1^2} + \frac{W_1}{(W_1+W_2)}\frac{k_BT}{m\omega_2^2}\right]. \end{aligned} \tag{5.31}$$

A plot of the total MSD given by Eq.(5.31) has been illustrated in Fig.(5.2). It can be observed that it is in good agreement with experimental data over all temperature ranges.

5.3.2 SNR due to intra-well motion

When a particle in the neighborhood of the meta-stable state $x_n,\ n = 1, 2$ is subject to a linearized potential and a weak harmonic force, the Langevin equation is given by:

$$m\ddot{x} + \gamma\dot{x} + m\omega_0^2 x = \xi(t) + A\cos\omega_s t. \tag{5.32}$$

Taking the Fourier transform of Eq.(5.32) we get

$$X(\omega) = \frac{\xi(\omega) + \pi A\left(\delta(\omega-\omega_s) + \delta(\omega+\omega_s)\right)}{(m(\omega_n^2-\omega^2) - i\omega\gamma)}. \tag{5.33}$$

The power spectral density is then given by

$$< X^*(\omega')X(\omega) >= \frac{2\pi E_\xi\delta(\omega-\omega')}{(m(\omega^2-\omega_n^2))^2+(\gamma\omega)^2}$$

$$+(\pi A)^2 \frac{(\delta(\omega-\omega_s)+\delta(\omega+\omega_s))(\delta(\omega'-\omega_s)+\delta(\omega'+\omega_s))}{(m(\omega_n^2-\omega^2)-i\omega\gamma)(m(\omega_n^2-\omega'^2)+i\omega'\gamma)}. \tag{5.34}$$

For positive frequencies, the PSD for a single well is then given by

$$S(\omega) = \frac{E_\xi}{[m^2(\omega_n^2-\omega^2)^2+(\omega\gamma)^2]} + \frac{\pi A^2}{2}\left[\frac{\delta(\omega-\omega_s)}{m^2(\omega_n^2-\omega^2)^2+(\omega\gamma)^2}\right]. \tag{5.35}$$

It follows that for two potential wells of different depths the PSD due to intra-well motion is given by:

$$\begin{aligned} < S(\omega) >_{intra} &= E_\xi\left[\frac{\pi_1}{m^2(\omega_1^2-\omega^2)^2+(\omega\gamma)^2}+\frac{\pi_2}{m^2(\omega_2^2-\omega^2)^2+(\omega\gamma)^2}\right] \\ &+\frac{\pi A^2}{2}\left[\frac{\pi_1}{m^2(\omega_1^2-\omega^2)^2+(\omega\gamma)^2}+\frac{\pi_2}{m^2(\omega_2^2-\omega^2)^2+(\omega\gamma)^2}\right]\delta(\omega-\omega_s). \end{aligned} \tag{5.36}$$

Therefore, the combined PSD due to inter-well motion and intra-well motion, is given by

$$\begin{aligned} &< S(\Omega) >=< S(\Omega) >_{inter} + < S(\Omega) >_{intra} \\ = \;& \left[R_1\frac{2\mu}{\mu^2+\omega^2}+E_\xi\left\{\frac{\pi_1}{m^2(\omega_1^2-\omega^2)^2+(\omega\gamma)^2}+\frac{\pi_2}{m^2(\omega_2^2-\omega^2)^2+(\omega\gamma)^2}\right\}\right] \\ &+A^2\left[\pi R_2+\frac{\pi}{2}\left\{\frac{\pi_1}{m^2(\omega_1^2-\omega^2)^2+(\omega\gamma)^2}+\frac{\pi_2}{m^2(\omega_2^2-\omega^2)^2+(\omega\gamma)^2}\right\}\right]\delta(\omega-\omega_s). \end{aligned} \tag{5.37}$$

Therefore, the SNR is then given by:

$$R = \frac{\pi A^2}{4mk_BT}\frac{\left[\beta^2\left(\frac{W_1W_2}{W_1+W_2}\right)^2+(g_1+g_2)\right]}{\left[\beta\left(\frac{W_1W_2}{W_1+W_2}\right)+\omega_d(g_1+g_2)\right]}, \tag{5.38}$$

where A^2 can be found separately for solvent α- fluctuations or for approaching ligands and

$$\begin{aligned} &\beta = \frac{m(x_1-x_2)^2}{k_BT}, \qquad \omega_d = \gamma/m, \\ &g_i = \frac{\pi_i(\mu^2+\omega^2)}{(\omega_i^2-\omega^2)^2+(\omega\omega_d)^2}, \; i=1,2. \end{aligned} \tag{5.39}$$

It is observed that for low and high frequencies respectively, the SNR is a monotonically decreasing function or a monotonically increasing function. For intermediate frequencies,

the SNR shows a transition from decreasing to increasing behavior.

5.4 Conclusions

This chapter considers the possibility of stochastic resonance (SR) in an effective potential model for myoglobin. If the potential is approximated by an asymmetric bimodal well, it is shown in some frequency regimes, that the Signal-to-Noise Ratio (SNR) increases with temperature. This effect persists even at physiological temperatures of ~ 300K. This has the extremely interesting interpretation that the response of myoglobin to weak, harmonic forces arising from solvent fluctuations or approaching (NO/CO) ligands, modelled by the Vogel-Tammann-Fulcher relations or the Lennard-Jones Potential, is enhanced by ambient thermal fluctuations. Alternatively, this chapter gives a theoretical argument for the vibrational statistics of myoglobin based on Kramers' theory and the Langevin equation. The temperature dependence of these statistics has drawn numerous computational and theoretical efforts, variously based on conformational kinetics [131]; the harmonic approximation [133]; molecular dynamics [174, 173]; and non-Gaussian statistics [187, 188, 189]. It has been repeatedly argued in analyses of these fluctuation statistics [2, 128, 129, 131, 133, 134, 135, 187, 188, 189] that myoglobin exhibits an effective potential with multiple minima corresponding to its stable conformations. We use a simple, yet self-consistent model developed in [189] where the potential is modeled by an asymmetric bistable potential well in one reaction co-ordinate. The transitions between two wells, often referred to as *inter-well* transitions [122] can then be described by Kramers' rate theory. They account for the anomalous, almost ten-fold increase in the mean-squared-displacement of myoglobin in the high-temperature range $180-300$K. The fluctuations in the vicinity of each well, referred to as *intra-well* fluctuations, can then be described by the Langevin equation using the harmonic approximation. In this description, they are shown to be dominant in the low-temperature regime. The sum of these two terms gives an estimate for the mean-squared-displacement of myoglobin. These results are seen to be in excellent agreement with experimental data. It is noteworthy that the measurements in [31] analyzed in this chapter, are intrinsically time-dependent due to the lifetime of the Mossbauer excited state of approximately 140ns. This raises the possibility that kinetic effects resulting from a time-dependent rate distribution should be considered. This will be done in a forthcoming work. The biological significance of these results is as follows: thermal vibrations, mediated by dielectric fluctuations, induce fluctuations in the position of the iron atom in myoglobin (corresponding to the reaction coordinate of the system). Such fluctuations are linked to the binding and unbinding

of ligands, and therefore to myoglobin's capacity to serve as an oxygen buffer and as a regulator of the concentration of nitric oxide in the bloodstream. Therefore, stochastic resonance exemplifies a means by which the effect of temperature can be evident of these crucial physiological functions of myoglobin.

Chapter 6

Stochastic resonance in tubulin dimers

6.1 Introduction

The electrical properties, signaling and information processing capabilities of microtubules (MTs) have been the subject of increasing interest in computational neuroscience [15, 182]. This stems from the fact that MTs play an essential role in transport and neuronal plasticity through their regulation of cell shape [33, 149]. It has been shown that MTs modeled as dipole lattices with some overall polarization [15] may assume ferroelectric phase long-range order, optimal for signaling and assembly/ disassembly [182]. Local conformation changes in tubulin dimers could lead to the formation of solitonic excitations detectable through Mossbauer spectroscopy [165]. Such a ferroelectric phase can be shown to be formally equivalent to a liquid crystal model, which can then be used to study the stability of such excitations [166]. Implications of this model for the dynamic instability of MTs and transport properties have been studied in [167]. A biophysical mechanism for the effect of MT on neuronal function given in [143] goes thus: (i) electrical signals from a presynaptic neuron, which arrive at a postsynaptic neuron within the dendritic spine, trigger ionic waves to travel along actin filaments to the connected MT network; (ii) the MT network then evolves these states via protein conformational changes, or changes in the electromagnetic signal; (iii) these signals or conformational changes are propagated to remote voltage sensitive ion channels where they regulate temporal gating states, thereby regulating membrane conductive properties. In addition to such classical approaches, the quantum information processing capabilities of microtubules have also been investigated [62, 17], though the existence of quantum behavior is

yet to fully reconciled with persistent decoherence effects at physiological temperatures [180]. Such properties can be related to quantum information processing in neurons implicated in the phenomena of consciousness [143, 62, 138]. These results gain additional focus because in conventionally accepted models of the brain each neuron, modelled by the Hodgkin-Huxley relations [70, 68], passively integrates synaptic signals received by its dendrites generating an action potential spike if the total membrane potential exceeds a certain threshold. However, such a model cannot account for the complexity of dendritic integration, or the inter-spike variability of neuron thresholds amongst other features [127]. This suggests a need for an alternative, more viable, model based on active integration, in a sub-cellular structure such as the neuronal cytoskeleton [62, 138]. Much indirect evidence also suggests that MTs are computationally relevant to cognitive processes [60, 53, 144] and in references in [17]. Certain other theoretical results of interest include: the dynamical instability of individual MTs leading to assembly and disassembly [16]; and treatment of nucleation and oscillations in an MT plasma using the Landau-Ginzburg formalism [169].

MTs are tubular polymers consisting of long fibers of the protein tubulin, arranged in a cylindrical manner [184] as shown in Fig.(6.1.B). Each tubulin molecule is a heterodimer consisting of α- tubulin and β-tubulin monomers (Fig.(6.1.A)). The $\alpha-$ and $\beta-$ monomers are homologous with an average weight of $50-55kDa$ and consisting of approximately 450 amino-acids [185]. On average, each tubulin molecule, or $\alpha\beta$-heterodimer, has dimensions of $46 \times 80 \times 65\mathring{A}$ and is polar. Based on the crystal structure of tubulin, it has been shown to have an electric dipole moment of 1740 Debye, a refractive index of 2.90, a high-frequency dielectric constant of 8.41 and a high-frequency polarizability of $2.1 \times 10^{-33} Cm^2/V$ [124]. Also, an electrostatic potential map of the crystal structure has shown that the interior of the tubulin molecule contains a confining potential for a mobile electron [17, 185] (Figs.(6.1.C, 6.1.D)). Physical consequences of these results in terms of effects of neighboring microtubules, and length-scales over which electrostatic effects are significant for interactions with biomolecules and ions are outlined therein. Recent studies based on electron crystallography have produced a refined structure of the tubulin molecule with a $3.5\mathring{A}$ resolution [107], the resulting map having the following cross-sections: two regions of positive potential surrounded by negative potential [8] (Fig.(6.1.C)). This region is located near the separation between the $\alpha-$ and $\beta-$ tubulin monomers, approximately 4.5 nm from the tip of the $\alpha-$ monomer, with the positive potential regions separated by 2 nm. This structure may provide a local double-well potential for a mobile electron transfer process within the protein. Though it is common to have hydrophobic neutral residues in the interior of a protein, yet the double-well po-

tential seems decidedly polar: a negative electron with two positive holes. It was found that the amino-acids around the double-well region were mainly charged with only a few hydrophobic residues in the vicinity. Such a double-well structure is a prime candidate for observing stochastic resonance (SR) [46, 64, 94, 122]. SR refers to the phenomenon whereby the addition of random noise enhances the propagation of signals within a system. This phenomenon has been observed in numerous biological detection systems such as sensory neurons [104], mechano-receptor cells of crayfish [32], cercal systems of crickets [100] and passive receptors of electrical signals in paddlefish (*Polyodon spathula*). At the sub-cellular level SR has been observed experimentally in an artificial system of ion channels [11] and theoretically in a single Shaker potassium channel [55]. An important biomedical application of SR concerns the use of electrical and mechanical noise to detect sub-threshold mechanical cutaneous stimuli [28]. For other details and references on the topic the interested reader is referred to [63].

A proper study of this phenomenon in tubulin dimers is of biophysical relevance for the following reasons:

- at physiological temperatures, long-range tunneling over distances upto $10\mathring{A}$ is a viable mechanism for electron transfer in proteins, processes which are believed to mediate protein function [107]. In our system, the residue tryptophan is located approximately $8\mathring{A}$ from the left well [56] and could supply a mobile electron to the double well for such transfer processes;

- the double-well is located within $5\mathring{A}$ from a colchicine binding site and within $8\mathring{A}$ from a non-hydrolyzable GTP on the $\alpha-$ tubulin monomer. Since colchicine is an MT inhibitor, and GTP must be bound to both the $\alpha-$ and $\beta-$ monomers for the formation of MT through polymerization, such a location may be related to the stability of the dimer and its ability to polymerize [17];

- the maximum energy of a bound electron calculated from the Coulomb interaction between mobile electrons in adjacent (nearest neighbor) sites is found to be approximately 0.6 eV, much less than the reported energy gap to the conduction band for most proteins [17]. Therefore, it can be assumed these mobile valence electrons cannot reside in the conduction band;

- tubulin dimers can be modeled as quantum well structures containing an electron that can exist in at least two distinct quantum states: its ground state and its first excited state. These excitonic states and microtubule (MT) lattice vibrations (i.e. phonons) determine the state space of individual tubulin dimers within the MT lat-

tice. Following mechanisms of exciton energy propagation based on Scheibe aggregates [186], the strength of exciton and phonon interactions and their influence on the formation and dynamics of coherent exciton domains within MTs can be studied [17]. It has been shown that sufficiently long-lived coherent exciton/ phonon structures cannot exist in the absence of thermal isolation mechanisms;

- in stochastic resonance (SR) the effect of thermally mediated transitions between adjacent wells on the long-time dynamics of the system is considered [46, 64, 94, 122]. Thus SR constitutes a thermal effect.

The remainder of this chapter is organized as follows: Section 6.2 provides necessary background theory; Section 6.3 presents the main results and finally Section 6.4 concludes the chapter.

6.2 Background theory

6.2.1 An effective potential for the problem

The double well described above can be modeled by a symmetric bistable potential in a single reaction co-ordinate of the form

$$V(x) = V_0 - \frac{a}{2}x^2 + \frac{b}{4}x^4. \tag{6.1}$$

with the coefficients

$$a = 1.578\ eV/nm^2 \quad b = 4.152\ eV/nm^4. \tag{6.2}$$

A plot of the potential given by Eqs.(6.1) and (6.2) has been illustrated in Fig.(6.1.D). The positions and the depths of the potential wells are denoted by $x_{1,2}$ and $V_{1,2}$, where S_1 and S_2 refer to the left and right wells respectively. Their numerical values are found to be $x_{1,2} = \pm 0.616\ nm$ and $V_1 = V_2 = 150\ meV$. The Langevin equation for the damped motion of a particle of mass m in the effective potential is given by

$$m\ddot{x} + \gamma\dot{x} = F(x) + \xi(t), \tag{6.3}$$

where x denotes the reaction co-ordinate of the effective potential or the amplitude of the "principal mode"; m denotes the mass; γ denotes the viscosity; $F(x) = -\frac{\partial V(x)}{\partial x}$ denotes the deterministic force due to the effective potential; $\xi(t)$ denotes the random force. The fluctuating random force $\xi(t)$ denotes Gaussian white noise with zero mean, and has a

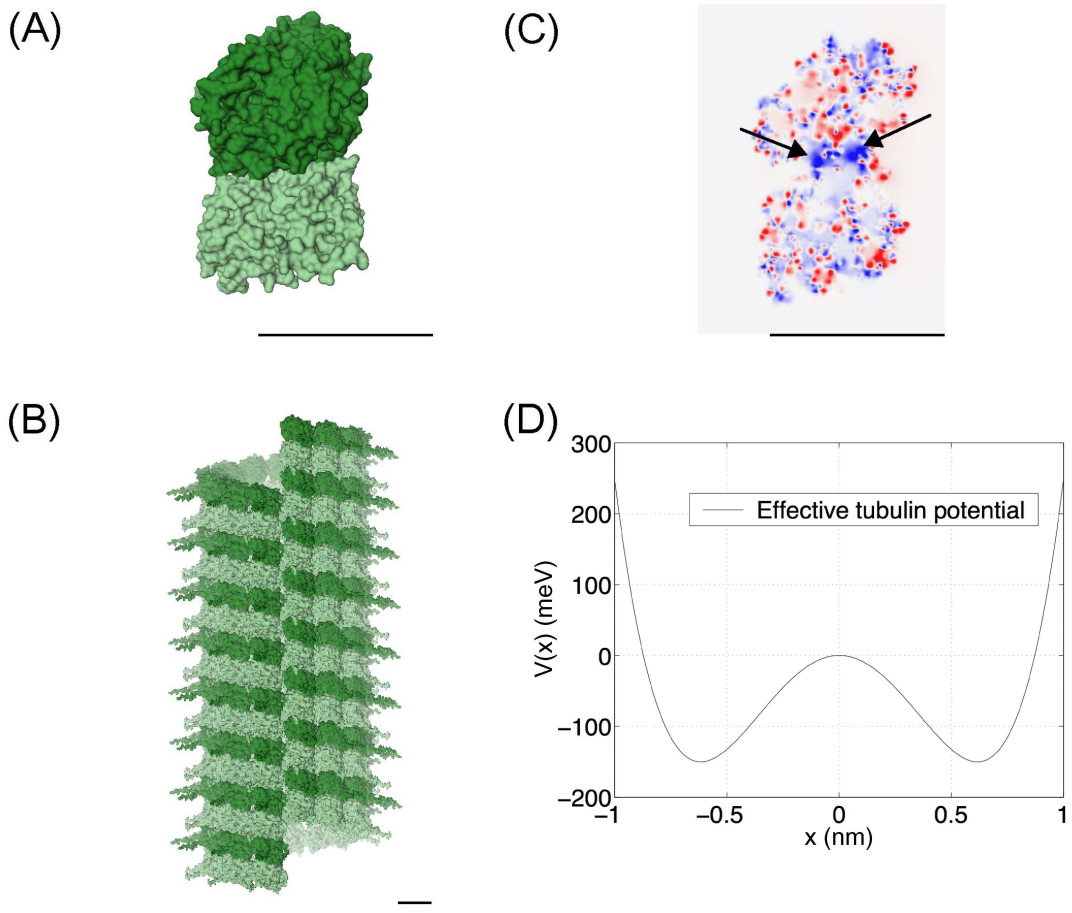

Figure 6.1: (A) A molecular surface representation of a tubulin dimer (α-monomer, pale green; β-monomer, forest green); (B) A molecular surface representation of a B-lattice microtubule; (C) An in-plane slice of the electrostatic map of tubulin showing the double well potential (black arrows) (red negative, blue positive; values between -75 and 75 $k_B\ T/e$); (D) The effective potential of tubulin as given in Eq.(6.1); Scale bars in (A) through (C) are 5 nm in length.

correlation function given by:

$$\begin{aligned} < \xi(t) > &= 0, \\ < \xi(t)\xi(t') > &= E_\xi \delta(t - t'), \end{aligned} \tag{6.4}$$

where $E_\xi = 2\gamma k_B T$. The probabilities of inter-well transitions between S_1 and S_2, given by Kramers' rate theory [64, 94] in the overdamped limit, are

$$\begin{aligned} p_{12} &= \frac{\sqrt{V''(x_1)|V''(0)|}}{2\pi\gamma} e^{-V_1/k_B T}, \\ p_{21} &= \frac{\sqrt{V''(x_2)|V''(0)|}}{2\pi\gamma} e^{-V_2/k_B T}. \end{aligned} \tag{6.5}$$

The numerical values were found from Eq.(6.1) to be:

$$W = p_{12} = p_{21} = \frac{1}{\sqrt{2}\pi} \frac{a}{\gamma} e^{-\frac{\frac{a^2}{4b}}{k_B T}}. \tag{6.6}$$

From the symmetry of the potential it also follows that the natural oscillation frequencies in both wells have the common value $\omega_0^2 = a/m$. The symbol π denotes the constant pi with a numerical value of 3.1453, and does not denote a probability. Based on results in this section, we are now in a position to derive quantitative estimates for the mean-squared displacement (MSD) and the signal-to-noise-ratio (SNR) which follow from Kramers' theory [64, 94].

6.2.2 Preliminary results from Kramers' theory

When considering inter-well transitions the details of intra-well dynamics can be conveniently ignored. The master equation governing the change of probabilities of states S_1 and S_2 [122] is given by

$$\begin{aligned} \dot{\pi_1} &= W(\pi_2 - \pi_1), \\ \dot{\pi_2} &= W(\pi_1 - \pi_2). \end{aligned} \tag{6.7}$$

The solution of Eq.(6.7) is given by [122]. It follows that the long-time limiting values of the probabilities and the inter-well mean-square displacement are given by:

$$\pi_1 = \pi_2 = 1/2. \tag{6.8}$$

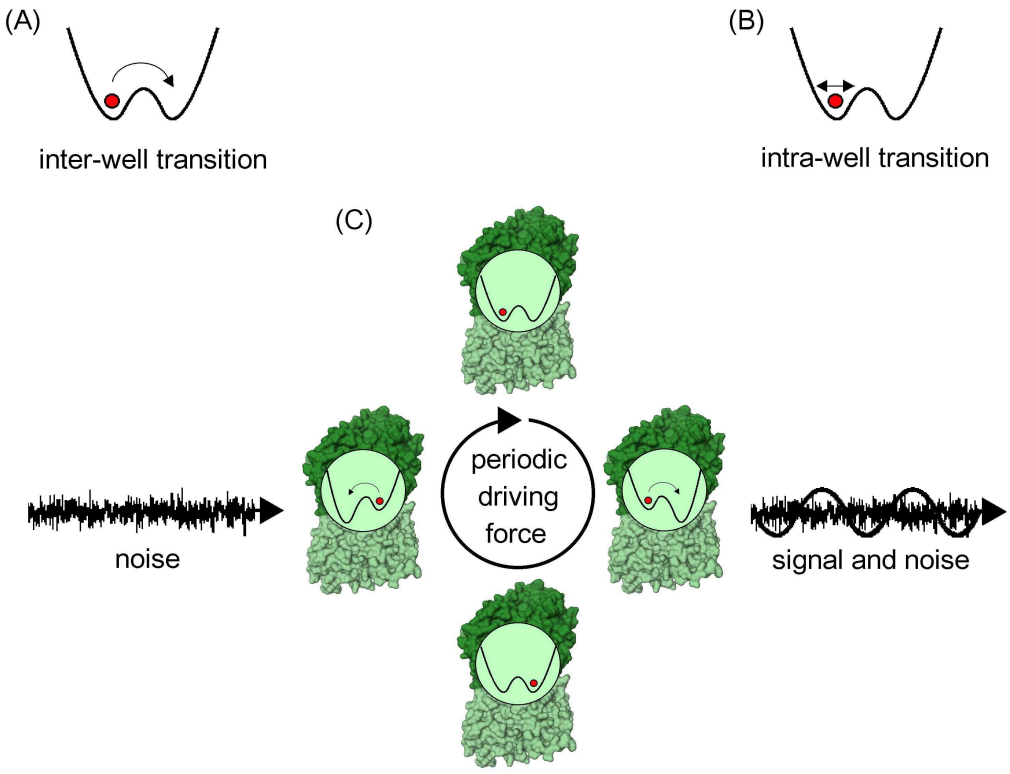

Figure 6.2: (A) Inter-well transition; (B) Intra-well fluctuation; (C) Noise impingent on a symmetric double-well potential cannot cause a transition. A weak periodic driving signal, which cannot cause well transitions on its own, rocks the double well allowing an optimal amount of noise to induce synchronized transitions between wells creating an semi-periodic output signal with enhanced amplitude.

$$\begin{aligned} MSD_{inter} &= < x^2(t)|x_0, t_0 > - (< x(t)|x_0, t_0 >)^2 , \\ &= a/b. \end{aligned} \tag{6.9}$$

When such a system is subject to weak, periodic forces the effective potential is modified to

$$V(x) = V_0 - \frac{a}{2}x^2 + \frac{b}{4}x^4 + Ax\cos(\omega_c t). \tag{6.10}$$

If the amplitude A is assumed to be sub-dominant to the depth of the potential wells V_1 and V_2 such that $A \ll V_1, V_2$, the modified time-dependent inter-well transition probabilities denoted by $W_1(t)$ and $W_2(t)$ are found to be:

$$\begin{aligned} W_1(t) &= W_1 \left[1 - \frac{A\sqrt{a/b}}{k_B T} \cos(\omega_c t) \right], \\ W_2(t) &= W_2 \left[1 + \frac{A\sqrt{a/b}}{k_B T} \cos(\omega_c t) \right]. \end{aligned} \tag{6.11}$$

It follows that the long-time limiting values of the probabilities and the inter-well mean-square displacement are given by

$$\begin{bmatrix} \pi_1 \\ \pi_2 \end{bmatrix} = \frac{1}{2\ W} \begin{bmatrix} W - a\cos\omega_c t \\ W + a\cos\omega_c t \end{bmatrix}, \tag{6.12}$$

where the coefficient a is given by

$$a = \frac{2WA\sqrt{a/b}}{k_B T}. \tag{6.13}$$

For a symmetric bistable well the auto-correlation function is given by [122] to be

$$C(\tau)_{inter} = (a/b)\ e^{-2W|\tau|} + \frac{A^2 a^2 W^2}{b^2(\omega^2 + W^2)(k_B T)^2} \left(e^{j\omega_c \tau} + e^{-j\omega_c \tau} \right). \tag{6.14}$$

The power spectral density (PSD) is given by [122] to be

$$S(\omega)_{inter} = \frac{(a/b)4W}{(\omega^2 + 4W^2)} + \frac{2\pi A^2 a^2 W^2}{b^2(\omega^2 + W^2)(k_B T)^2} \delta(\omega - \omega_c). \tag{6.15}$$

The SNR, defined as the ratio of the strength of the output signal and the output

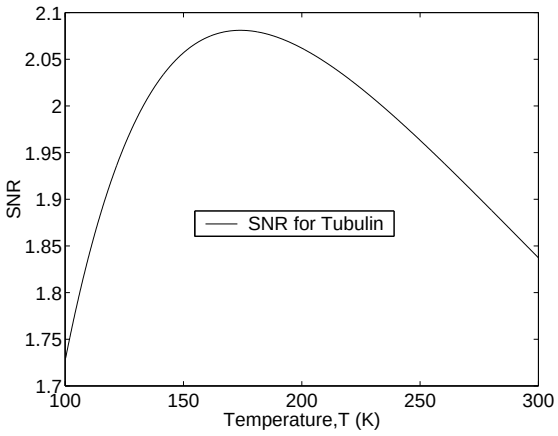

Figure 6.3: The signal-to-noise ratio (SNR) in a tubulin hetero-dimer as given by Kramers' theory and the effective potential as given in Eq.(6.1)

broadband noise at the signal frequency, denoted by R can be found from [122] to be

$$R = \frac{a^2}{\sqrt{2}bk_BT}e^{-\frac{a^2}{8bk_BT}}. \tag{6.16}$$

For dipole oscillations of tubulin dimers in a microtubule lattice the amplitude squared of the resultant force, denoted by A^2, can be approximated by

$$A^2 = \frac{e^2D_T^2\tau_0}{m_Tr_T^2\omega_T^2}k_BT, \tag{6.17}$$

where D_T, r_T, m_T and ω_T are the dipole moment, approximate radius, mass and oscillation frequency of the tubulin dimer; $\tau_0 = m/\gamma$ represents the non-zero correlation time [71]. For numerical simulations we have taken the values $D_T = 1740D, r_T = 50\mathring{A}, m_T = 50kDa$ and approximating ω_T by the frequency of a MT protofilament $\omega_T = 3.17 \times 10^{11} rad/s$.

6.3 Effect of intra-well motion

In this section we will compute the MSD and the SNR due to intra-well motion of tubulin dimers in a multi-well potential. The canonical approach would require a numerical solution of the Langevin equation as outlined in [122]. However, in this chapter we follow an alternative approach. A massive particle trapped in a multi-well potential can execute two distinct forms of motion: transitions from one well to another (termed

inter-well motion in literature [122]) shown in Fig.(6.2.A); and fluctuations within a well (termed intra-well motion) shown in Fig.(6.2.B). Observables such as the mean-squared-displacement (MSD) and the signal-to-noise ratio (SNR) due to inter-well motion can be found from Kramers' theory as given by Eqs.(6.14) and (6.16). The effect of intra-well motion remains to be found. This is now done.

6.3.1 MSD due to intra-well motion

For motion in the neighborhood of the meta-stable state $x_n,\ n = 1, 2$ we can use the harmonic approximation $F(x) = -m\omega_0^2(x - x_n)$ in Eq.(6.3) as in [75], thereby getting

$$m\ddot{x} + \gamma\dot{x} + m\omega_0^2 x = \xi(t). \tag{6.18}$$

Taking the Fourier transform of Eq.(6.18) we get

$$X(\omega) \quad = \frac{\xi(\omega)}{(m(\omega_0^2 - \omega^2) - i\omega\gamma)}. \tag{6.19}$$

The power spectral density is given by

$$< X^*(\omega')X(\omega) >= \frac{< \xi^*(\omega')\xi(\omega) >}{(m(\omega_0^2 - \omega'^2) + i\gamma\omega')\,(m(\omega_0^2 - \omega^2) - i\gamma\omega)}. \tag{6.20}$$

From Eq.(6.4) it follows that

$$\begin{aligned} < \xi(\omega) > &= 0, \\ < \xi^*(\omega')\xi(\omega) > &= 2\pi E_\xi \delta(\omega - \omega'). \end{aligned} \tag{6.21}$$

Therefore,

$$< X^*(\omega')X(\omega) >= \frac{2\pi E_\xi \delta(\omega - \omega')}{(m(\omega^2 - \omega_0^2))^2 + (\gamma\omega)^2}. \tag{6.22}$$

The auto-correlation function is then given by

$$< x(t)x(t') >= \frac{E_\xi}{2\pi} \int_{-\infty}^{\infty} \frac{e^{i\omega(t'-t)} d\omega}{[(m(\omega^2 - \omega_0^2))^2 + (\gamma\omega)^2]}. \tag{6.23}$$

It follows that the MSD in the n^{th} well is given by

$$< x^2(t) >_n \quad = \quad \frac{E_\xi}{2\pi} \int_{-\infty}^{\infty} \frac{d\omega}{[(m(\omega^2 - \omega_0^2))^2 + (\gamma\omega)^2]}$$

$$= \frac{E_\xi}{2m\gamma\omega_0^2} = \frac{k_B T}{m\omega_0^2}. \tag{6.24}$$

Therefore, combining Eqs.(6.9) and (6.24) we get

$$MSD = \frac{a^2}{4b} + \frac{k_B T}{m\omega_0^2}. \tag{6.25}$$

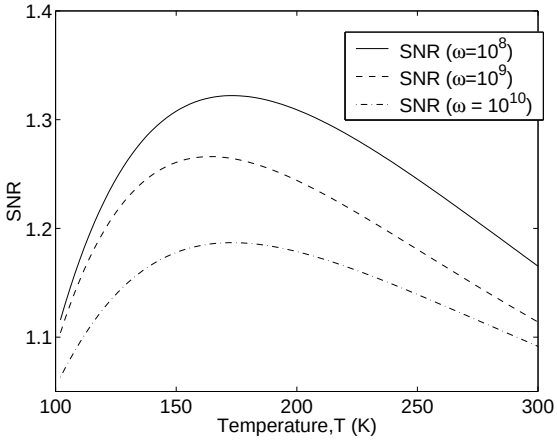

Figure 6.4: The signal-to-noise ratio (SNR) in a tubulin hetero-dimer due to dipolar oscillations at angular speeds $\omega = 10^8, 10^9$ and 10^{10} rads/s.

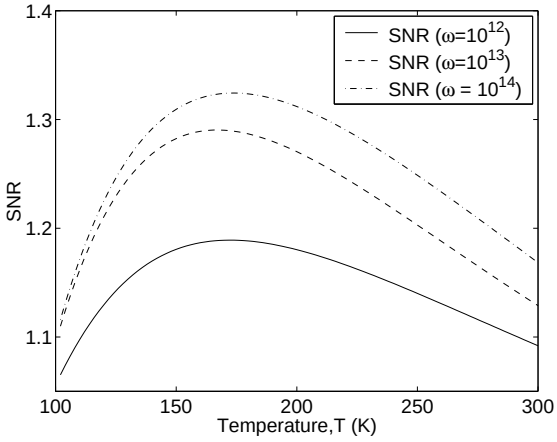

Figure 6.5: The signal-to-noise ratio (SNR) in a tubulin hetero-dimer due to dipolar oscillations at angular speeds $\omega = 10^{12}, 10^{13}$ and 10^{14} rads/s.

6.3.2 SNR due to intra-well motion

When a particle in the neighborhood of $x_n,\ n = 1, 2$ is subject to a linearized potential of the form Eq.(6.1) and a weak harmonic force, the Langevin equation is given by

$$m\ddot{x} + \gamma\dot{x} + m\omega_0^2 x = \xi(t) + A\cos\omega_c t. \tag{6.26}$$

Taking the Fourier transform of Eq.(6.26) we get

$$X(\omega) \quad = \frac{\xi(\omega) + \frac{A}{2}\left(\delta(\omega-\omega_c) + \delta(\omega+\omega_c)\right)}{(m(\omega_0^2-\omega^2) - i\omega\gamma)}. \tag{6.27}$$

Now

$$\begin{aligned} < X^*(\omega')X(\omega) > &= \frac{2\pi E_\xi \delta(\omega-\omega')}{(m(\omega^2-\omega_0^2))^2 + (\gamma\omega)^2} \\ &+(\pi A)^2 \frac{\left(\delta(\omega-\omega_c)+\delta(\omega+\omega_c)\right)\left(\delta(\omega'-\omega_c)+\delta(\omega'+\omega_c)\right)}{\left(m(\omega_0^2-\omega'^2)+i\gamma\omega'\right)\left(m(\omega_0^2-\omega^2)-i\gamma\omega\right)}. \end{aligned} \tag{6.28}$$

It follows that the power spectral density due intra-well motion is given by

$$< S(\omega) >_{intra} = \frac{E_\xi}{[(m(\omega^2-\omega_0^2))^2 + (\gamma\omega)^2]} + \frac{\pi A^2}{2}\left[\frac{\delta(\omega-\omega_c)}{m^2(\omega_0^2-\omega^2)^2 + (\gamma\omega)^2}\right]. \tag{6.29}$$

It follows that the power spectral density due to inter-well and intra-well motion, given by the coherent sum of Eqs.(6.15) and (6.29), is

$$\begin{aligned} < S(\omega) > &= < S(\omega) >_{inter} + < S(\omega) >_{intra} \\ &= \left[\frac{(a/b)4W}{\omega^2+4W^2} + \frac{E_\xi}{[(m(\omega^2-\omega_0^2))^2 + (\gamma\omega)^2]}\right] \\ &\quad +A^2\left[\frac{2\pi a^2 W^2}{b^2(\omega^2+W^2)(k_BT)^2} + \frac{\pi}{2}\frac{1}{m^2(\omega_0^2-\omega^2)^2 + (\gamma\omega)^2}\right]\delta(\omega-\omega_c). \end{aligned} \tag{6.30}$$

Therefore, the SNR is given by

$$R = \frac{\pi A^2}{mak_BT}\left(\frac{\beta^2W^2+g}{\beta W + \omega_d A}\right), \tag{6.31}$$

where A^2 is given by Eq.(6.17) and

$$\beta = \left(\frac{2ma}{bk_BT}\right), \omega_d = \gamma/m \quad \text{and} \quad g = \frac{\omega^2 + 4W^2}{(\omega^2 - \omega_0^2)^2 + (\omega\omega_d)^2}. \tag{6.32}$$

Plot of the SNR given by Eqs.(6.31) and (6.32) are shown in Figs.(6.4) and (6.5). It is observed that for all frequency regimes, the SNR shows a distinct peak at $T \sim 150$K, indicative of stochastic resonance (SR). Simulations indicate that the SR effect is robust to a wide range of model parameters.

6.4 Conclusions

This chapter investigates stochastic resonance (SR) in the electrostatic double-well potential located in tubulin dimers. Delocalized electrons can be transferred within a tubulin dimer (shown in Fig.(6.1.A)) by the process of tunneling. This process has an appealing, geometric explanation: the electrostatic map of a tubulin dimer (Fig.(6.1.C)) shows a double-well potential at the interface of the two constituent monomers (shown in greater resolution in Fig.(6.1.D)). Within the double well, indicated by arrows in Fig.(6.1.C) or plotted with respect to inter-well distance (the reaction coordinate of the system), the electron can make interwell or intrawell transitions induced by thermal fluctuations. In the system considered here, SR refers to the phenomenon by which noise, in the form of random thermal fluctuations, together with a weak, sub-threshold, input signal, such as molecular vibrations (phonon modes) or dipole oscillations, assists the delocalized electron/ small polaron in crossing the energy threshold between adjacent wells as shown in Fig.(6.2.C). The combination of a weak periodic driving force and noise induce synchronized transitions resulting in an increased output signal-to-noise ratio resulting in a more meaningful transfer of information. It is shown that for frequencies ranging from 10 MHz to 10 THz the SNR is unimodal, with a distinct peak at a temperature of $T \sim 150$ K, a characteristic of SR. The effective potential is modeled by a symmetric bimodal well in one reaction co-ordinate. The transitions between two wells, often referred to as inter-well transitions [122], can then be described by Kramers' rate theory. The fluctuations in the vicinity of each well, referred to as intra-well transitions, can then be described by the Langevin equation using the harmonic approximation. The sum of these two terms also gives an estimate for the mean-squared-displacement (MSD) of tubulin. These results imply that the response of a tubulin dimer to weak, harmonic forces arising from molecular vibrations or dipolar oscillations reaches a maximum at $T \sim 150$K, thereafter decreasing monotonically with temperature. While this indicates

the occurence of SR in the tubulin protein, the peak is well below physiological temperatures where cold-induced depolymerization and denaturation of microtubules (MTs) and the tubulin protein would be expected. However, even at physiological temperatures of $\sim$ 300K, the output signal-to-noise ratio is still above unity, allowing the possibility of meaningful information transfer. In addition, the synchronization of transitions induced by SR can be regarded as a clocking mechanism. The 10 MHz range is of particular interest as MTs exhibit a natural resonance at 8.085 MHz, for which thermally induced resonance has been suggested as a possible cause [139]. It has also been suggested that the 8.085 MHz MT resonance is due a weak Frolich condensate [146]. These results show SR in a single tubulin dimer within a classical framework. In a future correspondence, they will be extended to an array of dimers using a quantum many-body formalism.

Chapter 7

Conclusions

This thesis explores the possibility of stochastic resonance (SR) in: (i) single (hard) threshold devices used to model neurons; (ii) averaging structures of carbon nanotubes (CNTs); (iii) myoglobin atoms; and finally (iv) tubulin dimers.

In chapter 3, we consider a nonlinear detector of weak acoustic signals in a realistic noisy environment. As the performance of such a detector is dependent on the PDF governing noise, a technique to estimate the PDF, based on Beaulieu series, is also proposed (Appendix B). Physically, the SR detector consists of a threshold system followed by a correlator. The convergence properties, perturbative corrections and signal detection statistics are derived in the weak signal limit. A deterministic algorithm is developed to globally optimize the performance of the SR detector. It is established that this algorithm converges with logarithmic complexity. Scaling arguments demonstrate an improvement over standard, deterministic algorithms in two important limiting cases: (i) increasing accuracy of the optimization procedure; and (ii) increasingly heavy tailed probability density functions (PDFs). It is demonstrated that the detection performance of the SR detector is better than that of the matched filter for a large class of PDFs. Numerical simulations indicate that the SR detector is stable under most perturbative corrections. The architecture of efficient and inexpensive hardware devices based on these results, for possible use in cochlear implants, is briefly outlined.

In chapter 4, we demonstrate the possibility of observing Stochastic Resonance (SR) in arrays of *averaging structures* of carbon nanotubes using theoretical arguments. The scope of the SR phenomenon is extended to summing arrays (averaging structures) of carbon nanotubes. Such arrays are considered in two different configurations: (i) when all devices have dynamically adjustable conductance gains and threshold voltages; and (ii) when all devices have static, equal conductance gains and threshold voltages. Both

configurations are described using Shannon's Information theoretic formalism. Asymptotic expressions for the mutual information of both configurations are derived in the limiting cases of high and low noise. These formulas indicate that: (i) both configurations are equivalent at high noise; (ii) the mutual information of an array of nanotubes with fixed parameters is non-monotonic and is maximized for non-zero noise intensity, thereby fulfilling the criterion for SR. Our results can be used to establish performance bounds on nanoscale architectures with high redundancy factors and to gauge the effect of quantum coherence in such mesoscopic systems. A numerical estimate for the value of noise intensity where the SR peak is reached is derived.

In chapter 5, we present a theoretical explanation for the observed mean square displacement (MSD) vs. temperature curve of myoglobin. The effective potential of myoglobin is modeled as an asymmetric bimodal potential well. It is shown that the anomalous increase in the mean-square-displacement (MSD) for high temperatures (180K-300K) is due to thermally mediated inter-well transitions. It is also shown that the dominant contribution to the MSD at lower temperatures is due to intra-well vibrations in the vicinity of the meta-stable states. Our approach is rooted in Kramers' rate theory and the Langevin formalism. It is shown that these results are in agreement with existing experimental data. Another prominent result which follows from Kramers' rate theory is that the response of the myoglobin globule to ambient harmonic forcing terms is enhanced by temperature. Two example calculations of this phenomenon are cited for (i) transduced molecular vibrations and (ii) fluctuations originating in the solvent/ hydration shell.

In chapter 6, we consider the possibility of stochastic resonance (SR) in tubulin dimers. A formula for the signal-to-noise ratio (SNR) of tubulin as a function of temperature is derived. The effective potential experienced by a delocalized electron in such a dimer is postulated to be a symmetric bimodal well. Inter-well and intra-well motion are described by Kramers' rate theory and the Langevin formalism respectively. The frequency-dependent expression for the SNR shows that the response of the electron-tubulin dimer system is enhanced by ambient dipolar oscillations in some frequency regimes. This is a characteristic of SR. Biophysical implications of this property such as the relevance to 8.085 MHz microtubule resonance and the clocking mechanism are detailed.

Finally, it could be mentioned that these results lead to significant avenues for future investigation.

Bibliography

[1] M. Abramowitz and I. A. Stegun, *Handbook of mathematical functions*, Dover, New York (1970).

[2] K. Achtergold, C. Keppler, A. Ostermann, U. van Burck, W. Sturhahn, E. E. Alp, F. G. Park, Phys. Rev. E **65**, 051916 (2002) .

[3] R. Adams, *Sobolev spaces*, 2nd Ed. Academic press (2003).

[4] V. C. Anderson, Jl. Acoust. Soc. Am. **32(7)**, 867–870 (1960).

[5] E. Antonini and M. Brunori, *Hemoglobin and myoglobin in their reactions with ligands*, (Amsterdam, North-Holland, 1971).

[6] R. D. Antonov and A. T. Johnson, Phys. Rev. Lett. **83**, 3274–3276 (2006)

[7] R. L. Badzey and P. Mohanty, Nature Letters, **437**, 020104(R) 995–998 (2005).

[8] N. A. Baker, D. Sept, S. Joseph, M. J. Holst and M. J. McCammon, Proc. Natl. Acad. Sci. USA **98**, 10037–10041 (2001).

[9] N. C. Beaulieu, IEEE Trans. Comm. **38**, 1463–1474 (1990).

[10] R. Benzi, A. Sutera and A. Vulpiani, J. Physics A: Math. and Gen. **14**, 453–457 (1981).

[11] S. M. Bezrukov and I. Vodyanoy, Nature **378**, 362–364 (1995).

[12] R. S. Blum, IEEE Trans. Info. Th. **41(1)**, 204–215 (1995).

[13] R. P. Brent, *Algorithms for minimization without derivatives*, Dover (2002).

[14] A. R. Bulsara, A. Zador, Physical Review E, **54**,R2185 (1996).

[15] J. A. Brown, J. A. Tuszynski, Phys. Rev. E **56**, 5834–5840 (1997).

[16] H. Bolterauer, H.-J. Limbach and J. A. Tuszynski, Jl. Biol. Phys. **25** 1–22 (1999).

[17] T. J. A. Craddock and J. A. Tuszynski, J. Biol. Phys. **36**, 53–70 (2010).

[18] H. S. Carslaw, *Introduction to the theory of Fourier series and integrals*, Dover, New York (1930).

[19] F. Chapeau-Blondeau, Physical Review E, **53**, 5469 (1996).

[20] F. Chapeau-Blondeau, Physics Letters A, **232**, 41–48 (1997).

[21] F. Chapeau-Blondeau, IEEE Sig. Proc. Lett. **7**, 205–207 (2000).

[22] F. Chapeau-Blondeau, Digital Signal Processing, **9**, 162–177 (1999).

[23] F. Chapeau-Blondeau, Phys. Rev. E, **53**, 5469–5472 (1996).

[24] F. Chapeau-Blondeau and X. Godivier, Signal Processing, **56**, 293–303 (1997).

[25] F. Chapeau-Blondeau and X. Godivier, Phys. Rev. E, **55**, 1478–1495 (1997).

[26] C. L. Cheung, A. Kurtz, H. Park and C. M. Lieber, J. Phys. Chem. B **106**, 2429–2434 (2002).

[27] R. V. Churchill and J. W. Brown, *Fourier series and boundary value problems*, Mc-Graw Hill, New York (1978).

[28] J. J. Collins, T. T. Imhoff and P. Grigg, Nature **383**, 700 (1996).

[29] A. Cossins, M. Berenbrink, Nature **454**, 416–417 (2008).

[30] A. DeHon, IEEE Transactions on Nanotechnology 4, 681 (2005).

[31] W. Doster, S. Cusack, W. Petry, Nature **337**, 754 (1989).

[32] J. K. Douglass, L. Wilkens, E. Pantazelou and F. Moss, Nature **365**, 337 (1993).

[33] P. Dustin, *Microtubules*, (Springer, NY, 1978).

[34] M. I. Dykman, R. Mannella, P. V. E. McClintock and N. G. Stocks, Phys. Rev. Lett. **65**, 48 (1990a).

[35] M. I. Dykman, R. Mannella, P. V. E. McClintock and N. G. Stocks, Phys. Rev. Lett. **65**, 2606 (1990b).

[36] M. I. Dykman, D. G. Luchinsky, R. Mannella, P. V. E. McClintock, N. D. Stein and N. G. Stocks, Nuovo Cimento D **17**, 661 (1995).

[37] M. I. Dykman, R. Mannella, P. V. E. McClintock and N. G. Stocks, Phys. Rev. Lett. **68**, 2985 (1992).

[38] T. W. Ebbesen and P. M. Ajayan, Nature **358**, 220–224 (1992).

[39] S. Fauve and F. Heslot, Phys. Lett. **97A**, 5 (1983).

[40] W. Feller, *An introduction to probability theory and its applications, Vol. 1* (Wiley, 1968).

[41] P. W. Fenimore, H. Frauenfelder, B. H. MacMahon, R. D. Young, Proc. Natl. Acad. USA **101 (40)**, 14408 (2004).

[42] U. Flogel, M. W. Merx, A. Godecke, U. K. M. Decking and J. Schrader, Proc. Natl. Acad. Sci. USA **98**, 735–740 (2001).

[43] G. Floquet, Ann. de l'Ecole Norm. Suppl. **12**, 47 (1883).

[44] R. F. Fox, Phys. Rev. A, **39**, 4148 (1989).

[45] H. Frauenfelder, G. Chen, J. Berendzen, P. W. Fenimore, H. Jansson, B. H. McMahon, I. R. Stroe, J. Swenson, R. D. Young, Proc. Nat. Acad. (USA) **106 (13)**, 5129 (2009).

[46] L. Gammaitoni, P. Hanggi, P. Jung and F. Marchesoni, Rev. Mod. Phys. **70**, 223 (1998).

[47] L. Gammaitoni, F. Marchesoni and S. Santucci, Phys. Rev. E, **52(5)**, 4691–4698 (1995).

[48] L. Gammaitoni, F. Marchesoni, E. Menichella-Saetta and S. Santucci, Phys. Rev. Lett. **62**, 349 (1989).

[49] L. Gammaitoni, F. Marchesoni, E. Menichella-Saetta and S. Santucci, Phys. Rev. Lett. **65**, 2607 (1990).

[50] L. S. Garcia-Colin, L. F. del Castillo and P. Goldstein, Phys. Rev. B **40 (10)**: 7040–7044 (1989).

[51] Z. Gingl, L. B. Kiss and F. Moss, Europhys. Lett. **29**, 191 (1995).

[52] Z. Gingl, L. B. Kiss and F. Moss, Il Nuovo Cimento **17**, 795 (1995).

[53] G. Glanz, Science **276** 678–679 (1997).

[54] X. Godivier, J. Rojas-Varela and F. Chapeau-Blondeau, Electronics Lett. **33**, 1666-1668 (1997).

[55] I. Goychuk and P. Hanggi, Phys. Rev. E **61**, 4272–4280 (2000).

[56] H. B. Gray and J. R. Winkler, Ann. Rev. Biochem. **65**, 537–561 (1996).

[57] R. M. Gray, D. L. Neuhoff, IEEE Trans. Info. Th. **44(6)**, 2325–2383 (1998).

[58] M. Grifoni and P. Hanggi, Phys. Rev. Lett. **76**, 1611 (1996).

[59] M. Grifoni and P. Hanggi, Phys. Rev. E **54**, 1390 (1996).

[60] G. G. Gundersen and T. A. Cook, Cell Biol. **11**, 81–94 (1999).

[61] J. Hafner, M. Bronikowski, B. Azamian, P. Nikolaev, D. Colbert and R. Smalley, Chem. Phys. Lett. **296** (1998).

[62] S. Hameroff, Phil. Trans. R. Soc. Lond. A **365**, 1869–1896 (1998).

[63] P. Hanggi, Eur. Jl. Phys. Chem. Phys. **3**, 285–290 (2002).

[64] P. Hanggi, P. Talkner and M. Berkovec, Rev. Mod. Phys. **62(2)**, 251–341 (1990).

[65] P. Hanggi and H. Thomas, Phys. Rep. **88**, 207 (1982).

[66] G. P. Harmer, B. R. Davis and D. Abbott, IEEE Trans. Instr. Meas. **51**, 299–309 (2002).

[67] G. P. Harmer and D. Abbott, Microelectronics Jl. **32(12)**, 959–967 (2001).

[68] J. Hertz, A. Krogh and R. G. Palmer, *Introduction to the theory of neural computation*, (Santa Fe Institute studies in the science of complexity, 1991).

[69] T. Hoch, G. Wenning and K. Obermayer, Physical Review E 68, 011911 (2003).

[70] A. Hodgkin and A. Huxley, Jl. Physiol. **117**, 500–544 (1952).

[71] J. Howard, *Mechanics of motor proteins and the cytoskeleton*, (Sinauer associates, 2001).

[72] G. Hu, T. Ditzinger, C. Z. Ning and H. Haken, Phys. Rev. Lett. **71**, 807 (1993).

[73] G. Hu, H. Haken and C. Z. Ning, Phys. Lett. A **172**, 21 (1992).

[74] G. Hu, G. Nicolis and C. Nicolis, Phys. Rev. A **42**, 2030 (1990).

[75] K. Huang, *Introduction to statistical physics*, (Taylor and Francis, 2001).

[76] S. Huang, X. Cai and J. Liu, J. Amer. Chem. Soc. **125(19)**, 5636–5637 (2003).

[77] Y. Jin, W. Xu, M. Xu, Chaos, Solitons and Fractals **26**, 1183 (2005).

[78] A. Joshi, Phys. Rev. E, **77**, 020104(R) 1–4 (2008).

[79] P. Jung, Phys. Rev. E **50**, 2513 (1994).

[80] P. Jung, Phys. Lett. A **207**, 93 (1995).

[81] P. Jung and P. Hanggi, Europhys. lett. **8**, 505 (1989).

[82] P. Jung and P. Hanggi, Phys. Rev. A **41**, 2977 (1990).

[83] P. Jung and G. Mayer-Kress, Phys. Rev. Lett. **74**, 2130 (1995).

[84] P. Jung, Phys. Rep. **234**, 175 (1993).

[85] P. Jung and P. Hanggi, Phys. Rev. A **44**, 8032 (1991a).

[86] P. Jung and P. Hanggi, Z. Phys. B **90**, 255 (1993).

[87] S. M. Kay, *Fundamentals of statistical signal processing, Vol. II: Detection Theory*, Prentice-Hall, New Jersey (1998).

[88] S. M. Kay, IEEE Sig. Proc. Lett. **7**, 8–10, (2000).

[89] J. Kong, H. Soh, A. Cassell, C. F. Quate and H. Dai, Nature **395**, 878–881 (1998).

[90] B. Kosko, *Noise*, Viking (2006).

[91] B. Kosko and S. Mitaim, Phys. Rev. E, **64**, 051110 (2001).

[92] B. Kosko and S. Mitaim, Neural networks **16**, 755–761 (2003).

[93] B. Kramer, *Quantum coherence in mesoscopic systems* (Springer, 2007).

[94] H. A. Kramers, Physica (Utrecht) **7**, 284 (1940).

[95] R. Kubo, J. Phys. Soc. Jpn. **12**, 570 (1957).

[96] R. Kubo, Rep. Prog. Phys. **29**, 255 (1966).

[97] K. Lau, H. Chang, J. Lu, Y. Yin, D. Hui and H. Li, J. Comput. Theor. Nanosci. **2**, 23 (2008).

[98] I. Y. Lee, X. Liu, B. Kosko and C. Zhou, Nanoletters, **3(12)**, 1683-1686 (2003).

[99] I. Lee, X. Liu, C. Zhou and B. Kosko, IEEE Transactions on Nanotechnology **5**, 613 (2006).

[100] J. E. Levin and J. P. Miller, Nature (London) **380**, 165 (1996).

[101] J. L. Liu, Science **280**, 1253–1256 (1998).

[102] M. Locher, G. A. Johnson and E. R. Hunt, Phys. Rev. Lett, **77**, 4698 (1996).

[103] A. Longtin, J. Stat. Phys. **70**, 309(1993).

[104] A. Longtin, A. Bulsara and F. Moss, Phys. Rev. Lett. **67**, 656–659 (1991).

[105] R. Lofstedt and S. N. Coppersmith, Phys. Rev. E, **49**, 4821 (1994b).

[106] R. Lofstedt and S. N. Coppersmith, Phys. Rev. Lett, **72**, 1947 (1994a).

[107] J. Lowe, H. Li, K. H. Downing and E. Nogales, Jl. Mol. Biol. **313**, 1045–1057 (2001).

[108] V. Lubchenko, P. G. Wolynes and H. Frauenfelder, Jl. Phys. Chem. B **1009**, 7488 (2005).

[109] D. G. Luchinsky, R. Mannella, P. V. E. McClintock and N. G. Stocks, IEEE Trans. Cir. Sys.-II, **46(9)**, 1205–1214 (1999).

[110] F. W. Machell, C. S. Penrod and G. E. Ellis, in *Topics in non-Gaussian signal processing*, ed. E. J. Wegman, S. C. Schwartz and J. B. Thomas, Springer-Verlag, New York (1989), Chapter 3, 29–57.

[111] V. K. Madisetti, D. B. Williams, *The Digital Signal Processing Handbook*, CRC Press, Boca Raton, FL (1999).

[112] S. Mallat, *A wavelet tour of signal processing*, Academic press (1998).

[113] M. K. Mandal and A. A. Saha, Intl. Conf. Acoust. Sp. Sig. Proc. *(ICASSP 2008)*.

[114] F. Martorell, S. D. Cotofana and A. Rubio, IEEE Trans. Nanotech. **7**, 24 (2008).

[115] F. Martorell and A. Rubio, Microelectronics Jl. **39**, 1041 (2008).

[116] M. D. McDonnell, Proc. Austr. Comm. Th. Workshop (IEEE), Christchurch, New Zealand, 23–28 (2008).

[117] M. D. McDonnell, N. G. Stocks and D. Abbott, Phys. Rev. E **75**, 061105 (2007).

[118] M. D. McDonnell, D. Abbott and C. E. M. Pearce, Microelectronics Jl. **33**, 1079 (2002).

[119] M. D. McDonnell, N. G. Stocks, C. E. M. Pearce and D. Abbott, Fluc. Noise Lett. **5**, L457 (2005).

[120] M. D. McDonnell, N. G. Stocks, C. E. M. Pearce and D. Abbott, Phys. Lett. A **352**, 183 (2006).

[121] R. Martel, T. Schmidt, H. R. Shea, T. Hertel and P. Avouris, Appl. Phys. Lett. **73**, 2497–2449 (1998).

[122] B. McNamara and K. Wiesenfeld, Phys. Rev. A **39**, 4854 (1989).

[123] B. McNamara, K. Wiesenfeld and R. Roy, Phys. Rev. Lett. **60**, 2626 (1988).

[124] A. Mershin, H. Sanabria, J. H. Miller D. Nawarathna, E. M. C. Skoulakis, N. E. Mavromatos, A. A. Kolomenski, H. A. Schuessler, R. F. Luduena and D. V. Nanopoulos, in *The emerging physics of consciousness*, ed. J. A. Tuszynski, 95–170 (Springer, Berlin, 2006).

[125] S. Mitaim and B. Kosko, Proc. IEEE **86**, 2152–2183 (1998).

[126] F. Moss, L. M. Ward and W. G. Sannita, Clin. Neurophys. **115**, 267–281 (2004).

[127] B. Naundorf. F. Wolf and M. Volgushev, Nature **440**, 1060 (2006).

[128] G. U. Nienhaus, J. Heinzl, E. Huenges and F. Parak, Nature **338**, 665 (1989).

[129] G. U. Nienhaus, R. Waschiply, K. Nienhaus, O. Minkow, A. Ostermann and F. G. Parak, *Proc. first biological physics conference, Bangkok, Thailand*, 56 (World Scientific, 2001).

[130] K. Nikolic, A. S. Sadek and M. Foreshaw, Nanotechnology **13**, 357 (2003).

[131] A. Ostermann, R. Waschipky, F. G. Parak and G. U. Niehaus, Nature **404**, 205 (2000).

[132] A. Papoulis, *Probability, random variables and stochastic processes*, Mc-Graw Hill, New York (1984).

[133] F. G. Parak and K. Achtergold, Hyperfine interactions **123**, 825 (1999).

[134] F. G. Parak, E. Knapp and D. Kucheida, Jl. Mol. Biol. **161**, 177 (1982).

[135] F. G. Parak, *Proc. first biological physics conference, Bangkok, Thailand*, 7, (World Scientific, 2001).

[136] A. Patel and B. Kosko, Neural networks, **18**, 467–478 (2005).

[137] A. Patel and B. Kosko, Phys. Rev. E, **64**, 051110 1–11 (2001).

[138] R. Penrose, *Shadows of the mind*, (Oxford University Press, NY, 1994).

[139] J. Pokorny, J. Hasek, F. Jelinek, J. Saroch and B. Palan, Electro- and Magnetobiology **20 (3)**, 371–396 (2001).

[140] D. R. Powell and G. R. Wilson, in *Topics in non-Gaussian signal processing*, ed. E. J. Wegman, S. C. Schwartz and J. B. Thomas, Springer-Verlag, New York (1989), Chapter 2, 17–28.

[141] C. Presilla, F. Marchesoni and L. Gammaitoni, Phys. Rev. A, **40**, 2105 (1989).

[142] W. H. Press, S. A. Teukolsky, W. T. Vetterling and B. P. Flannery, *Numerical recipes in C: The art of scientific computing*, (Cambridge University Press, 1995).

[143] A. Priel, J. A. Tuszynski and H. F. Cantiello, in *The emerging physics of consciousness*, ed. J. A. Tuszynski, 293–325, (Springer, Berlin, 2006).

[144] A. Priel, J. A. Tuszynski and N. J. Woolf, Eur. Biophys. Jl. **35** 40–52 (2005).

[145] W. J. Rappel and S. H. Strogatz, Phys. Rev. E, **50**, 3249 (1994).

[146] J. R. Reimers, L. K. McKemmish, R. H. McKenzie, A. E. Mark and N. S. Hush, Proc. Natl. Acad. Sci. USA **106 (11)**, 4219–4224 (2009).

[147] H. Risken, *The Fokker-Planck equation*, Springer series in synergetics **18**, (Springer, Berlin, New York, 1999).

[148] D. Rousseau, F. Duan and F. Chapeau-Blondeau, Phys. Rev. E **68**, 031107 (2003).

[149] K. Roberts and J. S. Hyams, *Microtubules* (Academic press, NY, 1979).

[150] S. Roy and V. Beiu, IEEE Trans. Nanotech. **4**, 441 (2005).

[151] W. Rudin, *Functional analysis, 2nd Ed.* McGraw Hill (1991).

[152] W. Rudin, *Principles of mathematical analysis*, Mc-Graw Hill (1976).

[153] P. Rudnick, Jl. Acoust. Soc. America **32(7)**, 871–877 (1960).

[154] A. S. Sadek, K. Nikolic and M. Foreshaw, Nanotechnology **15**, (2005).

[155] A. A. Saha and G. V. Anand, Sig. Proc. **83**, 1193–1212 (2003).

[156] A. A. Saha and G. V. Anand, Sig. Proc. **86**, 3466–3471 (2006).

[157] A. A. Saha and V. G. Guha, Sig. Proc. **87**, 134–147 (2007).

[158] A. A. Saha and J. A. Tuszynski, Adv. Media and Comm. Research **6**, 122–156 (2010).

[159] A. A. Saha and J. A. Tuszynski, Jl. Comput. Theor. Nanosci. **8**, 1–9 (2011).

[160] A. A. Saha and J. A. Tuszynski, Jl. Biol. Phys. *to appear*.

[161] A. A. Saha, T. J. A. Craddock and J. A. Tuszynski, Biosystems *submitted*.

[162] R. Saito, M. Fujita, G. Dresselhaus and M. S. Dresselhaus, Appl. Phys. Lett. **60**, 2204–2206 (1992).

[163] J. J. Sakurai, *Modern quantum mechanics*, Pearson Education (1994).

[164] A. Samarbakhsh and J. A. Tuszynski, J. Comput. Theor. Nanosci. **5** 2041 (2008).

[165] M. V. Sataric, S. Zekovic, J. A. Tuszynski and J. Pokorny, Phys. Rev. E **58**, 6333–6339 (1997).

[166] M. V. Sataric and J. A. Tuszynski, Phys. Rev. E **67**, 011901-1-11 (2003).

[167] M. V. Sataric and J. A. Tuszynski, Jl. Biol. Phys. **31**, 487–500 (2005).

[168] E. E. Scott, Q. H. Gibson and J. S. Olson, J. Biol. Chem. **276**, 5177–5188 (2001).

[169] D. Sept and J. A. Tuszynski, Jl. Biol. Phys. **26** 5–15 (2000).

[170] Y. Shibata, H. Takahashi, A. Kurita and T. Kushida, Jl. Luminescence **72–74**, 605–606 (1997).

[171] M. R. Stan, P. D. Franzon, S. C. Goldstein, J. C. Lach and M. M. Zeidler, Proc. IEEE **91**, 1940 (2003).

[172] P. J. Steinbach and B. R. Brooks, Jl. Comput. Chem, **15**: 667–683 (1993).

[173] P. J. Steinbach and B. R. Brooks, Proc. Natl. Acad. USA **93**, 55 (1996).

[174] P. J. Steinbach and B. R. Brooks, Proc. Natl. Acad. USA **90**, 9135 (1993).

[175] N. G. Stocks, Phys. Rev. Lett. **84**, 2310 (2000).

[176] N. G. Stocks, Phys. Rev. E **63**, 041114 (2001).

[177] N. G. Stocks, D. Allingham and R. P. Morse, Fluc. Noise Lett. **2**, L169 (2002).

[178] R. L. Stratonovitch, *Topics in the theory of random noise, Vol.1*, Gordon and Breach, New York.

[179] S. J. Tans, R. M. Verschueren and C. Dekker, Nature **393**, 49–52 (1998).

[180] M. Tegmark, Phys. Rev. E **61**, 4194–4206 (2000).

[181] L. Turin, Chem. Sens. **21 (6)**, 773 (1996).

[182] J. A. Tuszynski, S. Hameroff, M. V. Sataric, B. Trpisova and M. L. A. Nip, J. Theor. Biol. **174**, 371–380 (1995).

[183] J. A. Tuszynski, Travis J. A. Craddock and Eric J. Carpenter, J. Comput. Theor. Nanosci. **5** 2022 (2008).

[184] J. A. Tuszynski and M. Kurzynski, *Introduction to biophysics*, (CRC Press, Florida, 2003).

[185] J. A. Tuszynski, J. A. Brown, E. Crawford, E. J. Carpenter, M. L. A. Nip, J. M. Dixon and M. V. Sataric, Math. Comput. Model. **41** 1055–1070 (2005).

[186] J. A. Tuszynski, M. F. Jorgensen and D. Mobius, Phys. Rev. E **59**, 4374–4382 (1999).

[187] J. A. Tuszynski, M. J. Clouter and H. Kiefte, Phys. Lett. A **108** 272 (1985).

[188] J. A. Tuszynski and A. Wierzbicki, Phys. Rev. B **43**, 8472 (1991).

[189] J. A. Tuszynski, E. J. Carpenter, J. M. Dixon and Y. Engelborghs, Eur. Biophys. Jl. **33**, 159 (2004).

[190] N. G. van Kampen, *Stochastic processes in physics and chemistry, 2nd. Ed.* (North-Holland, Amsterdam, New York, 1978).

[191] J. Wang, R. M. Wolf, J. W. Caldwell, P. A. Kollman and D. A. Case, Jl. Comput. Chem. **25**, 1157–1174 (2004).

[192] K. Wiesenfeld, D. Pierson, E. Pantazelou, C. Dames and F. Moss, Phys. Rev. Lett. **72**, 2125 (1994).

[193] J. M. G. Wildoer, L. C. Venema, A. G. Rinzler, R. E. Smalley and C. Dekker, Nature **391**, 59–62 (1998).

[194] H. S. Wio and S. Bouzat, Braz. Jl. Phys. **29**, 136 (1999).

[195] D. Witthaut, S. Trimborn and S. Wimberger, Phys. Rev. A **79**, 033621 (2009);

[196] http://focus.ti.com/docs/toolsw/folders/print/tmdsdsk6713.html

[197] S. Zdravkovic, J. A. Tuszynski and M. V. Sataric, J. Comput. Theor. Nanosci. **2** 263 (2005).

[198] T. Zhou and F. Moss, Phys. Rev. A **41**, 4255 (1990).

[199] T. Zhou, F. Moss and P. Jung, Phys. Rev. A **42**, 3161 (1990).

[200] C. Zhou, J. Kong and H. Dai, Appl. Phys. Lett. **76**, 1597 (2000).

[201] S. Zozor and P.-O. Amblard, IEEE Trans. Sig. Proc. **47 (1)**, 108–122 (1999) and **49 (5)**, 1107–1109 (2001).

[202] S. Zozor and P.-O. Amblard, Sig. Proc. **82 (3)**, 353–367 (2002).

[203] S. Zozor, P.-0. Amblard and C. Duchene, Fluct. Noise Lett. **7**, L39 (2007).

Appendix A

Miscellaneous relations

A.1 Upper bound of search interval

Eq.(3.29) describes a Gaussian-Gaussian mixture. Since the first component Gaussian is larger than the second component Gaussian, we get

$$f(x) < \frac{c}{\sqrt{2\pi}}\left[\alpha + \frac{1-\alpha}{\beta}\right]\exp\left(-\frac{c^2x^2}{2}\right).$$

Inverting the RHS of this inequality, we get $f(x) \leq \tilde{\epsilon}\ \forall x \geq B$ for

$$B = \frac{1}{c}\left[2\log\left(\frac{\alpha + (1-\alpha)/\beta}{\sqrt{2\pi}\tilde{\epsilon}}c\right)\right]^{1/2}.$$

For our simulations we choose $\tilde{\epsilon} = 0.01$ and the corresponding value of B.

A.2 Formulas for partial derivatives

From the definition of the Gamma integral

$$\Gamma(u,a) = \int_u^\infty e^{-t}t^{-1+a}dt.$$

Therefore, $\Gamma'(u,a) = -e^{-u}u^{-1+a}$. From the definition of c in (3.30) it follows

$$\frac{\partial c^2}{\partial \alpha} = (1-\beta^2) \quad \text{and} \quad \frac{\partial c^2}{\partial \beta} = 2(1-\alpha)\beta.$$

For mixtures-of-Gaussians, integrating (3.29), we get

$$[1 - F(x)] = \frac{\alpha}{2\sqrt{\pi}}\Gamma((cx)^2/2, 1/2) + \frac{1-\alpha}{2\sqrt{\pi}}\Gamma((cx)^2/2\beta^2, 1/2). \tag{A.1}$$

Therefore,

$$\begin{aligned}
\frac{\partial F}{\partial \alpha} &= -\frac{1}{2\sqrt{\pi}}\left[\Gamma((cx)^2/2, 1/2) - \Gamma((cx)^2/2\beta^2, 1/2)\right] \\
&\quad + \frac{x(1-\beta^2)}{2c\sqrt{2\pi}}\left[\alpha e^{-(cx)^2/2} + \frac{1-\alpha}{\beta}e^{-(cx)^2/2\beta^2}\right], \\
\frac{\partial F}{\partial \beta} &= \frac{x\alpha(1-\alpha)}{c\sqrt{2\pi}}\left[\beta e^{-(cx)^2/2} - \frac{1}{\beta^2}e^{-(cx)^2/2\beta^2}\right].
\end{aligned} \tag{A.2}$$

Similarly, from (3.29) it also follows

$$\begin{aligned}
\frac{\partial f}{\partial \alpha} &= \frac{1}{2c\sqrt{2\pi}}[\{\alpha(1-\beta^2)(3-(cx)^2) + 2\beta^2\}e^{-(cx)^2/2} \\
&\quad + \frac{1}{\beta}\{(1-\alpha)(1-\beta^2)(3-(cx/\beta)^2) - 2\}e^{-(cx)^2/2\beta^2}], \\
\frac{\partial f}{\partial \beta} &= \frac{\alpha(1-\alpha)}{c\sqrt{2\pi}}\left[\beta(1-(cx)^2)e^{-(cx)^2/2} - \frac{1}{\beta^2}(1-(cx/\beta)^2)e^{-(cx)^2/2\beta^2}\right].
\end{aligned} \tag{A.3}$$

In the above formulae, the dependence of the LHS on the argument x has been suppressed for convenience.

A.3 Structured version of Brents' algorithm

The classical version of Brent's algorithm [13] requires GOTO and break statements. A slightly modified version of Brent's algorithm without such unstructured programming is presented. The step numbers to the left margin do not have any functional purpose and have been kept to indicate a correspondence with the original [13].

The Algorithm:

Initialize $lx = 0$; $ux = B$; $M = 10$; flag1=0; $\epsilon = 0.0001$

$\delta = \min(|\epsilon/M|, \sqrt{|\epsilon/M|})$.

1. $\phi \leftarrow \min(G(lx), G(ux))$,
   if($\phi == G(lx)$) then $\mu \leftarrow lx$, else $\mu \leftarrow ux$.
   $x_2 \leftarrow lx$.
2. flag1=1, $x_3 \leftarrow$ some point in $(x_2, ux]$.
   while(flag1==1){

if$((x_2 >= (ux - \delta))$or$(|x_3 - x_2| < \delta))$ then flag1=0.
else $x_3 \leftarrow$ some point in $(x_2, ux]$.
flag2 = 1;
while(flag2==1){
3. if$(G(x_3) < \phi)$ then $\mu \leftarrow x_3$,$\phi \leftarrow G(x_3)$.
4. if the parabola $y = P(x)$ defined by $P''(x) = M$,
$P(x_2) = G(x_2)$ and $P(x_3) = G(x_3)$ satisfies
the condition $P(x) \geq \phi - \delta \forall x \in [x_2, x_3]$
then flag2 $\leftarrow 0$,
else $x_3 \leftarrow (x_2 + x_3)/2$.
}end (of flag2 loop)
5. $x_2 \leftarrow x_3$;
}end (of flag1 loop)

Certain details necessary to the implementation of the above algorithm are mentioned now.

1. The condition in step 4 is equivalent to stating, *"if the minimum of the parabola $y = P(x)$ ... denoted by P_{min} satisfies $P_{min} \geq \phi - \epsilon$"*. P_{min} is found to be

$$P_{min} = G(x_3) - \frac{DG.M}{2}(x_3 - x_2) - \frac{M}{4}(x_3 - x_2)^2 - \frac{DG^2}{4},$$

where $DG = \frac{G(x_3)-G(x_2)}{x_3-x_2}$.
In step 2, a good choice of x_3 is given in[13] to be

$$x_3 = min\left\{ux, x_2 + \sqrt{\frac{G(a_2) - \phi + \epsilon}{M/2}}\right\}$$

The implementation and the convergence properties are seen to depend crucially on M the upper bound of the absolute value to the second derivative of the Gain functional i.e. $Sup|G''(x)| \leq M$. M can be estimated to be ~ 10.

A.4 A bound for M

The polynomial factors in both terms in Eq.(3.16) can be bounded over finite intervals giving,

$$|f''(x)| \leq \frac{c^3}{\sqrt{2\pi}} \left[\alpha M_1 e^{-(cx)^2/2} + \frac{1-\alpha}{\beta^3} M_2 e^{-(cx)^2/2\beta^2} \right]. \tag{A.4}$$

where

$$\begin{aligned} M_1 &= Max_{[0,B]} \left((cx)^2 - 1 \right), \\ M_2 &= Max_{[0,B]} \left((cx/\beta)^2 - 1 \right), \\ &= Max_{[0,B/\beta]} \left((cx)^2 - 1 \right) \end{aligned} \tag{A.5}$$

Since the maximum taken over a smaller interval/set must necessarily be smaller, it follows

$$M_2 \leq M_1. \tag{A.6}$$

Combining the inequalities (A.4,A.6) and Eq.(3.16) we get

$$\begin{aligned} |G''(x)| &\leq \left[M_1 \frac{c^3}{\sqrt{2\pi}} \right] \frac{2f^2(x)}{1-F(x)}, \\ &\leq \left[M_1 \frac{c^3}{\sqrt{2\pi}} \right] G(x) \end{aligned} \tag{A.7}$$

Therefore taking the supremum of both sides,

$$Sup|G''(x)| \leq \left[M_1 \frac{c^3}{\sqrt{2\pi}} \right] SupG(x) \tag{A.8}$$

For large values of B the bound M_1 can be approximated as $M_1 \approx (cB)^2$ and from numerical simulations we know that for ranges of α and β considered, $Sup\ G(x) \leq 12$. Therefore,

$$Sup|G''(x)| \leq \frac{12c^5B^2}{\sqrt{2\pi}} \tag{A.9}$$

Though rigorous, this bound give a value of ~ 100 which is very conservative, the maximum value observed from numerical simulations being ~ 5. Such an over-estimate

would result in 20 times more computation than for an ideal, exact estimate. In order to reduce complexity, a sharper bound is therefore necessary.

Appendix B

Noise characterization using Beaulieu series

In this section we propose a computational technique for estimating parameters of probability density functions (PDFs) governing marine noise, using Beaulieu series. The PDFs are assumed to be mixtures-of-Gaussians from the widely used Middleton's Class A model. The Beaulieu series for such PDFs are derived. Such an approach is orders of magnitude more efficient than approaches based on convolution integrals, and can be done in real-time. The computational complexity for the technique is then derived. Such a procedure can be used in conjunction with existing detectors on sonar platforms.

B.1 Problem formulation:

The inverse problem of characterizing marine noise from sonar data requires the repeated computation of the PDF of sums of random variables. Let $X_i, i = 1, \ldots M$ denote independent R.V's each with a PDF $f(.)$. Denote the sum of the M Random Variables (RVs) by Y i.e. $Y = \sum_{i=1}^{M} X_i$ and its probability density function (PDF) and cumulative distribution function(CDF) by $g(.)$ and $G(.)$, respectively. The classical formulae for $g(.)$ and $G(.)$ given by (i) the $M-1$-fold convolution $g(x) = f * f * \ldots f * (x)$ and (ii) the integral $G(x) = \int_{-\infty}^{x} g(u)du$ represent a computationally exorbitant task. In [9] Beaulieu developed an infinite series representation for the CDF $G(.)$. The utility of Beaulieu series lies in the fact that M successive integrals by quadrature, have been replaced by a single rapidly convergent summation. In this section we derive the Beaulieu series for a large class of marine noise PDFs, and propose an iterative technique for estimating the parameters defining the PDF from sonar time-series. An estimate of of the computational

complexity is also derived.

B.2 Proposed technique:

Our proposed technique has three main components: (i) Derivation of the *Beaulieu series* for mixture-of-Gaussian PDFs which largely govern marine noise; (ii) Calculation of a cost functional which relates the theoretical estimate of CDF $G_{\alpha,\beta}(.)$ from Beaulieu series to that observed from sonar data; and lastly (iii) Calculation of the optimal values for the parameters α and β which the define marine noise PDF. These components are now described in succession.

Phenomenological studies of marine environments [110] show the PDF governing ocean acoustic noise can be modelled as a weighted sum of two Gaussians as given by Eqs.(3.29) and (3.30). The *Beaulieu series* for mixture-of-Gaussian PDFs can be expressed as

$$G_{\alpha,\beta}(y) = \frac{1}{2} + \frac{2}{\pi} \sum_{n=1,odd}^{\infty} \frac{\sin(n\omega y/M)}{n} \times \left[\alpha e^{-n^2\omega^2/2c^2} + (1-\alpha) e^{-n^2\omega^2\beta^2/2c^2}\right]. \tag{B.1}$$

where $\omega = 2\pi/T$. Some relevant values are $T = 196.8$ and $\omega = \pi/98.4$ [9].

The mean squared error (MSE) between the theoretical and empirical estimates of the CDF for particular values of (α, β) is then given by

$$MSE(\alpha,\beta) = \int_{y=-\infty}^{\infty} |G_{\alpha,\beta}(y) - G_{obs}(y)|^2 dy. \tag{B.2}$$

Typical surface plots of $MSE(\alpha, \beta)$ using synthetic data and Beaulieu series generated from assumed values of the mixing parameters (α, β) show the functional to be unimodal in nature [113]. The optimal estimates $(\alpha_{opt}, \beta_{opt})$ are given by the values which minimize the MSE as follows:

$$(\alpha_{opt}, \beta_{opt}) = Argmin_{\alpha,\beta} MSE(\alpha,\beta). \tag{B.3}$$

These estimates can be found by a classical, deterministic algorithm developed by Brent [13]. In addition, this benchmark algorithm is guaranteed to converge to the global optimum in a finite number of steps.

The proposed technique can then be summarized as follows:

- Minimize $MSE(\alpha, \beta)$ defined in Eq.(B.2) using Brent's algorithm;

- At each iteration evaluate $G(\alpha, \beta)$ using Beaulieu series given in Eq.(B.1).

The stopping criterion is achieved when within 0.1% of the global minimum of $MSE(\alpha, \beta)$. Numerical studies of the stability of these estimates were done in [113].

B.3 Computational complexity:

The computational complexity of the proposed algorithm is evidently the product of the complexities of (i) the Beaulieu series summation given by Eq.(B.1); (ii) the computation of the integral in Eq.(B.2) by quadrature and lastly (iii) Brent's algorithm, denoted by C_1, C_2 and C_3 respectively.

C_1 can be taken to be the number of terms after which the series in Eq.(B.1) is truncated. It can be shown [9] that the error incurred by truncating the summation at the ${N_1}^{th}$ term, denoted here by R_{N_1} is upper bounded by: $|R_{N_1}| \leq \left\{ [\sup f(x)] \left[\frac{T}{4} - \frac{2T}{\pi^2} \sum_{n=1,odd}^{N_1} \frac{1}{n^2} \right] \right\}^{1/2}$. Inverting this bound we get

$$C_1 = \sqrt{\frac{2}{\pi^5}} Tc \left[\alpha + \frac{1-\alpha}{\beta} \right] \epsilon^{-1}. \tag{B.4}$$

Theoretical estimates of C_2 and C_3 are found [13] and [142] to be:

$$\begin{aligned} C_2 &= 2B^2 \frac{\sqrt{U_\alpha U_\beta}}{\epsilon} \log_2 \left(2B \sqrt{\frac{U_\alpha}{2\epsilon}} \right) \log_2 \left(2B \sqrt{\frac{U_\beta}{2\epsilon}} \right), \\ C_3 &= \left[\frac{2}{3} B^3 U_y \right]^{1/2} \epsilon^{-1/2}, \end{aligned} \tag{B.5}$$

where U_α, U_β and U_y denote upper bounds on various second order partial derivatives of the functional being optimized given by $Sup|\frac{\partial^2 MSE(\alpha,\beta)}{\partial \alpha^2}| \leq U_\alpha$, $Sup|\frac{\partial^2 MSE(\alpha,\beta)}{\partial \beta^2}| \leq U_\beta$ and $Sup|\frac{\partial^2 MSE(\alpha,\beta)}{\partial y^2}| \leq U_y$, respectively.

The total computational complexity of the procedure C_{total} is then given by

$$\begin{aligned} C_{total} &= C_1 \times C_2 \times C_3, \\ &= \left[(16/3\pi^5)^{1/2} B^{7/2} (U_y U_\alpha U_\beta)^{1/2} \right] Tc \left[\alpha + \frac{1-\alpha}{\beta} \right] \epsilon^{-5/2} \\ &\quad \log_2 \left(2B \sqrt{\frac{U_\alpha}{2\epsilon}} \right) \log_2 \left(2B \sqrt{\frac{U_\beta}{2\epsilon}} \right) \end{aligned} \tag{B.6}$$

It can be inferred for sufficiently high accuracy i.e. as $\epsilon \to 0_+$, the complexity is propor-

tional to

$$C_{total} \propto \epsilon^{-5/2}(\log_2 \epsilon)^2 \tag{B.7}$$

For a typical marine ocean acoustic environment, this translates to $\sim 10^7$ elementary arithmetic operations for the entire optimization routine. On a cluster of 4 Pentium-5 160Mhz computers this would require $0.01 - 0.02$ secs, and $0.02 - 0.04$ secs on a Texas Instruments(TI) DSP platform (Model: TMS320C6713).

B.4 Conclusions:

We develop a procedure for the application of Beaulieu series to the estimation of PDFs governing marine noise. The Beaulieu series for a large class of marine noise PDFs are first derived. An iterative procedure to compute the optimal estimates of the parameters defining the PDF, from sonar time-series is then formulated. Unlike existing methods, this procedure can be performed in real-time. These results indicate that such a procedure can be used in tandem with nonlinear detectors with system parameters which depend on marine noise PDFs.

Appendix C

Derivations for Chapter 4

C.1 Miscellaneous (useful relations, values etc)

For $|a_n| \leq 1$ the following expansion can be used:

$$\log(1 + a_n(x)) \approx a_n(x) - 0.5a_n(x)^2. \tag{C.1}$$

For symmetric PDFs it can be shown:

$$F(-u) = 1 - F(u). \tag{C.2}$$

The following inequality can be found by integrating by parts [40]:

$$\begin{aligned} & f\left(\frac{\Theta_i - x}{\sigma_\eta}\right)\left[\left(\frac{\sigma_\eta}{\Theta_i - x}\right) - \left(\frac{\sigma_\eta}{\Theta_i - x}\right)^3\right] \\ & \leq 1 - F\left(\frac{\Theta_i - x}{\sigma_\eta}\right) \leq f\left(\frac{\Theta_i - x}{\sigma_\eta}\right)\left(\frac{\sigma_\eta}{\Theta_i - x}\right). \end{aligned} \tag{C.3}$$

where $f(\cdot)$ and $F(\cdot)$ represent the unit-variance PDF and CDF governing noise respectively, as defined in Eq.(4.6). The first inequality in (4.17) is straightforward from Ineq.(C.3) and Eq.(4.5). From Eq.(4.5) and the assumed symmetry of the PDF it also follows

$$\begin{aligned} 1 - P_i(x) &= \int_{-\infty}^{\Theta_i - x} f_\eta(x)dx = \int_{x-\Theta_i}^{\infty} f_\eta(x)dx \\ &= 1 - F_\eta(x - \Theta_i) = 1 - F\left(\frac{x - \Theta_i}{\sigma_\eta}\right). \end{aligned} \tag{C.4}$$

The second inequality in (4.17) then follows.

The term B_1 in Eq.(4.21) is a function of the threshold values $(\Theta_i)_{i=1}^N, i = 1 \dots N$ which in turn are functions of the noise intensity σ_η^2. It can be empirically observed that $(\Theta_i)_{i=1}^N, i = 1 \dots N$ form a symmetric set for low values of σ_η. Since $f_x(.)$ is a symmetric PDF, it follows that B_1 can be regarded as a constant in this interval.

The integral B_2 in Eq.(4.21) must in general be evaluated numerically. For a few important PDFs it is given by $B_2 = -\sqrt{3}\log 2/2 = -1.2494$ (Uniform); -1.3030 (Gaussian); -1.3082 (Logistic); and -1.3010 (Laplacian). The integrals (I_1, I_2) in Eq.(4.29) must also be evaluated numerically. For a few important PDFs they are given by $(0.3447, -0.5939)$ (Uniform); $(I_1, I_2) = (0.3183, -0.6578)$ (Gaussian); $(0.5530, -0.6905)$ (Logistic) and $(0.3989, -0.5756)$ (Laplacian).

C.2 Derivation of Eq.(4.12)

The set $(\Theta_i)_{i=1}^N$ being real-valued and of finite cardinality is bounded. Our derivation relies on the condition $\frac{|x-\Theta_i|}{\sigma_\eta} \ll 1 \; \forall \; i$. It will be shown later that the probability of x assuming a value beyond these bounds remains negligible. Case (i) All threshold levels independent: Eq.(4.5) can be rewritten as

$$P_i(x) \;\; = \;\; \int_0^\infty f_\eta(u)du - \int_0^{\Theta_i - x} f_\eta(u)du.$$

The median of the noise being zero, the first term equals 1/2. Through a change of variable $u \rightarrow u/\sigma_\eta$ the second term becomes:

$$\int_0^{\Theta_i - x} f_\eta(u)du = \int_0^{\frac{\Theta_i - x}{\sigma_\eta}} f(u)du = f(\xi_i)\left(\frac{\Theta_i - x}{\sigma_\eta}\right).$$

The last equality follows from the Mean Value Theorem [152] where ξ_i denotes a point in the interval $\left[0, \frac{\Theta_i - x}{\sigma_\eta}\right]$. For sufficiently large σ_η, the interval length becomes negligible for relevant values of x and $f(\xi_i)$ can be approximated by $f(0)$ up to a second order correction, giving us

$$P_i(x) = \frac{1}{2} - f(0)\left(\frac{\Theta_i - x}{\sigma_\eta}\right). \tag{C.5}$$

Substituting the above into Eq.(4.7) and linearizing, and then proceeding to Eq.(4.4), we get

$$P_{y|x}(n|x) = D_n\left(1 + a_n(x)\right), \qquad P_y(n) = D_n\left(1 + b_n\right), \tag{C.6}$$

where the terms $D_n, a_n(x)$ and b_n are given by

$$D_n = \frac{\binom{N}{n}}{2^N}, \quad a_n(x) = \frac{(N-2n)}{\sigma_\eta} 2f(0)(\overline{\Theta} - x),$$
$$\text{and} \qquad b_n = \frac{(N-2n)}{\sigma_\eta} 2f(0)(\overline{\Theta} - \mu_x). \tag{C.7}$$

The mean of the threshold values is denoted by $\overline{\Theta} = \left(\sum_{i=1}^{N} \Theta_i\right)/N$. Provided $|a_n(x)| \leq 1$, the first term of the mutual information in Eq.(4.3) then has the following asymptotic form:

$$\int_{-\infty}^{\infty} f_x(x) \sum_{n=0}^{N} P_{y|x}(n|x) \log_2 P_{y|x}(n|x) dx \approx \int_{-\infty}^{\infty} f_x(x) \times$$
$$\sum_{n=0}^{N} \frac{\left(D_n \log D_n + (1 + \log D_n) D_n a_n(x) + \frac{1}{2} D_n a_n(x)^2\right)}{\log 2} dx$$
$$\approx \sum_{n=0}^{N} \frac{D_n \log D_n}{\log 2} + \sum_{n=0}^{N} \frac{D_n}{2 \log 2} \left(\int_{-\infty}^{\infty} f_x(x) a_n(x)^2 dx\right). \tag{C.8}$$

The first relation follows from Eq.(C.6), (C.7) and the approximation (C.1). The first term in the intermediate expression is independent of x and can be taken outside the integral which then becomes $\int f_x(x)dx = 1$. As $a_n(x) \propto N - 2n$ and D_n given by Eq.(C.7) are anti-symmetric and symmetric in n respectively, it follows that the second term is anti-symmetric in n, and vanishes on summation. The second relation then follows. Analogously for the second term we get,

$$\sum_{n=0}^{N} P_y(n) \log_2 P_y(n)$$
$$\approx \sum_{n=0}^{N} \frac{\left(D_n \log D_n + (\log D_n + 1) D_n b_n + \frac{1}{2} D_n b_n^2\right)}{\log 2}$$
$$\approx \sum_{n=0}^{N} \frac{D_n \log D_n}{\log 2} + \sum_{n=0}^{N} \frac{D_n}{2 \log 2} b_n^2. \tag{C.9}$$

Substituting Eqs.(C.7), (C.8) and (C.9) into Eq.(4.3) and rearranging the result we get

$$I(x,y) \quad = \quad \sum_{n=0}^{N} \frac{D_n}{2 \log 2} \left(\int_{-\infty}^{\infty} f_x(x) a_n(x)^2 dx - b_n^2\right)$$

$$= \left(\sum_{n=0}^{N} \frac{2D_n}{\log 2} \left(\frac{f(0)(N-2n)}{\sigma_\eta} \right)^2 \right) \sigma_x^2. \tag{C.10}$$

Noting that $D_n,\ n = 0, .., N$ is the probability mass function of a binomial distribution with equal probabilities of success or failure (of 1/2), we get $\sum (N-2n)^2 D_n = N$, and the prefactor in Eq.(C.10) reduces to $\frac{2N}{\log 2} f^2(0)/\sigma_\eta^2$. Therefore, the mutual information simplifies to as given in Eq.(4.12).

Case (ii) All threshold levels equal: All $(\Theta_i)_{i=1}^N$ are constrained to a common value Θ. This trivially reduces to the previous case with $\overline{\Theta} = \Theta$.

The condition for validity of this expression may now be derived as follows. The starting approximation used to derive Eq.(C.5) is valid if $|x - \Theta_i| \ll \sigma_\eta$. Since x denotes a random variable it follows the approximations are valid only in the event space $\cap_{i=1}^N \{|x - \Theta_i| \ll \sigma_\eta\}$. It follows that the probability measure of the complement of the above set given by $Prob\left[\cup_{i=1}^N \{|x - \Theta_i| > \sigma_\eta\}\right]$ should be sufficiently small. From the sub-additivity of probability measures it follows

$$\text{Prob}\left[\cup_{i=1}^N \{|x - \Theta_i| > \sigma_\eta\}\right] \leq \sum_{i=1}^{N} \text{Prob}\left[|x - \Theta_i| > \sigma_\eta\right]. \tag{C.11}$$

The Chernoff bound [132] for each component term gives:

$$\text{Prob}\left[|x - \Theta_i| > \sigma_\eta\right] \leq \frac{E\left(x - \Theta_i\right)^2}{\sigma_\eta^2}. \tag{C.12}$$

Combining Eqs.(C.11) and (C.12) we get

$$\text{Prob}\left[\cup_{i=1}^N \{|x - \Theta_i| > \sigma_\eta\}\right] \leq \frac{N\sigma_x^2 + \sum_{i=1}^N (\Theta_i - \mu_x)^2}{\sigma_\eta^2}. \tag{C.13}$$

It follows that a sufficient, but not necessary, condition for the approximations to be valid is given by $\sigma_\eta^2 \gg N\sigma_x^2 + \sum_{i=1}^N (\Theta_i - \mu_x)^2$. For sufficiently high values of σ_η it is empirically observed that the threshold converges to the signal mean: $\Theta \to \mu_x$. Then the condition for validity can be modified to $\sigma_\eta^2 \gg N\sigma_x^2$.

C.3 Derivation of Eq.(4.21)

The proof follows from computing the dominant order corrections to the unperturbed values given by Eqs.(4.14,4.15) and (4.16) due to the perturbed values given by Eqs.(4.19)

and (4.20). The first term in Eq.(4.3) has the following asymptotic form

$$\begin{aligned}
&\int_{-\infty}^{\infty} f_x(x) \sum_{n=0}^{N} P_{y|x}(n|x) \log_2 P_{y|x}(n|x) dx \\
&\approx \int_{-\infty}^{\infty} f_x(x) \times \sum_{i=1}^{N} \left[F\left(\frac{\Theta_i - x}{\sigma}\right) \log_2 F\left(\frac{\Theta_i - x}{\sigma_\eta}\right) \right. \\
&\left. + \left(1 - F\left(\frac{\Theta_i - x}{\sigma_\eta}\right)\right) \log_2 \left(1 - F\left(\frac{\Theta_i - x}{\sigma_\eta}\right)\right) \right] dx \\
&\approx \int_{-\infty}^{\infty} \left\{ \sum_{i=1}^{N} f_x(\Theta_i - \sigma_\eta u) \right\} [F(u) \log_2 F(u) + \\
&\qquad (1 - F(u)) \log_2 (1 - F(u))] \, \sigma_\eta du. \qquad \text{(C.14)}
\end{aligned}$$

The second relation follows from the change of variable $u = \frac{\Theta_i - x}{\sigma_\eta}$ in each summand and re-summing the resultant integrals. Also $\lim_{\sigma_\eta \to 0} \left\{ \sum_{i=1}^{N} f_x(\Theta_i - \sigma_\eta u) \right\} = \sum_{i=1}^{N} f_x(\Theta_i)$, which being a constant can be pulled out of the integral. By the symmetry relation (C.2) we then get:

$$\begin{aligned}
&\int_{-\infty}^{\infty} f_x(x) \sum_{n=0}^{N} P_{y|x}(n|x) \log_2 P_{y|x}(n|x) dx \approx \\
&2\sigma_\eta \left\{ \sum_{i=1}^{N} f_x(\Theta_i) \right\} \times \left\{ \int_{-\infty}^{\infty} F(u) \log_2 F(u) du \right\}. \qquad \text{(C.15)}
\end{aligned}$$

It can be shown that the absolute value of the term within brackets can be upper bounded as:

$$|f_x(\Theta_1 + \sigma_\eta u) - f_x(\Theta_1 - \sigma_\eta u)| \leq 2K_1 \sigma_\eta u. \qquad \text{(C.16)}$$

where K_1 can be taken to be an upper bound on the absolute value of the derivative of $f'_x(.)$ for differentiable PDFs, or the Lipschitz constants for non-differentiable, but Lipschitz continuous PDFs (such as the Laplacian). Therefore, by the Mean Value Theorem [152] it follows:

$$P_y(0) = \frac{1}{N+1} + \mathcal{O}(\sigma_\eta^2). \qquad \text{(C.17)}$$

The correction terms of $\mathcal{O}(\sigma_\eta^2)$ are sub-dominant to the linear order terms in Eq.(C.15) and can be ignored. As the same relation holds for all i, it then follows that the second

term of Eq.(4.3) is given by

$$\sum_{n=0}^{N} P_y(n) \log_2 P_y(n) \approx -\log_2(N+1). \tag{C.18}$$

Summing Eqs.(C.15) and (C.18) we get Eq.(4.21).

C.4 Derivation of Eq.(4.29)

The first term of the mutual information given by Eq.(4.3) can be approximated as follows:

$$\begin{aligned}
&\int_{-\infty}^{\infty} f_x(x) \sum_{n=0}^{N} P_{y/x}(n/x) \log_2 P_{y/x}(n/x) dx \\
&\approx \int_{-\infty}^{\infty} f_x(x) \left[N\epsilon(x) \log_2 N\epsilon(x) \right. \\
&\quad \left. + (1 - N\epsilon(x)) \log_2 (1 - N\epsilon(x)) \right] dx \\
&\approx N\overline{\epsilon}(\log_2 N - 1) + N \int_{-\infty}^{\infty} f_x(x)\epsilon(x) \log_2 \epsilon(x) dx.
\end{aligned} \tag{C.19}$$

The intermediate expression can be found by keeping only the dominant terms in the sum (given by $n = 0, 1$ for $x < 0$ and by $n = N-1, N$ for $x > 0$ in Eqs.(4.26) and (4.27) respectively. Applying Eq.(C.1) to the first term in the summand and then substituting Eq.(4.25) the second expression follows.

The second term of $I(x, y)$ in Eq.(4.3) can be found from Eqs.(4.28) and (C.1) to be

$$\begin{aligned}
&\sum_{n=0}^{N} P_y(n) \log_2 P_y(n) \\
&\approx (1 - N\overline{\epsilon}) \log_2 \frac{1 - N\overline{\epsilon}}{2} + N\overline{\epsilon} \log_2 \frac{N\overline{\epsilon}}{2} \\
&\approx N\overline{\epsilon} \log_2 \overline{\epsilon} + N\overline{\epsilon} \left(\log_2 N - 1 \right) - \log_2 2.
\end{aligned} \tag{C.20}$$

The other terms in the sum being sub-dominant can be ignored. Combining Eqs.(C.19) and (C.20) we get

$$I(x, y) = 1 + N \left\{ \int_{-\infty}^{\infty} f_x(x)\epsilon(x) \log_2 \epsilon(x) dx - \overline{\epsilon} \log_2 \overline{\epsilon} \right\}. \tag{C.21}$$

From Eqs.(4.24,C.2) the following linear scaling relations can be derived

$$\int_{-\infty}^{\infty} f_x(x)\epsilon(x)\log_2\epsilon(x)dx = I_2\sigma_\eta, \qquad \overline{\epsilon} = I_1\sigma_\eta. \tag{C.22}$$

where $I_2 = 2f_x(0)\left[\int_0^\infty (1-F(u))\log_2(1-F(u))\,du\right]$ and $I_1 = 2f_x(0)\left[\int_0^\infty (1-F(u))\,du\right]$. Substituting Eq.(C.22) into Eq.(C.21), and keeping both terms, as there are no corrections to linear order, we get Eq.(4.29).